



HAL
open science

Detection of molecular changes induced by different classes of antibiotics against *Escherichia coli* and *Vibrio parahaemolyticus* using Raman and Infra-red spectroscopies

Ngoc Thanh Xuan Nguyen

► **To cite this version:**

Ngoc Thanh Xuan Nguyen. Detection of molecular changes induced by different classes of antibiotics against *Escherichia coli* and *Vibrio parahaemolyticus* using Raman and Infra-red spectroscopies. Bacteriology. Le Mans Université, 2017. English. NNT : 2017LEMA1025 . tel-01661578

HAL Id: tel-01661578

<https://theses.hal.science/tel-01661578>

Submitted on 12 Dec 2017

HAL is a multi-disciplinary open access archive for the deposit and dissemination of scientific research documents, whether they are published or not. The documents may come from teaching and research institutions in France or abroad, or from public or private research centers.

L'archive ouverte pluridisciplinaire **HAL**, est destinée au dépôt et à la diffusion de documents scientifiques de niveau recherche, publiés ou non, émanant des établissements d'enseignement et de recherche français ou étrangers, des laboratoires publics ou privés.

Thèse de Doctorat

Ngoc Thanh Xuan NGUYEN

*Mémoire présenté en vue de l'obtention du
grade de Docteur de Le Mans Université*

sous le sceau de l'Université Bretagne Loire

École doctorale : 3MPL

Discipline : Physique

Spécialité : Environnement et Biologie

Unité de recherche : IMMM

Soutenue le 24 octobre 2017

Thèse N° : 2017LEMA1025

**Detection of molecular changes induced by different classes of antibiotics
against *Escherichia coli* and *Vibrio parahaemolyticus*
using Raman and Infra-red spectroscopies**

JURY

Rapporteurs :	Michel FEDERIGHI , Professeur, ALIM-SCAN, Oniris,Nantes
	Genesh SOCKALINGUM , Professeur, Université de Reims Champagne Ardenne
Examinatrice	Françoise LEROI , Chercheur - HDR, IFREMER Nantes
Directeur de Thèse :	Philippe DANIEL , Professeur, Université du Mans
Co-directeurs de Thèse :	Samira SARTER , Docteur -HDR, CIRAD Montpellier
	Ngoc Hai NGUYEN , Professeur, Université de Nong Lam – Ho Chi Minh ville

Thèse de Doctorat

Ngoc Thanh Xuan NGUYEN

**Detection of molecular changes induced by different classes of antibiotics
against *Escherichia coli* and *Vibrio parahaemolyticus*
using Raman and Infra-red spectroscopies**

Résumé

Ce travail avait pour objectif principal l'étude par spectroscopie vibrationnelle Raman et IR, couplée à l'analyse statistique de type ACP, la détection des changements moléculaires induits par différentes classes d'antibiotiques (ampicilline, céfotaxime, tétracycline et ciprofloxacine) vis-à-vis de deux bactéries modèles (*E. coli* et *V. parahaemolyticus*). Dans le cas d'*E. coli*, l'ampicilline et le céfotaxime ont provoqué une baisse des bandes protéiques en Raman et IR, une augmentation des carbohydrates en IR. L'addition de la tétracycline a entraîné une augmentation des acides nucléiques, une forte baisse de la phénylalanine en Raman, une diminution des bandes protéiques et une augmentation de l'ADN en Raman et IR. Concernant la ciprofloxacine, une augmentation des acides nucléiques en Raman, une augmentation des bandes protéiques et de l'ADN en IR ont été observées. Chez *V. parahaemolyticus*, le

Abstract

The present study aimed to explore Raman and IR in combination with PCA to detect molecular changes induced by different classes of antibiotics (ampicillin, cefotaxime, tetracycline and ciprofloxacin) against two bacterial models (*E. coli* and *V. parahaemolyticus*). In *E. coli*, ampicillin and cefotaxime treatments led to a decrease of protein bands in both Raman and IR, an increase of carbohydrates in IR. Tetracycline addition caused an increase of nucleic acids, a sharp decrease of phenylalanine in Raman, a decrease of protein bands and an increase of DNA in both Raman and IR. For ciprofloxacin, an increase of nucleic acids in Raman, an increase of protein bands and DNA in IR were observed. In *V. parahaemolyticus*, cefotaxime resulted in a decrease of protein bands in both Raman and IR, an increase of polysaccharides in IR. Tetracycline

céfotaxime a provoqué une baisse des protéines en Raman et Infra-rouge, une augmentation des polysaccharides en Infra-rouge. L'addition de la tétracycline a entraîné une baisse de la phénylalanine en Raman, une baisse des protéines en Raman et Infra-rouge, une augmentation des polysaccharides en Infra-rouge. Concernant la ciprofloxacine, une augmentation des polysaccharides et une diminution des bandes protéiques en Raman et IR ont été détectées. Une nette discrimination entre les échantillons traités aux antibiotiques et le témoin a été enregistrée chez *E. coli* et *V. parahaemolyticus*. Pour cette dernière, le profil de résistance à l'ampicilline a aussi été observé. Ce travail jette les bases d'une compréhension des mécanismes d'antibio-résistance dans les systèmes bactériens.

Mots-clés: Raman, Infra-rouge, *Escherichia coli*, *Vibrio parahaemolyticus*, antibiotiques, antibio-résistance.

increase of polysaccharides and a decrease of proteins in both Raman and Infra-red were noticed. Clear discrimination of antibiotic-treated samples compared to the control was recorded for the three antibiotic classes in both *E. coli* and *V. parahaemolyticus*. For the latter, resistance pattern has also been observed for ampicillin. This work lays the foundations for an understanding of the mechanisms of antibiotic resistance in the bacterial systems.

Keywords: Raman ; Infra-red ; *Escherichia coli*; *Vibrio parahaemolyticus*; antibiotics; antibio-resistance.

Contents

INTRODUCTION	1
CHAPTER I: BIBLIOGRAPHY	4
Part I.1: Vibrational spectroscopy	5
I.1.1 Raman spectroscopy	6
I.1.1.1 History	6
I.1.1.2 Basic theory	6
I.1.1.3 Structure of Raman spectrometers	8
I.1.1.4 Other Raman techniques	9
I.1.2 IR spectroscopy	11
I.1.2.1 History	11
I.1.2.2 Basic theory	11
I.1.2.3 Structure of IR spectrometers.....	12
I.1.2.4 FT-IR spectroscopy	12
I.1.2.5 Selection rules for Raman and IR	13
I.1.2.6 Major advantages and disadvantages of Raman and IR.....	14
Although Raman and IR spectroscopies are similar in that both techniques provide information on vibrational frequencies, there are many advantages and disadvantages to each method (Table 1).....	15
I.1.3 Applications of Raman and IR spectroscopies	16
I.1.3.1 Applications of Raman and IR spectroscopies to micro-organisms	16
I.1.3.2 Applications of Raman and IR spectroscopies in food analysis	21
I.1.3.3 Applications in pharmaceutical analysis	23
I.1.4 Data processing.....	24
I.1.5 Chemometric analysis.....	25
Part I.2: Bacterial species	27
I.2.1 <i>Escherichia coli</i>	27
I.2.1.1 Morphology and culture conditions	27

I.2.1.2 Virulence strains	27
I.2.1.3 Resistance to antibiotics in <i>E. coli</i>	28
I.2.2 <i>Vibrio parahaemolyticus</i>	28
I.2.2.1 Morphology and culture conditions	28
I.2.2.2 Virulence factors	29
I.2.2.3 Resistance to antibiotics in <i>V. parahaemolyticus</i>	30
I.2.3 Biofilm in bacteria.....	30
I.2.3.1 Biofilm formation and influence factors.....	30
I.2.3.2 Role of biofilms for bacteria	32
Part I.3: Antibiotics.....	34
I.3.1 Beta-lactam antibiotics: penicillins and cephalosporins	35
I.3.1.1 History and structure	35
I.3.1.2 Applications of ampicillin and cefotaxime	36
I.3.1.3 Mechanism of action.....	37
I.3.1.4 Mechanisms of resistance to β -lactams.....	38
I.3.2 Tetracyclines	40
I.3.2.1 History and structure	40
I.3.2.2 Applications of tetracyclines.....	41
I.3.2.3 Mechanism of action.....	41
I.3.2.4 Mechanisms of resistance to tetracyclines:	42
I.3.3 Fluoroquinolones: ciprofloxacin	42
I.3.3.1 History and structure	42
I.3.3.2 Applications of fluoroquinolones.....	44
I.3.3.3 Mechanisms of action	44
I.3.3.4 Mechanisms of resistance to fluoroquinolones.....	45
CHAPTER II: MATERIAL AND METHODS.....	46
II.1 Spectroscopic instrumentation	47
II.1.1 Raman spectroscopy	47
II.1.2 IR absorption spectroscopy.....	47
II.2 Growth conditions of bacteria	48

II.2.1 Bacterial strains	48
II.2.2 Growth conditions of <i>E. coli</i>	48
II.2.3 Growth conditions of <i>V. parahaemolyticus</i>	48
II.3 Antibacterial activities of antibiotics against bacteria.....	49
II.3.1 Antibacterial activities of antibiotics against <i>E. coli</i>	49
II.3.2 Antibacterial activities of antibiotics against <i>V. parahaemolyticus</i>	50
II.4 Raman and IR spectroscopy investigations	50
II.4.1 Bacterial growth monitoring	50
II.4.2 Effects of antibiotics against bacteria.....	51
II.4.2.1 Effects of antibiotics against <i>E. coli</i>	51
II.4.2.2 Effects of antibiotics against <i>V. parahaemolyticus</i>	52
II.5 Data analysis	55
CHAPTER III: RESULTS AND DISCUSSION	56
Part III.1 Vibrational spectroscopic study of bacterial growth	57
III.1.1 Growth curve of bacteria	57
III.1.2 <i>Escherichia coli</i>	57
III.1.2.1 Raman spectrum of <i>E. coli</i>	57
III.1.2.2 IR absorption spectrum of <i>E.coli</i>	60
III.1.2.3 Characterization of <i>E. coli</i> growth curve.....	60
III.1.3 <i>Vibrio parahaemolyticus</i>	62
III.1.3.1 Raman spectrum of <i>V. parahaemolyticus</i>	62
III.1.3.2 IR absorption spectrum of <i>V. parahaemolyticus</i>	63
III.1.3.3 Characterization of <i>V. parahaemolyticus</i> growth curve	64
Part III.2: Effects of antibiotics against <i>Escherichia coli</i>	67
III.2.1 Effects of ampicillin and cefotaxime	67
III.2.2 Effects of tetracycline	71
III.2.3 Effects of ciprofloxacin.....	73
III.2.4 Conclusion	76

Part III.3 Effects of antibiotics against <i>Vibrio parahaemolyticus</i>	78
III.3.1 Effects of ampicillin	78
III.3.2 Effects of cefotaxime	80
III.3.3 Effects of tetracycline	84
III.3.4 Effects of ciprofloxacin	87
III.3.5 Conclusion	89
CHAPTER IV: SUMMARY AND OUTLOOK	92
IV.1 Summary	93
IV.2 Outlook: Further experiments	95
REFERENCES	96

List of figures

Figure 1: Different fundamental light processes during material interaction	5
Figure 2: Different vibrational modes in a typical diatomic molecule	6
Figure 3: Principle of Raman spectroscopy	7
Figure 4: Differences in mechanism of Raman and IR.....	7
Figure 5: Surface-enhanced Raman scattering. The proximity to a metallic surface or nanostructure resulting in plasmon resonance (right) leads to a much stronger Raman signal than the molecule alone (left)	10
Figure 6: ATR and interaction of IR light with a sample numerous times before exiting the cell ..	12
Figure 7: Changes in polarizability during vibration of CO ₂ molecule	14
Figure 8: Changes in dipole moment for H ₂ O molecule during each normal vibration	14
Figure 9: Typical Raman spectrum of <i>E. coli</i> in the range of 400 - 4000 cm ⁻¹	16
Figure 10: Typical IR spectrum of <i>E. coli</i> in the range of 400 - 4000 cm ⁻¹	17
Figure 11: Comparison before(upper spectrum) and after (lower spectrum) baseline, normalization processing of Raman spectrum of <i>E. coli</i> recorded 8h of incubation	25
Figure 12: Morphology of <i>E. coli</i> cells	27
Figure 13: Morphology of <i>V. parahaemolyticus</i> cells	29
Figure 14: Schematic representation of biofilm-formation steps.....	31
Figure 15: Chemical structures of β-lactam antibiotics	36
Figure 16: Cell wall structure of Gram-positive, Gram-negative bacteria and chemical bonds in peptidoglycan layer	38
Figure 17: Mechanisms of resistance to antibiotics in bacteria	39
Figure 18: Three primary mechanisms of resistance to β-lactams.....	40
Figure 19: Structure of tetracycline and its semi-synthetic analogs	41
Figure 20: Mechanism of action of tetracyclines	42
Figure 21: Selected examples representing each of the four fluoroquinolone generations	43
Figure 22: Mechanism of action of quinolones.....	44
Figure 23: Confocal Raman (Horiba) and IR (Bruker) spectrometers used in the study.....	48
Figure 24: Determination of MIC value of Amp against <i>E. coli</i>	50
Figure 25: Experimental protocol for detection of molecular changes induced by different classes of antibiotics (Amp, Ctx, Tet and Cip) against <i>E. coli</i>	53

Figure 26: Experimental protocol for differentiation Amp-resistant <i>V. parahaemolyticus</i> culture (Control) and culture with Amp at 20 µg/ml	54
Figure 27: Experimental protocol for detection of molecular changes induced by different classes of antibiotics (Ctx, Tet and Cip) against <i>V. parahaemolyticus</i>	54
Figure 28: Raman and IR absorption spectra of <i>E. coli</i> recorded 8h of incubation.....	58
Figure 29: Growth curve of <i>E.coli</i> in MHB at 37°C, shaking at 200 rpm (n = 3 ± SD).....	60
Figure 30: Average Raman and IR absorption spectra of <i>E. coli</i> with double standard deviation as grey corona at different growth time points (3, 6, 8 and 24 h of incubation)	62
Figure 31: Scores plot of Raman and IR absorption spectra of <i>E. coli</i> at different growth time points (3, 6, 8 and 24 h of incubation)	62
Figure 32: Raman and IR absorption spectra of <i>V. parahaemolyticus</i> recorded 8 h of incubation ..	63
Figure 33: Growth curve of <i>V. parahaemolyticus</i> in MHB at 38°C without shaking (n = 3 ± SD) .	64
Figure 34: Raman and IR absorption spectra of <i>V. parahaemolyticus</i> with double standard deviation as grey corona at different growth time points (8, 10 and 24 h of incubation).....	65
Figure 35: Scores plot of Raman and IR absorption spectra of <i>V. parahaemolyticus</i> at different growth time points (8, 10 and 24 h of incubation).....	66
Figure 36: Average Raman spectra with double standard deviation as grey corona of <i>E. coli</i> control (black line) and culture with Amp 8MIC (40 µg/ml) (red line), or with Ctx 8MIC (1.6 µg/ml) (blue line) recorded 120 min after the antibiotic addition.....	68
Figure 37: A) Scores plot of the first two PC of Raman spectra of <i>E. coli</i> control (blue points) and culture with Amp 8MIC (40 µg/ml) (red points) recorded 120 min after the antibiotic addition. B) Loading plot for the first PC from A.....	68
Figure 38: A) Scores plot of the first two PC of Raman spectra of <i>E. coli</i> control (blue points) and culture with Ctx 8MIC (16 µg/ml) (red points) recorded 120 min after the antibiotic addition. B) Loading plot for the first PC from A.....	69
Figure 39: Average IR absorption spectra with double standard deviation as grey corona of <i>E. coli</i> control (black line) and culture with Amp 8MIC (40 µg/ml) (red line), or with Ctx 8MIC (1.6 µg/ml) (blue line) recorded 120 min after the antibiotic addition	70
Figure 40: A) Scores plot of the first two PCs of IR absorption spectra of <i>E. coli</i> control (blue points) and culture with Amp 8MIC (40 µg/ml) (red points) recorded 120 min after the antibiotic addition. B) Loading plot for the second PC from A.....	70

Figure 41: **A)** Scores plot of the first two PCs of IR absorption spectra of *E. coli* control (blue points) and culture with Ctx 8MIC (1.6 µg/ml) (red points) recorded 120 min after the antibiotic addition. **B)** Loading plot for the second PC from A 71

Figure 42: **A)** Average Raman spectra with double standard deviation as grey corona of *E. coli* control (black line) and culture with Tet 8MIC (40 µg/ml) (red line) recorded 120 min after the antibiotic addition. **B)** Scores plot of the first two PCs. **C)** Loading plot of the first PC from B 72

Figure 43: **A)** Average IR absorption spectra with double standard deviation as grey corona of *E. coli* without (black line) and with Tet 8MIC (40 µg/ml) (red line) recorded 120 min after the antibiotic addition. **B)** Scores plot of the first two PCs. **C)** Loading plot of the first PC from B 73

Figure 44: **A)** Average Raman spectra with double standard deviation as grey corona of *E. coli* control (black line) and culture with Cip 8MIC (0.8 µg/ml) (red line) recorded 90 min after the antibiotic addition. **B)** Scores plot of the first two PCs. **C)** Loading plot of the first PC from B 74

Figure 45: **A)** Average IR absorption spectra with double standard deviation as grey corona of *E. coli* control (black line) and culture with Cip 8MIC (0.8 µg/ml) (red line) recorded 90 min after the antibiotic addition. **B)** Scores plot of the first two PCs. **C)** Loading plot of the first PC from B 75

Figure 46: **A)** Average Raman spectra with double standard deviation as grey corona of *V. parahaemolyticus* control (black line) and culture with Amp at 20 µg/ml (red line) recorded 17h after the antibiotic addition. **B)** Scores plot of the first two PCs. **C)** Loading plot of the second PC from B 79

Figure 47: **A)** Average IR absorption spectra with double standard deviation as grey corona of *V. parahaemolyticus* control (black line) and culture with Amp at 20 µg/ml (red line) recorded 17 h after the antibiotic addition. **B)** Scores plot of the first two PCs. **C)** Loading plot of the first PC from B 80

Figure 48: **A)** Average Raman spectra with double standard deviation as grey corona of *V. parahaemolyticus* control (black line) and culture with Ctx 12MIC (0.72 µg/ml) (red line) recorded 120 min after the antibiotic addition. **B)** Scores plot of the first two PCs. **C)** Loading plot of the second PC from B 81

Figure 49: **A)** Average IR absorption spectra with double standard deviation as grey corona of *V. parahaemolyticus* control (black line) and culture with Ctx 12MIC (0.72 µg/ml)(red line) recorded 120 min after the antibiotic addition. **B)** Scores plot of the first two PCs. **C)** Loading plot of the second PC from B 82

Figure 50: **A)** Average Raman spectra with double standard deviation as grey corona of *V. parahaemolyticus* culture with Amp (20 µg/ml) (black line) recorded 17 h after the antibiotic addition and with Ctx 12MIC (0.72 µg/ml) (red line) recorded 120 min after the antibiotic addition. **B)** Scores plot of the first two PCs. **C)** Loading plot of the first PC from B83

Figure 51: **A)** Average IR absorption spectra with double standard deviation as grey corona of *V. parahaemolyticus* with Amp (20 µg/ml) (black line) recorded 17 h after the antibiotic addition and with Ctx 12MIC (0.72 µg/ml) (red line) recorded 120 min after the antibiotic addition. **B)** Scores plot of the first two PCs. **C)** Loading plot of the first and second PCs from B 84

Figure 52: **A)** Average Raman spectra of *V. parahaemolyticus* control (black line) and culture with Tet 8MIC (0.8 µg/ml) (red line) recorded 120 min after the antibiotic addition. **B)** Scores plot of the first two PCs. **C)** Loading plot of the first PC from B 85

Figure 53: **A)** Average IR absorption spectra of *V. parahaemolyticus* control (black line) and culture with Tet 8MIC (0.8 µg/ml) (red line) recorded 120 min after the antibiotic addition. **B)** Scores plot of the first two PCs. **C)** Loading plot of the first PC from B 87

Figure 54: **A)** Average Raman spectra of *V. parahaemolyticus* control (black line) and culture with Cip 18MIC (0.9 µg/ml) (red line) recorded 120 min after the antibiotic addition. **B)** Scores plot of the first two PCs. **C)** Loading plot of the second PC from B 88

Figure 55: **A)** Average IR absorption spectra of *V. parahaemolyticus* control (black line) and culture with Cip 18MIC (0.9 µg/ml) (red line) recorded 120 min after the antibiotic addition. **B)** Scores plot of the first two PCs. **C)** Loading plot of the first PC from B 89

List of tables

Table 1: Major advantages and disadvantages of Raman and IR spectroscopies	15
Table 2: Raman bands of major food components	22
Table 3: Mid-IR bands of major food components	23
Table 4: Classification of antibiotics depending on their mechanisms of action	34
Table 5: Assignment of some bands frequently found in FT-IR and Raman spectra in biological samples	59

List of abbreviations

Antibiotics

Amp	Ampicillin
Ctx	Cefotaxime
Tet	Tetracycline
Cip	Ciprofloxacin

Bacterial strains

<i>E. coli</i>	<i>Escherichia coli</i>
<i>V. parahaemolyticus</i>	<i>Vibrio parahaemolyticus</i>

Biological index

DNA	Deoxyribonucleic acid
RNA	Ribonucleic acid
tRNA	Transfer ribonucleic acid
CFU	Colony Forming Unit
OD ₆₀₀	Optical density at 600 nm
MIC	Minimum inhibitory concentration
MBC	Minimum bactericidal concentration
IR	Infra-red spectroscopy
PC	Principal component
PCA	Principal components analysis
PCR	Polymerase chain reaction
AI	Autoinducer
EPSs	Extracellular polymeric substances
rpm	Rotation per minute
h	Hour

min Minute

UV Ultraviolet

Culture media

MHB Mueller Hinton broth

NA Nutrient agar

Vibrational spectroscopy

ATR Attenuated Total Reflectance

IR spectroscopy Infra-red spectroscopy

FT-IR Fourier transform – infra-red

FT-Raman Fourier transform -Raman

SERS Surface-enhanced Raman scattering

nm Nanometer

List of publications

1- Investigation of the effects of antibiotics against *Vibrio parahaemolyticus* using Raman and Infra-red spectroscopies. N. T. Xuan NGUYEN, N. Hai NGUYEN, Samira SARTER, Philippe DANIEL
Article is being finalized.

2- Detection of molecular changes induced by antibiotics in *Escherichia coli* using vibrational spectroscopy. N. T. Xuan NGUYEN, N. Hai NGUYEN, Samira SARTER, Philippe DANIEL. *Spectrochimica Acta Part A: Molecular and Biomolecular Spectroscopy* 183C (2017), pp 395-401.
<http://dx.doi.org/10.1016/j.saa.2017.04.077>

List of international and national communications

1- Oral presentation: Detection of molecular changes induced by antibiotics in *Escherichia coli* using vibrational spectroscopy. N. T. Xuan NGUYEN, N. Hai NGUYEN, Samira SARTER, Philippe DANIEL. International conference: The 19th Federation of Asian Veterinary Associations Congress, September 6-9, 2016 – Ho Chi Minh City, Viet Nam.

2- Oral presentation: Detection of molecular changes induced by antibiotics in *Escherichia coli* using Raman and Infra-red spectroscopies. N. T. Xuan NGUYEN, N. Hai NGUYEN, Samira SARTER, Philippe DANIEL. National conference: 7^{èmes} Rencontres Biologie Physique du Grand-Ouest, June 23 – 24, 2016 – Nantes, France.

List of posters and communications organized by Ecole doctorale

1- Poster presentation: Detection of molecular changes induced by antibiotics in *Escherichia coli* using vibrational spectroscopy. N. T. Xuan NGUYEN, N. Hai NGUYEN, Samira SARTER, Philippe DANIEL – Forum “Jeunes – Recherche”, November 2016, Université du Maine.

2- Oral presentation: Detection of molecular changes induced by antibiotics in *Escherichia coli* using Raman and Infra-red spectroscopies. N. T. Xuan NGUYEN, N. Hai NGUYEN, Samira SARTER, Philippe DANIEL - 8th Journées de l'Ecole doctorale, June 23-24, 2016 - Ecole des Mines, Nantes.

3- Poster presentation: Influence of antibiotics on the bacterial growth of *Escherichia coli* using micro-Raman spectroscopy. N. T. Xuan NGUYEN, N. Hai NGUYEN, Samira SARTER, Philippe DANIEL - June 2015, Université du Maine.

Acknowledgements

I would like to acknowledge my supervisor, Professor Philippe DANIEL, for giving me the opportunity to conduct this research project in his team PM2S at Le Mans University as well for the support and advices that he has given me to make this thesis possible. I would like to thank my co-supervisor, Professor Ngoc Hai NGUYEN, for his help, support and encouragement for more than 10 years. Also, I would like to express my sincere appreciation and utmost gratitude to my co-supervisor, Dr Samira SARTER, for her immense editing assistance in the preparation of papers, posters and this thesis. Your assistance was indispensable and your patience has made completion of this thesis possible. Thank you ever so much.

I am fully indebted to Dr Marie-José Durand-Thouand from GEPEA laboratory – Université de Nantes who provided the *E. coli* strain for the study. Also I wish especially to acknowledge Frédéric Amiard, Romain CHAUVET, Quang Huy NGUYEN who helped me in spectroscopy measurements and data treatments. I would like to thank Madame Brigitte MOREAU for giving me culture media in microbiology.

Special thanks to all thesis committee members: Professor Michel FEDERIGHI, Professor Ganesh SOCKALINGUM and Dr François LEROI

Last but not least, I would like to thank my parents, my younger sister and my brother-in-law. I could not have done this thesis without your love and encouragement. You are always in my heart.

**Detection of molecular changes induced by different classes of antibiotics
against *Escherichia coli* and *Vibrio parahaemolyticus*
using Raman and Infra-red spectroscopies**

Abstract

Raman and Infra-red spectroscopies are two complementary techniques that provide the biochemical composition of the cell, allowing rapid and accurate identification of micro-organisms. The present study aimed to explore these innovative methods to investigate the mechanisms of action of antibiotics against two bacterial models (*Escherichia coli* and *Vibrio parahaemolyticus*). Raman and IR spectroscopies were used in combination with principal components analysis to detect molecular changes induced by different classes of antibiotics (ampicillin, cefotaxime – cell wall inhibitors, tetracycline – protein synthesis inhibitor and ciprofloxacin – DNA replication inhibitor) against *Escherichia coli* and *Vibrio parahaemolyticus*. In *Escherichia coli*, ampicillin and cefotaxime treatments led to a decrease of protein bands in both Raman and Infra-red, an increase of carbohydrates in Infra-red. Tetracycline addition caused an increase of nucleic acids, a sharp decrease of phenylalanine in Raman, a decrease of protein bands and an increase of DNA in both Raman and Infra-red. For ciprofloxacin, an increase of nucleic acids in Raman, an increase of protein bands and DNA in Infra-red were observed. In *Vibrio parahaemolyticus*, cefotaxime resulted in a decrease of protein bands in both Raman and Infra-red, an increase of polysaccharides in Infra-red. Tetracycline treatment caused a decrease of phenylalanine in Raman, a decrease of proteins in both Raman and Infra-red, an increase of polysaccharides in Infra-red. For ciprofloxacin, an increase of polysaccharides and a decrease of proteins in both Raman and Infra-red were noticed. Clear discrimination of antibiotic-treated samples compared to the control was recorded for the three antibiotic classes in both *Escherichia coli* and *Vibrio parahaemolyticus*. For the latter, resistance pattern has also been observed for ampicillin.

Keywords: Raman; Infra-red, *Escherichia coli*, *Vibrio parahaemolyticus*, antibiotics, antibiotic-resistance.

**Détection des changements moléculaires induits par différentes classes d'antibiotiques
chez *Escherichia coli* et *Vibrio parahaemolyticus*
en utilisant les spectroscopies Raman et Infra-rouge**

Résumé

Les spectroscopies Raman and Infra-rouge sont deux techniques complémentaires qui fournissent la composition biochimique de la cellule, permettant l'identification rapide et précise des micro-organismes. Cette étude a exploré ces techniques innovantes pour comprendre les modes d'action des antibiotiques vis-à-vis de deux bactéries modèles (*Escherichia coli* et *Vibrio parahaemolyticus*). Les spectroscopies Raman et Infra-rouge ont été utilisées en combinaison avec l'analyse des composantes principales en vue de détecter les changements moléculaires induits par différentes classes d'antibiotiques (ampicilline, céfotaxime - inhibiteurs de la paroi cellulaire, tétracycline - inhibiteur de la synthèse protéique et ciprofloxacine – inhibiteur de la réplication d'ADN). Dans le cas d'*Escherichia coli*, l'ampicilline et le céfotaxime ont provoqué une baisse des bandes protéiques en Raman et Infra-rouge et une augmentation des carbohydrates en Infra-rouge. L'addition de la tétracycline a entraîné une augmentation des acides nucléiques, une forte baisse de la phénylalanine en Raman, une diminution des bandes protéiques et une augmentation de l'ADN en Raman et Infra-rouge. Concernant la ciprofloxacine, une augmentation des acides nucléiques en Raman, une augmentation des bandes protéiques et de l'ADN en Infra-rouge ont été observées. Chez *Vibrio parahaemolyticus*, le céfotaxime a provoqué une baisse des protéines en Raman et Infra-rouge, une augmentation des polysaccharides en Infra-rouge. L'addition de la tétracycline a entraîné une baisse de la phénylalanine en Raman, une baisse des protéines en Raman et Infra-rouge, une augmentation des polysaccharides en Infra-rouge. Concernant la ciprofloxacine, une augmentation des polysaccharides et une diminution des bandes protéiques en Raman et Infra-rouge ont été détectées. Une nette discrimination entre les échantillons traités aux antibiotiques et le témoin a été enregistrée chez *Escherichia coli* et *Vibrio parahaemolyticus*. Pour cette dernière, le profil de résistance à l'ampicilline a aussi été observé.

Mots-clés: Raman, Infra-rouge, *Escherichia coli*, *Vibrio parahaemolyticus*, antibiotiques, antibio-résistance.

INTRODUCTION

Antibiotic resistance is becoming a major threat to human and animal health. In particular, multidrug resistance in bacteria, such as *Escherichia coli* against cephalosporin and fluoroquinolones, *Klebsiella pneumoniae* against cephalosporin and carbapenems, *Staphylococcus aureus* against methicillin, aminoglycosides, macrolides, tetracycline, chloramphenicol and lincosamides, has emerged as a threat to public health all over the world [1,2]. Therefore, it is of great interest to understand the mechanisms of action of antibiotics on a molecular level to develop innovative methods for rapid detection of resistant bacterial strains. Indeed, to gain a better insight into the metabolism of the bacteria and to comprehensively understand about the action of antibiotics, especially non-destructive, highly sensitive characterization methods are urgently needed. During the last years, vibrational spectroscopic methods have been proven to have a great potential for the study of biological problems. Vibrational spectroscopy that is based on investigating the molecular vibration of the chemical bonds in a sample is the common term used to describe two techniques: Raman and IR. In Raman spectroscopy, the vibrational transitions are probed via an inelastic scattering process. Otherwise, the vibrational transitions are directly excited in IR spectroscopy [3]. In the recent years, Raman scattering and IR spectroscopies have been rapidly gaining ground in innovative research. The techniques offer significant benefits as non-invasive, non-destructive, reagent free and rapid diagnostic tools for single cell analysis. These approaches provide “whole organism fingerprinting” through an examination of spectral features corresponding to a wide range of important functional groups that together can give rich information about the complex chemical composition of the cell and the cell components also to identify and differentiate bacteria at a species level or strain level [4,5,6,7,8,9,10,11]. Raman spectroscopy offers some major advantages over IR spectroscopy for investigating biological specimens since interference of water spectrum is less problematic. Additionally, more spectral features are detectable in a Raman spectrum than in an IR spectrum over the same wavenumber range [12,13]. However, using a combination of both Raman and IR spectroscopies is powerful since the techniques are complementary. Moreover, it is important to apply advanced data processing (baseline, normalization correction) and statistical analysis to the raw Raman and IR spectra so that minor differences in the spectral features can be distinguished.

Objectives of the thesis

The important objectives of the thesis were to explore Raman (400-1800 cm^{-1}) and IR (400-4000 cm^{-1}) spectroscopies to investigate metabolic changes at different growth time and to detect molecular modifications induced by different classes of antibiotics (β -lactams: Amp, Ctx – cell wall synthesis inhibitors; tetracyclines: Tet – protein synthesis inhibitor and fluoroquinolones: Cip – DNA replication inhibitor) against *Escherichia coli* and *Vibrio parahaemolyticus* – two common bacterial models in food security. Therefore, to achieve these purposes the study focused on two main parts:

- ✓ Detection of metabolic changes occurring during the growth of *Escherichia coli* (3, 6, 8 and 24 h of incubation) and *Vibrio parahaemolyticus* (8, 10 and 24 h of incubation) using Raman and IR spectroscopies.
- ✓ Detection of molecular changes induced by different classes of antibiotics (Amp, Ctx, Tet and Cip) against *Escherichia coli* and *Vibrio parahaemolyticus* using Raman and IR spectroscopies

The observed subtle spectral changes were interpreted by means of chemometric analysis (Principal Components Analysis). The spectral region of interest from 400-1800 cm^{-1} for Raman and 900-2000 cm^{-1} for IR were analyzed by Principal Components Analysis.

CHAPTER I: BIBLIOGRAPHY

Part I.1: Vibrational spectroscopy

Vibrational spectroscopy is the common term used to describe collective movements of atoms or groupments atoms which are generally observed two analytical techniques - Raman and IR spectroscopies. These two techniques are non-destructive, non-invasive tools that provide information about the molecular composition, structure and interactions within a sample. Raman and IR spectroscopies measure vibrational energy levels which are associated with the chemical bonds in the sample. The sample spectrum is unique, like a fingerprint, thus vibrational spectroscopy is routinely used for identification, characterization, structure elucidation, reaction monitoring, quality control and quality assurance.

Principle of vibrational spectroscopy:

When light interacts with matter, the photons which make up the light may be absorbed (IR spectroscopy) or scattered (Raman spectroscopy) or may not interact with the material and may pass straight through it (Figure 1).

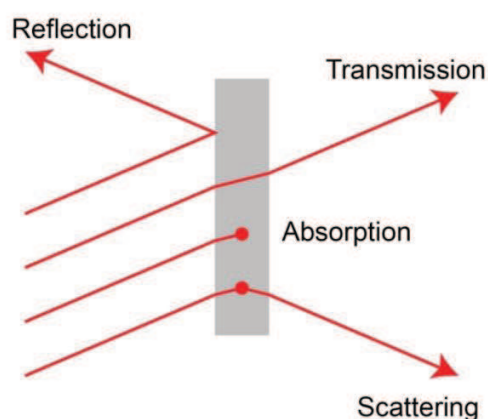


Figure 1: Different fundamental light processes during material interaction

(<http://www.renishaw.com/en/a-basic-overview-of-raman-spectroscopy--25805>)

The vibrational modes can be divided into valence vibrations (stretching vibrations) and different types of deformation vibrations (scissoring, wagging, rocking, twisting, torsion and bending vibrations) (Figure 2). The stretching vibrations change the distance along the bond between the involved atoms and can be either symmetric or anti-symmetric. The different deformation vibrations change the bond angle. The energy requirement for the stretching vibrations is greater than for the deformation vibrations [14,15].

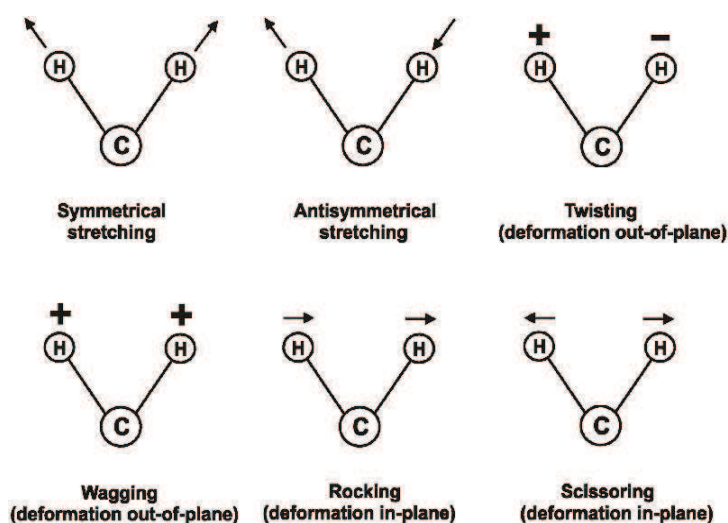


Figure 2: Different vibrational modes in a polyatomic molecule [16]

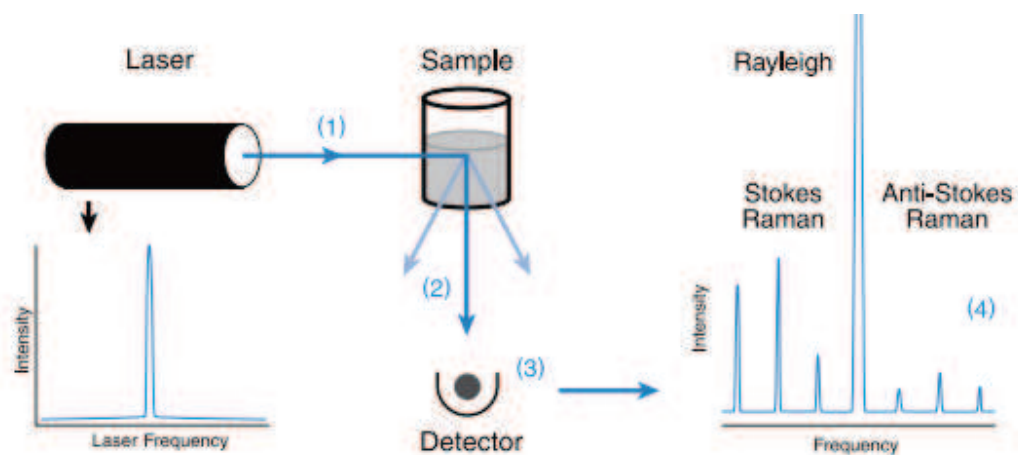
I.1.1 Raman spectroscopy

I.1.1.1 History

The phenomenon of inelastic scattering of light was discovered in 1928 by Raman C. V. and Krishnan K. F.. In 1930, Raman was awarded the Nobel prize in physics for his great discovery [12,17,18,19,20,21]. Since the phenomenon has been referred to as Raman spectroscopy. By the end of the 1930s, Raman spectroscopy had become one of the principle method of non-destructive chemical analysis. Although the development of lasers in the 1960s, Raman spectroscopy still required skilled operators to collect spectra and the process was quite labor intensive [21,14].

I.1.1.2 Basic theory

The technique is based on inelastic light scattering by a molecule or crystal. The scattered light consists of two types: one, called Rayleigh scattering, is strong and has the same energy and frequency as the incident photons (ν_0) and the other, called Raman scattering, is very weak (approximately 1 out of 10^7 photons) and has frequencies $\nu_0 \pm \nu_m$, where ν_m is a vibrational frequency of a molecule. The $\nu_0 - \nu_m$ and $\nu_0 + \nu_m$ lines are called the Stokes and anti-Stokes lines, respectively [19,22]. Thus, in Raman spectroscopy, we measure the vibrational frequency (ν_m) as a shift from the incident beam frequency (ν_0) (Figure 3 and 4)



- (1) Laser light excites the sample
- (2) This light is scattered in all directions
- (3) Some of this scattered light is directed to the detector, which records the Raman spectrum
- (4) This spectrum shows light at the original laser (or Rayleigh) frequency and the Raman spectral features unique to the sample

Figure 3: Principle of Raman spectroscopy

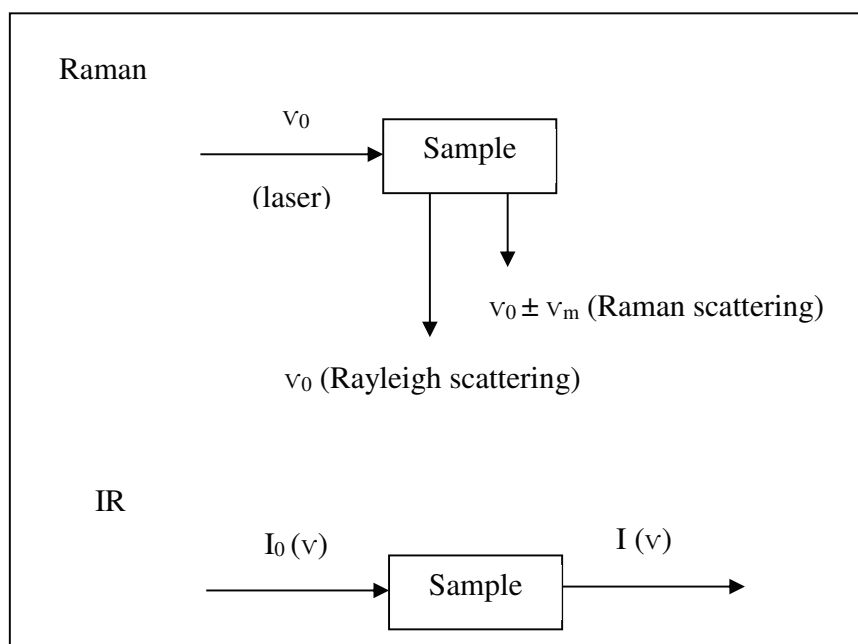


Figure 4: Differences in mechanism of Raman and IR

In Raman spectroscopy, a sample is irradiated with a strong monochromatic laser light whose frequency may vary from the visible to the near IR region. Raman spectroscopy experiences much smaller cross section compared to IR absorption spectroscopy. As a result, Raman scattering intensity is much weaker than that IR absorption intensity. Therefore, a powerful light

source is essential. Generally this radiation frequency is much higher than the vibrational frequencies but is lower than the electronic frequencies.

- ✓ Ultra-violet: 244 nm, 257 nm, 325 nm, 364 nm
- ✓ Visible: 457 nm, 473 nm, 488 nm, 514 nm, 532 nm, 633 nm, 660 nm
- ✓ Near infra-red: 785 nm, 830 nm, 980 nm, 1064 nm

For instance, three laser wavelengths investigated by confocal Raman XploRA ONE™(Jobin Yvon, Horiba) spectrometer: visible (532 nm – green, 633 nm – red), near-infra red (785 nm). Laser wavelengths can be chosen according to sample characteristic. For example:

- ✓ Blue or green lasers can be good for inorganic materials, resonance Raman experiments and surface enhanced Raman scattering.
- ✓ Red or near infra-red (660 – 830 nm) are good for fluorescence suppression.
- ✓ Ultra-violet lasers for resonance Raman on bio-molecules, such as proteins, DNA, RNA and fluorescence suppression.

Since Raman scattering is weak, the laser beam must be properly focused onto the sample and the scatter radiation collected efficiently. Spectra obtained from Raman spectroscopy are composed of three main components: the Raman signals, the background signal and noise. The background signal and noise are usually reduced in the recorded spectra using preprocessing techniques such as polynomial fitting, wavelet transform or the rolling ball technique before analysis [23].

1.1.1.3 Structure of Raman spectrometers

These systems consist of [14]:

- Laser excitation source (UV, visible or near-IR).
- Lenses (both to focus the light onto the sample and to collect the scattered light).
- Filters (to purify the reflected and scattered light so that only the Raman light is collected).
- A means of splitting the light into its constituents colors (normally a diffraction grating).
- A very sensitive detector (to detect the weak light).
- A device such as a computer to control the whole system, display the spectrum and enable this information to be analyzed.

I.1.1.4 Other Raman techniques

Confocal Raman microspectroscopy

The confocal Raman microscope was invented in 1990 and has been investigated for recording Raman spectra for a single human cell [24]. It is advantageous to couple the strength and the flexibility of Raman spectroscopy with a confocal microscope that allows analysis of very small samples. The goal of microscopy is to analyze the smallest samples possible and to distinguish the substance of interest from its surroundings. Raman microspectroscopy often takes advantage of a confocal setup to increase the spectral resolution, where two apertures (behind the light source and in front of the spectrometer) reduce stray light and eliminate out-of focus information and only information from the focal plane reaches the detector [20].

FT-Raman spectroscopy

One important advantage of FT-Raman lies in the near lack of sample fluorescence. An FT-Raman instrument typically employs a 1 μm excitation laser, an interferometer and a high-sensitivity near-infrared detector. By using the longer wavelength excitation laser, there is less energy supplied, so the virtual state is lower and less likely to overlap an upper electronic state. This greatly reduces fluorescence interferences [14].

Surface-enhanced Raman scattering

Surface-enhanced Raman scattering is a variation of Raman spectroscopy. The SERS effect is achieved when an analyte is absorbed onto or in close proximity to a prepared metal surface. The Raman excitation laser produces surface plasmons (coherent electron oscillations) on the surface of the metal. These surface plasmons interact with the analyte to greatly enhance the Raman emission up to $10^{14} - 10^{15}$ times. To obtain the most effective enhancement, there must be resonance between the metal and the laser, making the correct pairing of substrate and laser of critical importance. If the laser and metal are not properly matched, the signal will be weak, noisy and not produce any enhancement at all [25,26]. The most commonly used metals for SERS are silver and gold, although research involving a wide variety of metals is ongoing [27,28]. Other metals that have been shown to be useful include copper, platinum and palladium [13,29,30]. An important component for a good SERS enhancement is roughness of the metal surface. If the surface is too smooth or flat, there will not be effective surface plasmons generation. Surface roughness features are usually much smaller than the wavelength of the laser.

For example, particle sizes are commonly in the range of 20 to 100 nm for laser wavelengths in the range of 532 to 780 nm. Many researchers create their own SERS substrates, but commercially available kits offer a more routine approach. The other mechanism involved in signal enhancement is chemical effect. This mechanism contributes a 10^2 enhancement and is a result of molecular charge-transfer interactions between the nanoparticles and the analyte.

The main drawback of SERS is the rather poor quantitative reproducibility, since the SERS signal is exceedingly sensitive to the nature and shape of the metal surface roughness and a number of factors involving the adsorption process, such as the orientation at the metal surface and the extent of adsorption. In addition, it is possible that an impurity within a sample formed by surface photochemistry is preferentially enhanced. SERS shows great promise in a wide variety of fields including polymer and materials science, biochemistry and biosensing, catalysis, electrochemistry, food safety, threat detection and medical diagnostics [31].

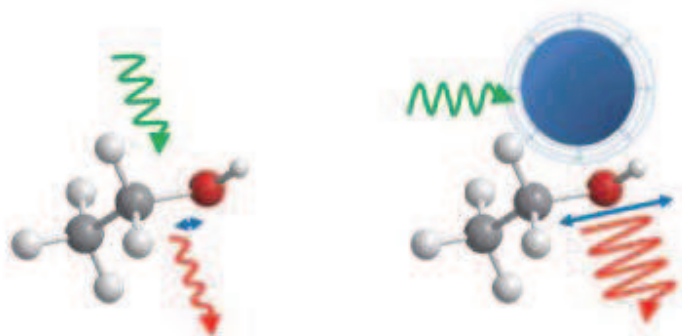


Figure 5: Surface-enhanced Raman scattering. The proximity to a metallic surface or nanostructure resulting in plasmon resonance (right) leads to a much stronger Raman signal than the molecule alone (left) [4]

Resonance Raman spectroscopy

In resonance Raman the excitation wavelength is carefully chosen to overlap with (or be very close to) an electronic transition –an area of UV-visible absorption. Such overlap can result in scattering intensities which are increased by factors of $10^2 - 10^6$ and thus detection limits and measurement times can be significantly decreased. Practically, resonance Raman can be explored on any Raman system and the actual measurement is made the standard way. The obvious requirement is to have suitable laser excitation in order to meet resonance conditions. Using the resonance Raman effect can selectively enhance vibrations of a particular chromophoric in the

molecule, such as aromatic amino acids, nucleic acids and lipids. For instance, at 231 nm spectral bands of aromatic amino acids are enhanced, at 251 nm spectral features of nucleic acids are most prominent in the spectrum. Besides, fluorescence occurs in biological molecules when the excitation wavelength is longer than 290 nm. This drawback can be avoided in case of resonance Raman spectroscopy. This is particularly advantageous in biological studies. However, a major disadvantage with using these excitation wavelengths in the UV range is the “burning” or other photochemical effects and thus leading to biochemical change of biological samples [17,19,32,33,34].

I.1.2 IR spectroscopy

I.1.2.1 History

The use of IR method began in the 1950s by Wilbur Kaye. He had designed a tool that tested the near-infrared spectrum and found the theory to describe the results. Karl Norris initiated using IR spectroscopy in the analytical field in the 1960s and as a result IR spectroscopy became an accepted technique [15,35].

I.1.2.2 Basic theory

IR spectroscopy is used to investigate the vibrational properties of a sample. The IR region ($10 - 14000 \text{ cm}^{-1}$) is divided into three regions: the near-, mid- and the far-IR. The mid-IR ($400 - 4000 \text{ cm}^{-1}$) is the most commonly employed region for analysis as molecular vibrations give rise to absorption bands generally located in the mid-IR range (between 400 and 4000 cm^{-1}) where they are the most intense. The far- and near-IR ranges are not usually used as only overtones (secondary vibrations) and combination vibrations are registered in those regions, being difficult to study and interpret from an analytical viewpoint [15,36]. Mid-IR spectroscopy is based on studying the interaction of IR radiation with samples. When IR radiation pass through a sample, specific wavelengths are absorbed, causing the chemical bonds in the material to undergo vibrations. Functional groups presented in a molecule tend to absorb IR radiation in the same wavenumber range regardless of other structures in the molecule. Thus there is a correlation between IR band positions and chemical structures in the molecule [36,37].

Attenuated Total Reflectance is a useful technique to obtain the IR spectrum of the surface of a material, which is too thick or too strongly absorbing to be analyzed by standard transmission methods. Samples can be powders, pastes, fibers, paper, foams, textiles or soils. Additionally, the ATR accessory shortened the time needed for sample preparation, increased

durability of IR instruments and reduced the analysis cost [13,15]. The sample is placed in contact with an internal reflection element, a material with a high refractive index, like ZnSe, Ge, Si or diamond. The light is totally reflected, several times and the sample interacts with the evanescent wave resulting in the absorption of radiation at each point of reflection. The intensity of the evanescent wave decays exponentially with the distance from the surface of the internal reflection element. Light longer wavelength penetrates deeper into the sample, which results in stronger bands. The angle of incidence is usually chosen to be between 45 and 60° (a smaller angle results in deeper penetration than a higher angle) (Figure 6)

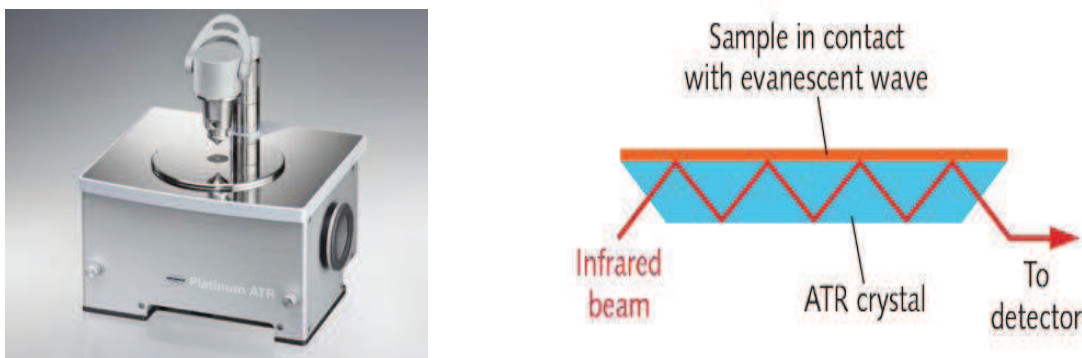


Figure 6: ATR and interaction of IR light with a sample numerous times before exiting the cell

I.1.2.3 Structure of IR spectrometers

An IR spectrometer is composed of four major components [15]:

- IR source
- Detector
- Beam splitter
- Generally ATR accessory

I.1.2.4 FT-IR spectroscopy

Along with conventional IR spectroscopy, FT-IR spectroscopy is a powerful tool extensively used to identify and discriminate bacteria. FT-IR spectroscopy exploits the interferometer, which gives simultaneous chemical information across a broad absorbance range

in the form of an interferogram. This is converted to the familiar absorbance spectrum through a mathematical process called the Fourier transform [15,18].

I.1.2.5 Selection rules for Raman and IR

The differences in mechanism of Raman and IR are presented in Figure 4 and their selection rules are distinctively different as well. IR bands arise from an interaction between light and the oscillating dipole moment of a vibrating molecule [15,38]. While Raman bands arise from an oscillating induced dipole caused by light waves interacting with the polarizability ellipsoid of a vibrating molecule [12,39]. Polarizability is related to the ability of electronic clouds surrounding the molecule to interact with an electric field. When a molecule is placed in an electric field (\vec{E}), it suffers distortion since the positively charged nuclei are attracted toward the negative pole and electrons toward the positive pole. This charge separation produces an induced dipole moment (\vec{P}) and results in scattering reactions.

$$\vec{P} = \alpha \vec{E}$$

The proportionality constant α is the polarizability of the molecule. The polarizability measures the ease with which the electron cloud around a molecule can be distorted. Figure 7 shows changes in polarizability during vibration of CO₂ molecule.

In order to obtain IR-active absorption, a molecular vibration must cause a change in the dipole moment of the molecule. It can be shown that the intensity of an IR absorption band is proportional to the square of the change in dipole moment caused by the molecular vibration giving rise to the absorption band.

To determine whether the vibration is active in the Raman and IR spectra, the selection rules must be applied to each normal vibration. For example, the dipole moment of the H₂O molecule is changed during each normal vibration (Figure 8). Thus, all these vibrations are IR-active [14].

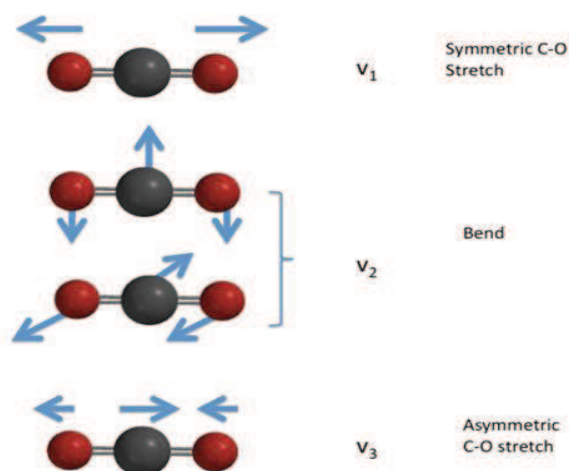


Figure 7: Changes in polarizability during vibration of CO₂ molecule
 (<http://chemistry.stackexchange.com/questions/18605/how-can-i-deduce-the-linearity-of-xef2-from-the-ir-spectrum>)

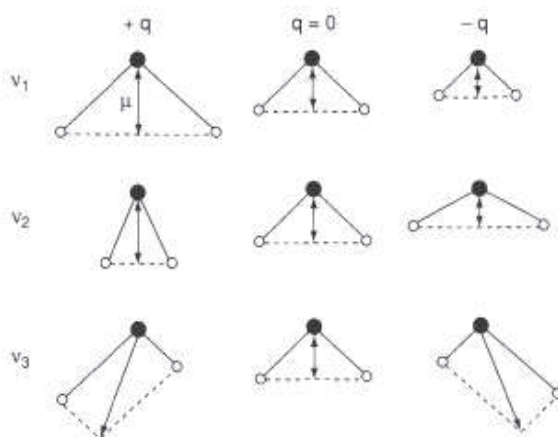


Figure 8: Changes in dipole moment for H₂O molecule during each normal vibration
 [14,16]

Raman and mid-IR spectroscopy are complementary techniques and usually both are required to completely measure the vibrational modes of a molecule. In general, Raman spectroscopy is best at symmetric vibrations of non-polar groups while IR spectroscopy is best at the asymmetric vibrations of polar groups.

I.1.2.6 Major advantages and disadvantages of Raman and IR

Although Raman and IR spectroscopies are similar in that both techniques provide information on vibrational frequencies, there are many advantages and disadvantages to each method (Table 1)

Table 1: Major advantages and disadvantages of Raman and IR spectroscopies
[14,15,17,28,38]

Raman spectroscopy	IR spectroscopy
Advantages	
<ul style="list-style-type: none"> - Sample preparation is not very elaborate, it can be in any state (solid, liquid, gaseous, hydrated films, crystalline or polycrystalline state). - Small amount of sample is required. - Since water and CO₂ are very weak Raman scatterers. Water can be used as a solvent. - The standard spectral range reaches well below 400 cm⁻¹, making the technique ideal for both organic and inorganic samples. - Raman spectroscopy can be used to measure bands of symmetric linkages which are weak in an IR spectrum. 	<ul style="list-style-type: none"> - The cost for equipment is comparatively inexpensive. - Existence of spectra libraries.
Disadvantages	
<ul style="list-style-type: none"> - The cost of required instrumentation is very high, which has been the main obstacle to the widespread adoption of Raman spectroscopy for routine analysis. - A major problem for Raman measurements lies in the high levels of fluorescence (intrinsic or caused by impurities), overlaying the Raman bands of sample (especially for biological samples). - A laser source is needed to observe weak Raman scattering. This may cause local heating and decomposition for sample. 	<ul style="list-style-type: none"> - Sample preparation can be elaborate - IR spectroscopy suffers from the strong absorption of water. Thus, water cannot be used as a solvent.

I.1.3 Applications of Raman and IR spectroscopies

Both Raman and IR spectroscopies have been extensively applied in various research areas, such as in microbiology (detection and discrimination of bacteria, detection of microbial cell injury, determination of mechanisms of action of antibiotics, assessment of antibiotic susceptibility, virus identification...), in food analysis (identification of water- and foodborne pathogens, studying properties of bacterial biofilms on contact surfaces), in pharmaceutical analysis...

I.1.3.1 Applications of Raman and IR spectroscopies to micro-organisms

Vibrational spectroscopy provides a wide range of biochemical constituents of bacteria in a single spectrum, most importantly characteristics of the cell membrane. Each bacterial species has a complex cell wall composition which gives a unique Raman and IR fingerprint due to the vibrational modes of molecular bonds or functional groups present in its proteins, lipids, carbohydrates, nucleic acids and polysaccharides. Therefore, Raman and IR spectra of the bacterial cell are usually complex (Figure 9 and 10).

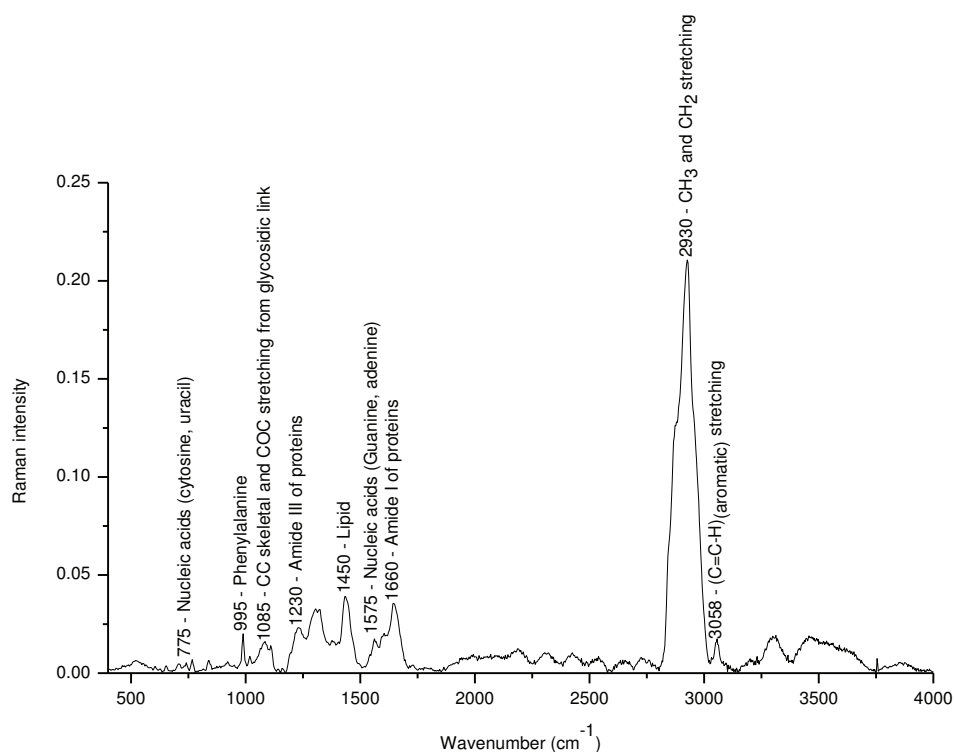


Figure 9: Typical Raman spectrum of *E. coli* in the range of 400 - 4000 cm⁻¹

In general, an IR absorption spectrum of bacteria is divided into five major windows [15,19,36,40,41]:

- ✓ Window 1 (~ 3000 – 2800 cm^{-1}): commonly dominated by C-H stretching of fatty acid compounds and therefore lipid content.
- ✓ Window 2 (~ 1700 – 1500 cm^{-1}): dominated by proteins
- ✓ Window 3 (~ 1450 – 1200 cm^{-1}): is the mixed region dominated by the carboxylic groups of proteins, free amino acids and polysaccharides (1450 – 1400 cm^{-1}), RNA/DNA and phospholipids (1250 – 1200 cm^{-1}).
- ✓ Window 4 (~1200 – 900 cm^{-1}): dominated by polysaccharides
- ✓ Window 5 (< 900 cm^{-1}): is referred to as the fingerprint region containing bands that cannot be assigned to specific functional groups

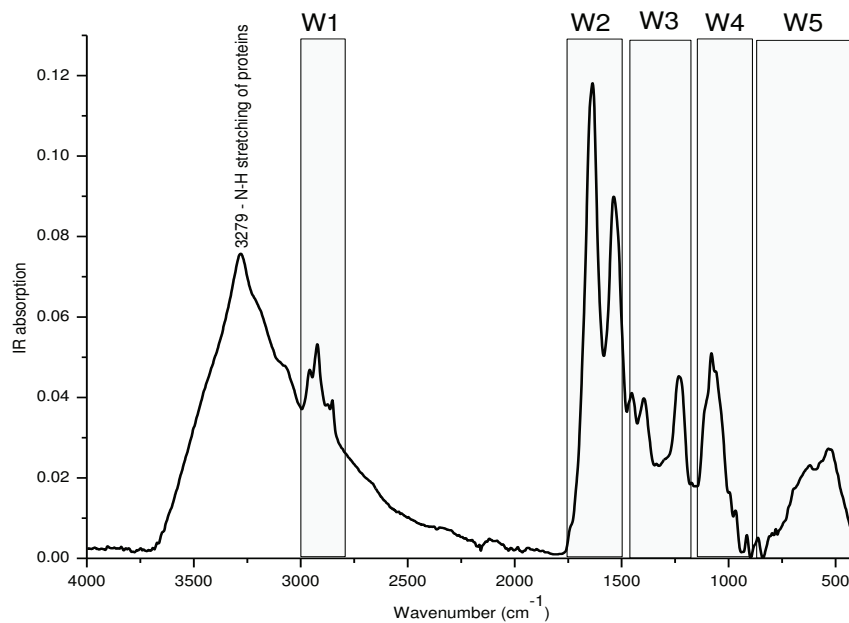


Figure 10: Typical IR spectrum of *E. coli* in the range of 400 - 4000 cm^{-1}

Analysis of structural components of bacteria

Raman and IR spectra of intact bacterial cells cannot provide complete information of specific cellular components due to overlapping spectral bands. Moreover, the spectra of bacteria may also change depending on the culture medium and culture conditions. Raman spectroscopy has gained a wider acceptance as a mature analytical tool for the non-invasive, rapid characterization and identification of micro-organisms. This technique provides several advantages such as a low cost, high speed of analysis, broad information content on the

chemical composition, the structure and the interaction of biomolecules within the microorganisms [42]. Each peak in Raman spectrum corresponds to a well-defined molecular vibration and consequently, a Raman spectrum is highly specific for that particular molecule. Raman spectra at the range of 500-2000 cm^{-1} contain rich biological information on nucleic acids, proteins, polysaccharides, carbohydrates and lipids [20]. A bacterial cell is composed of a multitude of complex biomolecules and therefore its Raman spectrum is very complex. However, based on the known Raman spectra of purified compounds, it is possible to assign peaks of the bacterial spectrum to particular cellular constituents.

Based on the different structure of cell wall, Raman spectroscopy was used to differentiate Gram-positive and Gram-negative plant-associated bacteria and offers the science of plant bacteriology a tool to further understand the mechanisms involved in host-pathogen interactions [43] or to analyze bio-membrane structure [44]. Furthermore, Raman spectroscopy has been used for investigation of the structure of supercoiled DNA in *E. coli* pUC19 [45]. In addition, surface functional group chemistry (hydroxyl, carboxyl, phosphoryl and amide groups) of Gram-positive and Gram-negative bacterial cells was examined using IR spectroscopy [46] or some particular cell components (polypeptide capsules) and formation of endospores can be detected using FT-IR spectroscopy [47]. As pointed out by Naumann *et al.* [48], IR spectroscopy was used as a tool for probing bacterial peptidoglycan. This technique was also employed to study structure and dynamics of membrane proteins [49].

Determination of molecular changes during bacterial growth

In general, bacterial growth curve is composed of four major phases: lag, log (exponential), stationary and death phases. Studying the changes in biochemical composition during bacterial growth could improve the understanding of microbial physiology as well as the behavior of bacterial strains in various batch culture systems. In this context, Raman spectroscopy was applied to *E. coli* and *Bacillus subtilis*. The augmentation of protein mass during the bacterial growth (lag, exponential and stationary phases) was detected. The protein peaks showed an increasing trend during the exponential phase and a decreasing trend in the stationary phase [50]. In addition to these changes, changes in nucleic acid and polysaccharide moieties were recorded between different growth phases of *E. coli* and *Listeria innocua* using FT-IR spectroscopy [51], of *E. coli* and *Staphylococcus epidermidis* using Raman spectroscopy [52]. The similar findings were confirmed by Neugebauer in *Staphylococcus epidermidis* using Raman and IR spectroscopies [17].

Identification and classification of micro-organisms

Vibrational spectroscopic techniques are suitable for the identification of micro-organisms due to the fact that the spectra reveal intrinsic chemical information of the cell. Different micro-organisms will differ in their molecular patterns and this will be reflected in their vibrational spectra. Raman spectroscopy has been used to classify different bacterial species at the colony [19,33,53,54,55,56,57,58] or at the single cell levels [59,60,61,62,63,64]. Raman spectroscopy has also been employed to classify three species of Gram-negative bacteria most commonly responsible for urinary tract infection (*E. coli*, *Klebsiella pneumoniae*, *Proteus* spp.) and to distinguish bacteria treated and not treated with ciprofloxacin after 2h of incubation [65]. Furthermore, IR spectroscopy coupled with chemometric analysis (PCA and classification method) has been used to identify and discriminate both vegetative and sporulated states of *Bacillus* due to peaks from the trihydrate salt of calcium dipicolinate found in the sporulated state spectra [66]. FT-IR spectroscopy has been applied for sub-typing 30 strains of *E. coli* O157:H7 [67], for differentiation of live and dead *E. coli* O157:H7 as well as cells subjected to various inactivation treatments, including heat, salt, UV, antibiotics and alcohol [68]. Maquelin *et al.* have used Raman and FT-IR spectroscopies for rapid identification of bacterial (*Staphylococcus aureus*, *E. coli*, *E. coli faecalis*, *Pseudomonas aeruginosa*) and fungal pathogens (*Candida* species) recovered from blood cultures [69]. However, in some cases the application of vibrational spectroscopy could not give positive results. Another study demonstrated that FT-IR technique was less effective to characterize and differentiate four *Pseudomonas* spp. that widely spread in surface water and soil [70].

Effects of antibiotics against bacteria

Because the difference between sensitive and resistant strains will be reflected in different molecular patterns of the cell, Raman and IR spectroscopies are promising for detection of molecular changes induced by different classes of antibiotics in bacteria, discrimination of sensitive and resistant bacterial strains towards antibiotics and thus allowing the comprehensive understanding of the mechanisms of antimicrobial resistance. Zeroual *et al.* [71] noticed FT-IR spectral changes in protein and nucleic acid bands in *E. coli* cells exposed to different concentrations of penicillin and nalidixic acid. In another research, profiles of *E. coli* phenotypes resulting from treatment with 15 different antibiotics from four classes were characterized using Raman spectroscopy [72]. Similarly, Neugebauer *et al.* [17,73] used IR absorption, micro-Raman and UV-resonance Raman spectroscopies to detect molecular changes

induced by different concentrations of moxifloxacin and ciprofloxacin in *Staphylococcus epidermidis* and *Bacillus pumilus*. Raman spectroscopy combined with laser tweezers was used to detect the cellular response of *E. coli* cells exposed to penicillin G-streptomycin and cefazolin [74]. In addition, ATR-FTIR was successfully used to discriminate isogenic strains of *Pseudomonas aeruginosa* with varying degrees of resistance to imipenem [75] and to identify antibiotic-resistant *Staphylococci* and epidemiological typing of methicillin-resistant *Staphylococcus aureus* [76]. Raman spectroscopy was employed to characterize antimicrobial reactions of tazobactam, sulbactam, clavulanic acid in solution, crystals and bacterial cells [77] and to detect physiology changes in plasmid-bearing *E.coli* with and without ampicillin treatment [78]. Moreover, Bouhedja *et al.* showed that IR spectroscopy has clearly discriminated the transconjugants β -lactams-resistance phenotype from *E. coli* K12 susceptible strain [79]. In this work, the low antibiotic concentration served not to kill the bacteria but rather to stimulate the expression of resistance genes. Additionally, uropathogenic *E. coli* strains were classified in terms of susceptibility or resistance to cephalothin on the basis of their IR spectra combined with artificial neural networks [80]. In another study, FT-IR spectroscopy has been used to investigate the effect of β -lactam antibiotic (oxacillin) in susceptible and resistant *Staphylococcus aureus* strains [81]. Sensitive and resistant strains of *Enterococcus faecalis* and *Enterococcus faecium* to vancomycin can be detected within 3h30 by using Raman spectroscopy [82].

Identification of biofilms

Biofilms are communities of microbial cells, which are embedded in a matrix mainly formed from water and extracellular polymeric substances such as polysaccharides, nucleic acids, lipids and proteins. Biofilms constitute a protected mode of growth that allows survival in hostile environment to most micro-organisms in natural ecosystems [83,84,85,86]. In addition, the biofilm formation provide advantages to bacteria, such as preventing the access of antibiotics to the bacterial cells within the biofilm [87,88], increasing resistance of bacteria to antibiotics [83,89,90]. Consequently, detection methods and characterization of the chemical composition of the biofilm are important. Raman spectroscopy has been used either for the identification of the biofilm formation in *Staphylococcus epidermidis* and in the determination of pathogenic strains [85] or for the differentiation of planktonic cells and biofilms in *Legionella* spp., *Pseudomonas aeruginosa*, *Klebsiella pneumonia* and *E. coli* [91]. In another study, confocal Raman microspectroscopy has been employed for studying the chemical

heterogeneities of biofilms in *Pseudomonas aeruginosa* [92]. In order to detect quickly and to forecast degradation of the microbial quality of drinking water, FT-IR was chosen to assess the responses of *Pseudomonas fluorescens* biofilms to variations in the dissolved organic carbon level [93]. Moreover, SERS was investigated to evaluate the chemical variations in the matrix of biofilm at different growth phases of *E. coli*, *Pseudomonas putida*, *Bacillus subtilis* [84].

I.1.3.2 Applications of Raman and IR spectroscopies in food analysis

Further trends in food analysis will involve combining vibrational spectroscopy with microscopy, mass spectroscopy or DNA-based methods to comprehensively investigate bacterial stresses. In addition, improved chemometric methods along with reduction in the cost of spectroscopic instrumentation may result in the development of reliable and real-time analytical systems. Foods are complex mixtures with the main components being water, proteins, fats and carbohydrates. Vibrational spectroscopy has been successfully applied as rapid analysis methods to evaluate the quality of agricultural products, such as determining the quality of cereals, cereals products and oils [16]. The important analytical Raman and mid-IR bands associated with the major components of foods are summarized in Table 2 and 3.

The detection of bacteria responsible for food contamination is a key step in the food industry. However, the current identification processes are laborious and time-consuming. For example, the detection of *Salmonella* in food samples is composed of several steps, including pre-enrichment, enrichment, selective isolation and biochemical tests. To simplify the procedure of analysis, Raman spectroscopy was employed to detect the presence of pathogenic bacteria in food samples. The results indicated that spectra of *Salmonella enterica* Typhimurium, *E. coli*, *Pseudomonas aeruginosa* were not correctly classified, proposing other methods for Raman sample preparation to discriminate pathogenic bacteria in food [94]. Likewise, FT-IR spectroscopy was used for detection and identification of *E. coli* O157:H7 and *Alicyclobacillus* strains in apple juice [95,96]. Additionally, Raman and FT-IR spectroscopies were also used to predict and monitor the microbial spoilage of meat. The results demonstrated that these two techniques can be applied reliably and accurately for the assessment of meat spoilage through the measurement of biochemical changes occurring in meat substrate [97,98,99]. Raman microspectroscopy in conjunction with chemometric analysis was applied to detect food-borne pathogens, including *E. coli*, *Listeria monocytogenes*, *Salmonella* spp., *Staphylococcus aureus*... from spiked meat and poultry products [10]. Another study was carried out for identification of pathogenic bacteria in drinking water (*Staphylococcus aureus*, *Bacillus*

anthracis, Bacillus cereus, Salmonella Typhimurium, Shigella sonnei, E. coli, Vibrio vulnificus, V. parahaemolyticus...) by IR spectroscopy using cellular fatty acid methyl esters [100]. Besides, Raman is also a promising and easy method for identification of water-borne bacteria. The technique has been used to discriminate *Legionella* strains, *E. coli* and coliform strains [6,101] and to detect and quantify filtered waterborne bacteria [102,103].

Table 2: Raman bands of major food components [16]

Frequency (cm ⁻¹)	Assignment
	<i>Water</i>
3200 - 3600	O-H stretching
	<i>Proteins</i>
510] 525] 545]	S-S stretching
630 – 670] 700 – 745]	C-S stretching
1235 – 1245	Amide III
1600 - 1700	Amide I
2550 - 2580	S-H stretching
2800 - 3000	C-H stretching
	<i>Fats</i>
1441	CH ₂ bending
1457	CH ₃ – CH ₂ bending
1656	C=C stretching
2855 - 2960	C-H stretching
	<i>Carbohydrates</i>
836	C-C stretching
1064	C-O stretching
2912] 2944]	C-H stretching
3451	O-H stretching

Table 3: Mid-IR bands of major food components [16]

Frequency (cm ⁻¹)	Assignment
	<i>Water</i>
3200 - 3600	O-H stretching
1650	H-O-H bending
	<i>Proteins</i>
1600 - 1690	Amide I
1565 – 1520	Amide II
1300 – 1230	Amide III
	<i>Fats</i>
3000 - 2800	C-H stretching
1745 - 1725	C=O stretching
967	C=C-H bending
	<i>Carbohydrates</i>
3000 – 2800	C-H stretching
1400 - 800	Coupled stretching and bending

Bacterial viability determination is one of the major concerns in food industry because some species enter into viable but non-culturable states in response to harmful factors in environment and thus are considered non-viable under traditional culture-based techniques, although they may still be metabolically active and may be able to reproduce during food storage and distribution, causing a significant health threat. In this context, Raman and IR spectroscopies were employed as rapid, non-culturable-based techniques to determine bacterial viability [104]. FT-IR methods have been used to study sonication-injured *Listeria monocytogenes* [105], heat-injured *Salmonella* Typhimurium and *Listeria monocytogenes* [106], chlorine-induced *Pseudomonas aeruginosa* and *E. coli* in water [51], radical-induced damage *Micrococcus luteus* [107], heat, starvation and sodium hypochlorite treatment in *Staphylococcus epidermidis* and *E. coli* [104], heat-killed *E. coli* O157:H7 in ground beef. The major differences between the spectra of live and dead cells were observed in the amide and nucleic acid regions due to heat-induced denaturation of these molecules [37,104].

I.1.3.3 Applications in pharmaceutical analysis

Raman and IR spectroscopies have been extensively applied in both qualitative and quantitative pharmaceutical analysis. These techniques are important for the evaluation of the raw materials used in production, the active ingredients and the excipients. However, spectral analysis of pharmaceuticals using Raman spectroscopy offers some additional benefits over IR

spectroscopy due to the fact that Raman is a scattering technique, there is no need for a reference light path (as needed for IR), thus it is amenable to fiber optics and allows for remote sampling. Moreover, higher lateral spatial and depth resolution is achievable by confocal Raman spectroscopy than by IR microspectroscopy. In pharmaceutical product design, it is important to understand the pharmacokinetic profile (absorption, distribution, metabolism, excretion) of the candidate drugs during early development [108]. Raman spectroscopy has been used in this research area [109,110]. In addition, the scattering method can be applied for microstructural characterization of drug delivery systems, analysis of pharmaceutical formulations [18], evaluation of drug uptake and reactions inside bacterial cell [111] as well as to understand drug – excipient interactions in the formulation [112,113,114]. Raman and IR spectroscopies can be also used for quantification of drug in semisolid formulations and tablets [115], visualization of drug distribution in formulations [116,117], quality control of finished pharmaceutical products [108].

I.1.4 Data processing

Before performance of chemometric analysis, Raman and IR spectra were preprocessed, such as baseline and normalization. Baseline correction allows to achieve flatter baselines and average the baseline to zero. Normalization correction allows to minimize differences due to sample amount [36,118]. The most common techniques are normalization using the highest peak (min-max) and vector normalization. In the first case, all the spectra are modified so that they have the same minimum and maximum values. In vector normalization, the samples are considered to be multidimensional vectors and are modified so that their magnitudes are equal [65].

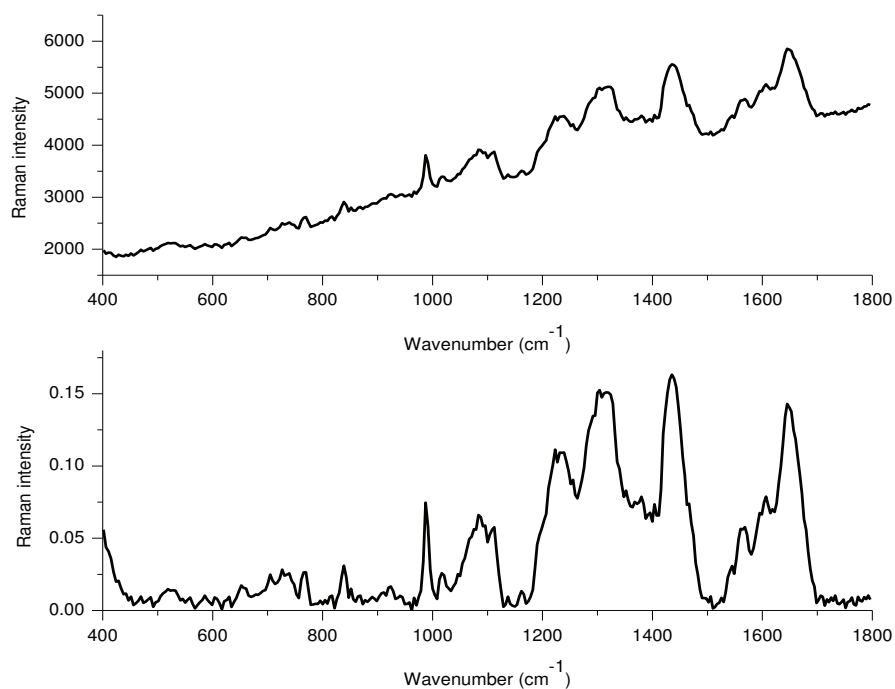


Figure 11: Comparison before(upper spectrum) and after (lower spectrum) baseline, normalization processing of Raman spectrum of *E. coli* recorded 8h of incubation

I.1.5 Chemometric analysis

Although Raman and IR spectroscopies are powerful techniques for analyzing various features, a significant amount of processing is required to extract useful information from raw spectra. Chemometric methods serve this purpose and can be used to analyze the huge spectral distribution, discriminate and classify spectra of different samples that show subtle changes. Chemometrics (also called multivariate statistical methods) are defined as the application of the mathematical and statistical methods to physics, chemistry or biology. The tool helps researchers to understand and manage the enormous amount of data effectively. The most frequently used chemometric methods in research are principal components analysis, discriminant analysis, principal component regression, multiple linear regression, cluster analysis and partial least squares regression [12]. Some software packages can be used for data analysis, such as Matlab, Unscrambler, OPUS...

Principal Components Analysis

Principal Components Analysis uses a linear transformation to represent the original

date into a new coordinate space. PCA reduce the multidimensionality of the data set into its most dominant components while maintaining the relevant variation between the data points. The largest variance will be positioned as the first coordinate (PC1), the second largest variance, orthogonal to the first one, will be the second coordinate (PC2) and so on [65]. Score plots can be used to interpret the similarities and differences of samples [36]. From the loadings of the principal components, the spectral peaks having the highest variance can be identified [17].

Part I.2: Bacterial species

I.2.1 *Escherichia coli*

Since its identification in 1885, *E. coli* has become one of the most comprehensively studied bacterial species. *E. coli* strains are easy to grow and manipulate in the laboratory.

I.2.1.1 Morphology and culture conditions

E. coli is a Gram-negative, rod-shaped, aerobe and facultative anaerobe bacterium that is commonly found in the gut of humans and warm-blooded animals. The optimal temperature for growth is 37°C [119]. Capsules and fimbriae are found in some strains. The major surface antigens of *E. coli* are the cell wall lipopolysaccharides (O antigens) and the capsular polysaccharides (K antigens) [120].

I.2.1.2 Virulence strains

Most strains of *E. coli* are harmless. However, some strains have evolved pathogenic mechanisms to cause disease in humans and animals, such as urinary tract infections (caused by uropathogenic *E. coli*/UPEC), meningitis (caused by neonatal meningitis *E. coli*/NMEC), enteric infections (caused by enteropathogenic *E. coli*/EPEC, enterohamorrhagic *E. coli*/EHEC, enteroinvasive *E. coli*/EIEC, enteroaggregative *E. coli*/EAEC, enterotoxigenic *E. coli*/ETEC and diffusely adherent *E. coli*/DAEC). It is transmitted to humans primarily through consumption of contaminated food, drinking water contaminated with animal or human waste or through direct person-to-person spread from poor hygiene [121].

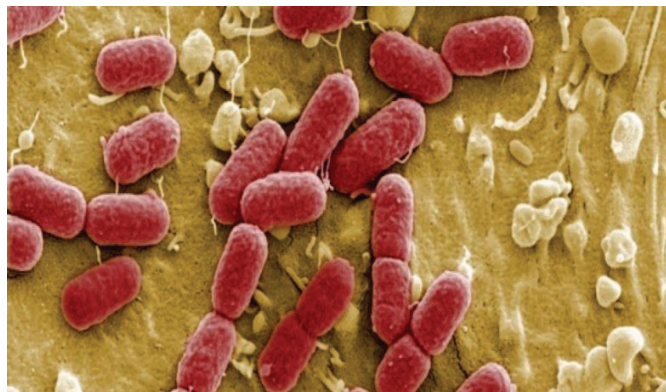


Figure 12: Morphology of *E. coli* cells

(<http://www.slate.fr/story/39015/e-coli-escherichlia-coli-origine>)

I.2.1.3 Resistance to antibiotics in *E. coli*

Antibiotic resistance of *E. coli* is of particular concern because it is the most common Gram-negative pathogen in humans. On the other hand, commensal *E. coli* that are defined as bacteria isolated from healthy animals without known virulence (toxic, adhesive, invasive) are considered as potential reservoirs of resistance determinants. Multidrug resistance to ampicillin, tetracycline, nalidixic acid, ciprofloxacin...have been reported on commensal *E. coli* isolated from animals. Consequently, the prevalence of antimicrobial resistance in commensal *E. coli* should be monitored regularly [122,123]. Out of 96 isolates from commercial and cooked foods in Korea, 17 isolates were resistant to one or more antimicrobial agents tested. High rates of resistance to the following drugs were observed: tetracycline (15.6%), streptomycin (12.5%), ampicillin (10.4%), nalidixic acid (9.4%) and ticarcillin (9.4%) [124]. According to Van *et al.* [125], 84% of 99 isolates from foods commonly sold in the market place in Vietnam were resistant to one or more antibiotics. The rates of multi-resistance were up to 89.5% in chicken, 95% in chicken faeces and 75% in pork isolates. The isolates displayed resistance to tetracycline (77.8%), sulfafurazole (60.6%), ampicillin (50.5%), amoxicillin (50.5%), trimethoprim (51.5%), chloramphenicol (43.4%), streptomycin (39.4%), nalidixic acid (34.3%), gentamicin (24.2%) and fluoroquinolones (ciprofloxacin 16.2%, norfloxacin 17.2% and enrofloxacin 21.2%).

I.2.2 *Vibrio parahaemolyticus*

I.2.2.1 Morphology and culture conditions

V. parahaemolyticus is a Gram-negative, halophilic bacterium, facultatively anaerobic motile curved rods with a single polar flagellum. The bacterium is widespread in the coastal and estuarine environments [126,127,128,129,130]. NaCl concentrations for the optimum growth range from 2 to 4% and poor growth is exhibited in media below 0.5% NaCl. The bacterium is inactivated rapidly in distilled water and growth is inhibited at 10% NaCl. The organism grows at a temperature range between 10 and 44°C, with optimum temperature of 35 - 37°C [131]. The optimum pH range for growth is 7.8 to 8.6, although it can grow in the pH range of 4.8 to 11.

V. parahaemolyticus was first identified as a food-borne pathogen in Japan in the 1950s [132]. Nowadays, *V. parahaemolyticus* is the leading cause of seafood-associated bacterial gastroenteritis in Asia and the United States. The bacterium causes gastroenteritis characterized by watery diarrhea and abdominal cramps. Other symptoms include nausea, vomiting, headache,

fever and chills. The incubation period is usually between 12 and 24 hours and the disease is normally resolved in 3 days [133,134,135,136,137,138] .



Figure 13: Morphology of *V. parahaemolyticus* cells

(<https://www.cdc.gov/media/subtopic/library/diseases.htm>)

V. parahaemolyticus occurs in a variety of fish and shellfish, including clams, shrimp, lobster, crayfish, scallops and crabs as well as oysters [126,132,139]. In temperate regions, *V. parahaemolyticus* is often detected in warmer months and the organism has been reported to survive in the sediment during winter. However, in tropical regions, *V. parahaemolyticus* can be detected throughout the year [140]. While salinity and temperature are important factors influencing the prevalence and levels of *V. parahaemolyticus* in temperate waters [141,142], salinity appears to be the main factor in tropical regions [140].

I.2.2.2 Virulence factors

The pathogenicity of *V. parahaemolyticus* is related to the presence of virulence factors, such as adhesins, thermostable direct hemolysin (TDH), thermostable direct hemolysin related to hemolysin (TRH) genes and two type 3 secretion systems, T3SS1 and T3SS2 [127,129,134,137,143,144,145,146,147]. In Asia, *V. parahaemolyticus* is a common cause of foodborne disease. In general, outbreaks are more prevalent in the summer with a peak in August. From 1996 to 1998 there were 496 outbreaks and 24,373 cases of *V. parahaemolyticus* reported, while 25,211 cases were reported from 1999 to 2005. During 1997 and 1998 there were more than 700 cases of illness due to *V. parahaemolyticus* in the United States. The majority of which were associated with the consumption of raw oysters [132]. More recently, an outbreak of *V. parahaemolyticus* involving 177 cases in 2006 was linked to contaminated oysters harvested in

Washington and British Columbia. *V. parahaemolyticus* infections are rarely reported in European countries. Sporadic outbreaks have been reported in Spain and France [126,129,130].

I.2.2.3 Resistance to antibiotics in *V. parahaemolyticus*

Antibiotic resistant bacteria have emerged due to the excessive use of antimicrobials in human, agriculture and aquaculture [148,149,150,151]. Letchumanan *et al.* [152] have reported a high frequency of antibiotic resistance of *V. parahaemolyticus* isolated from shrimp toward ampicillin, aminoglycosides and the third generation cephalosporins. Han *et al.* [153] investigated the antimicrobial susceptibility of 168 *V. parahaemolyticus* isolates from raw oysters in Louisiana gulf and indicated that various antibiotics (tetracycline, cefotaxime, ceftazidime and fluoroquinolones) remained highly effective, except for ampicillin (MIC \geq 16 $\mu\text{g/ml}$). Recently, virulent *V. parahaemolyticus* strain which showed high antibiotic resistance has caused an emerging disease to shrimp, known as early mortality syndrome (EMS), leading to significant losses up to 100% mortality in intensive ponds in leading Asian countries such as Vietnam, Malaysia, China and Thailand [154].

I.2.3 Biofilm in bacteria

Bacteria exist in two principal forms, as planktonic cells or biofilms [90]. Biofilms were observed as early as 1674 when Antonie van Leuwenhoek used his microscope to describe aggregates of “animalcules” that he scraped from human tooth surfaces. Biofilms are communities of micro-organisms immobilized at a substratum and frequently embedded in a matrix of extracellular polymeric substances (EPSs) produced by the individual cells [155,156,157]. EPSs are responsible for binding micro-organisms to a surface (adhesion) and cell-to-cell (cohesion). The general composition of EPSs consists of polysaccharides, proteins, nucleic acids, lipids and phospholipids [85,86,90,158,159]. According to Tsuneda *et al.* [158], proteins and polysaccharides account for 75% – 89% of the biofilm EPSs composition. There are a lot of bacterial species forming biofilm, from several genera such as *Pseudomonas*, *Vibrio*, *Escherichia*, *Salmonella*, *Listeria*, *Streptococcus*, *Staphylococcus* and *Mycobacteria* [160].

I.2.3.1 Biofilm formation and influence factors

Bacterial adhesion – an accumulated biomass of micro-organisms on a solid surface - is the initial step in colonization and biofilm formation. The properties of a surface may have a significant effect on the rate and extent of attachment of micro-organisms. In general, the rougher and more hydrophobic materials will develop biofilms more rapidly. In addition, the

characteristics of the cell surface are also important. For example, the presence of flagella, pili, fimbriae or glycocalyx may influence the rate of microbial attachment [133,155,161,162,163,164]. The attachment of cell to the surface after this step is considered to be reversible, because micro-organisms can be removed by rinsing. Then micro-organisms produce EPSs to firmly bind cells to a surface and cell-to-cell, allowing change from reversible to irreversible attachment. After the irreversible attachment to surfaces, the cells will begin division, form micro-colonies and intensively produce EPSs, which help strengthen the bond between the bacteria and the substratum and stabilize the colony from environmental stress. The next step is the biofilm maturation. In order to reach structural maturity, periods of 10 days or more are required. Dispersion is the last step in the biofilm formation and it allows the cell to revert into their planktonic form [90,164]. In a mature biofilm, EPSs matrix accounts for 75 – 95% and bacterial cells 5 – 25% [90]. The formation and development of biofilms are affected by many factors, including the specific bacterial strain, material surface properties and environmental parameters such as pH, nutrient levels and temperature [162,164]. Optimum pH for EPSs production depends on the individual species but it is around pH 7 for the most bacteria. The effect of temperature is associated with an increase in nutrient intake, resulting in a rapid formation of biofilm [155]. For instance, strong biofilm formation was observed at 37°C, while 4°C has led to weak biofilm formation of *V. parahaemolyticus* [165] .

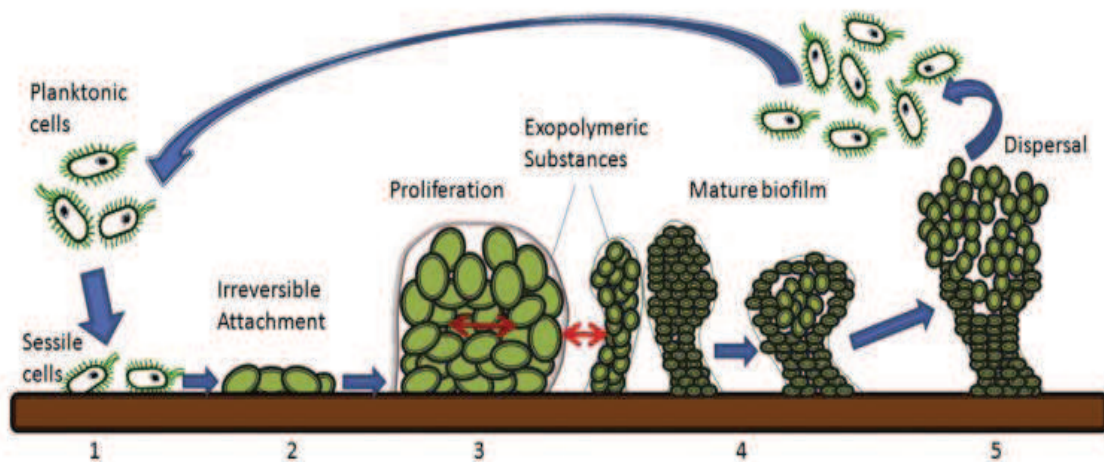


Figure 14: Schematic representation of biofilm-formation steps

(1) initial attachment, (2) irreversible attachment, (3) micro-colony development, (4) biofilm formation and (5) dispersal [166]

I.2.3.2 Role of biofilms for bacteria

Biofilms constitute a protected mode of growth of micro-organisms that allows their survival in unfavorable conditions [167,168]. In fact, the biofilm formation has many advantages for bacteria like protection of biomass from starvation, desiccation, antibiotics, disinfectants and other damaging agents [155,166,167]. Biofilm-associated organisms grow more slowly than planktonic organisms, probably because the cells are limited by nutrient and/or oxygen depletion [161].

In food industries, biofilm formation causes serious problems, such as impeding the flow of heat across a surface, increases in fluid frictional resistance of surfaces, leading to energy and production losses [155]. Sanitizers such as ozone, chlorine and organic acid were reported to be ineffective against microbial biofilm [164].

Inside the host, the matrix protects biofilm-growing bacteria from exposure to immune defenses and antibiotic treatments. Sessile bacteria cells release antigens and stimulate the production of antibodies, but the antibodies are not effective in killing bacteria within biofilms. In addition, biofilms act as barriers to limit the access of antimicrobial agents to the cells embedded in it [87]. Antibiotics are able to penetrate a thick mixture of EPSs to reach their biological targets. However, the antibiotic concentration after diffusion is not high enough for antibacterial activity, which results in an apparent increase in resistance. In this regard, the mutation frequency in biofilm-growing bacteria is significantly higher than in planktonic bacterial cells. Additionally, biofilms increase the opportunity for gene transfer between bacteria and may be significant for the transfer of resistance genes to susceptible bacteria [169]. According to the study conducted by Paraje [90], more than 60% of all microbial infections are caused by biofilms. Desai *et al.* [89] have reported that bacteria grown in biofilms were about 15 times more resistant than equivalent planktonic-grown bacteria. Furthermore, cells in biofilms may also exhibit increased resistance to UV light [170]. As a result, biofilm-growing bacteria easily become multidrug resistant against β -lactam antibiotics, aminoglycosides and fluoroquinolones [88,90,161,167,169,171]. Qi *et al.* [83] have demonstrated that the *Acinetobacter baumannii* isolates within biofilms exhibited 64 – 2048 fold greater resistance for cefotaxime, 32 – 512 fold for imipenem, 16 – 512 fold for ciprofloxacin than those under planktonic growth conditions and the increase of antibiotic resistance has been associated with the quantity of biofilm produced. Jung *et al.* [172] have used Raman spectroscopy to identify spectral differences in *Pseudomonas aeruginosa* biofilms

following treatment with three antibiotic agents (ceftazidime, patulin, epigallocatechin gallate). Outbreaks of pathogens associated with biofilms have been related to the presence of *Listeria monocytogenes*, *Yersinia enterocolitica*, *Campylobacter jejuni*, *Salmonella* spp., *Staphylococcus* spp. and *E. coli* O157:H7 [159]. In conclusion, bacteria within biofilms tend to be more resistant to antimicrobial agents than planktonic cells [169].

Virulence and pathogenicity of micro-organisms are often enhanced when growing as a biofilm and thus methods to control or eradicate biofilm formation are urgently required such as combination of broad spectrum microbial agents with modification of surface properties, using bacteriophage.... [163,169].

Part I.3: Antibiotics

Antibiotics are antimicrobial agents produced by micro-organisms (*Penicillium notatum*, *Cephalosporium* sp.). Natural antibiotics can be artificially modified to enhance their efficacy. Antibiotics are widely used for the treatment of infections caused by bacteria in both animal and human medicine. Antibiotics can be natural, semi-synthetic or synthetic products. Antibacterial agents can be classified as bactericidal (killing bacteria with an efficiency of > 99.9%) or bacteriostatic (inhibiting growth of bacteria but not killing them). In some cases, there can be overlaps between the two categories, for example some antibiotics may start out as bacteriostatic but as the concentration is increased, they could become bactericidal [173,174]. Antibiotics can be also classified by modes of action (Table 4).

Table 4: Classification of antibiotics depending on their mechanisms of action [41]

Mechanism of action	Group	Examples
Inhibitors of bacterial cell wall synthesis	β -lactams	Penicillins, cephalosporins, vancomycin, cycloserine, bacitracin
Inhibitors of bacterial protein synthesis: -Bacteriostatic: Affect function of 30S and 50S ribosomal subunits causing a reversible inhibition of protein synthesis - Bactericidal: Binding to 30S ribosomal subunit, altering protein synthesis, leading to bacterial cell death	Macrolides Tetracyclines Aminoglycosides	Erythromycin, azithromycin Tetracycline, doxycycline Gentamycin, tobramycin, streptomycin
Inhibitors of nucleic acid synthesis: - Directly via inhibition of topoisomerases (quinolones) or	Quinolones	Nalidixic acid, ciprofloxacin

inhibition of polymerases (rifamycins) -Indirectly via inhibition of dihydropteroate synthetase (sulfonamides) or inhibition of dihydrofolate reductase (diaminopyrimidines)	Rifamycins	Rifampin, rifabutin
	Sulfonamides	Sulfamethoxazole
	Diaminopyrimidines	Trimethoprim
Agents affecting membrane function	Polymyxins	Polymyxin B, colistin

I.3.1 Beta-lactam antibiotics: penicillins and cephalosporins

I.3.1.1 History and structure

Since the discovery of penicillin in 1928 by Alexander Fleming, β -lactam antibiotics, which contain a β -lactam nucleus in their molecular structure, are the first choice in treating bacterial infections. The original β -lactams were effective only against Gram-positive bacteria, but after many years of development derivatives have been produced against Gram-negative pathogens (ampicillin, carbenicillin, cefotaxime). The β -lactams account for over one-half of all of the antibiotics produced and used worldwide (52%) including cephalosporins (30%), penicillins (7%) and other β -lactams (15%). Improving upon the effectiveness of this class of antibiotics has been an ongoing challenge because of the emergence of multidrug-resistant strains of bacteria. Over the years, countless penicillin derivatives have been produced and tested, a variety of new β -lactam ring systems have been introduced. These systems are composed of the penams (penicillin, ampicillin), cephalosporins (cephems, cefotaxime), carbapenems, oxapenams as well as monocyclic, spirocyclic and multicyclic ring systems (Figure 15) [175].

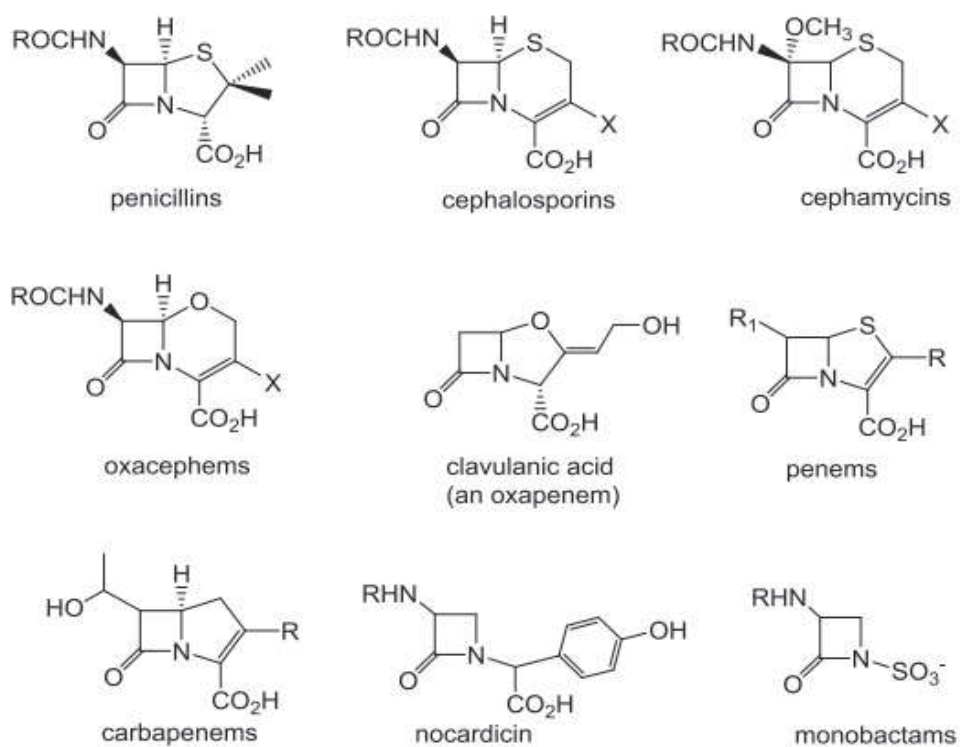


Figure 15: Chemical structures of β-lactam antibiotics [175]

I.3.1.2 Applications of ampicillin and cefotaxime

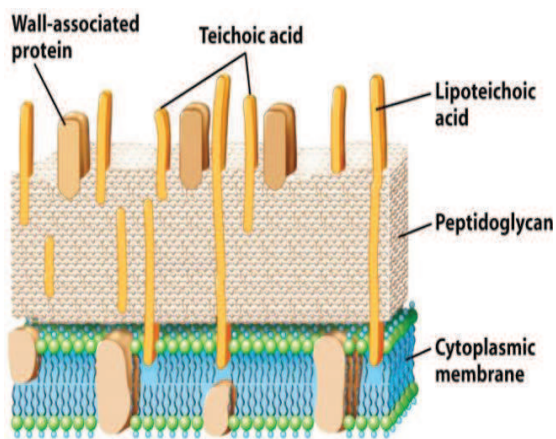
Amp was first described in 1962 and is effective against a wide variety of Gram-positive and Gram-negative organisms. The amino group of Amp allows it to penetrate the outer membrane of Gram-negative bacteria. Amp is commonly used to treat respiratory tract infections, bacterial meningitis, urinary tract infections, gastrointestinal infections caused by Gram-positive and Gram-negative bacteria (*Streptococcus pneumonia*, *Staphylococcus aureus*, *E. coli*, *Listeria monocytogenes*, *Salmonella* spp., *Shigela* spp. ...) [173].

The cephalosporins, produced by the fungus *Cephalosporium* sp., are a clinically important group of β-lactams. Ctx, 3rd generation of cephalosporins, has an aminothiazolyl side chain and possesses an iminomethoxy group on the acyl side chain. Owing to the modification of its chemical structure, Ctx possesses a high affinity for PBPs compared to the first and second generations and is protected from β-lactamase activity. In vitro, this antibiotic shows a potency of antibacterial activity against Gram-negative bacteria and is routinely used for treatment of enteric infections and respiratory tract infections [176]. In addition, Ctx can be used to treat acute urinary

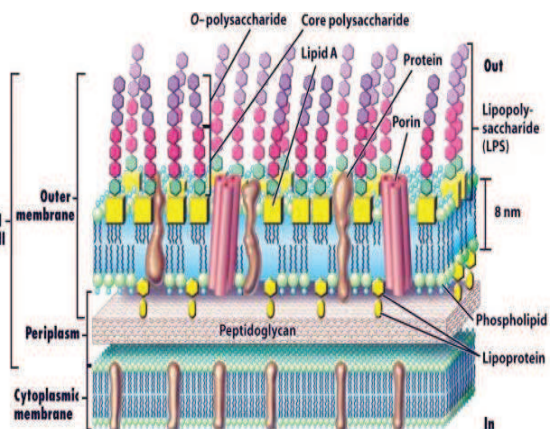
tract infections caused by *E. coli*, *Proteus mirabilis*, *Enterobacter* spp., *Klebsiella* spp. and *Staphylococcus epidermidis* [177].

I.3.1.3 Mechanism of action

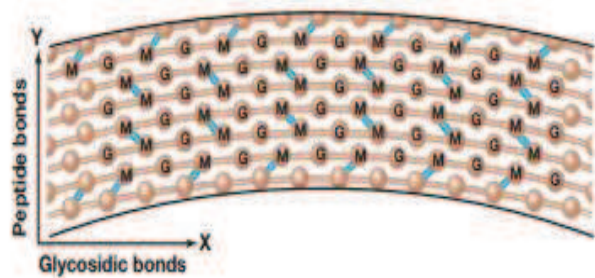
Beta-lactam antibiotics are bactericidal and inhibit the synthesis of the peptidoglycan layer of the bacterial cell wall. Structure of cell wall of Gram-positive and Gram-negative bacteria is shown in Figure 16. In Gram-positive bacteria, the cell wall consists of a thick layer of peptidoglycan (about 90%) and cytoplasmic membrane. In Gram-negative, the cell wall is composed of outer membrane, peptidoglycan (only about 10%), cytoplasmic membrane. In *E. coli*, up to 80% of the peptidoglycan consists of a monolayer with the rest being triple layered [178]. Nonetheless, peptidoglycan layer is extremely important for the preservation of cell shape and rigidity in Gram-negative organisms. Peptidoglycan is a polysaccharide composed of a basic repeating unit of an alternating disaccharide – N-acetyl glucosamine (G) and N-acetyl muramic acid (M). The alternating sugars are connected by glycosidic bonds in the X direction and peptides bonds in the Y direction (Figure 16) [179,180,181,182]. Inhibition of peptidoglycan synthesis in growing cells results in cell lysis. Therefore, peptidoglycan synthesis is an important antibiotic target [182] and there is a continuing interest in the development of new antibacterial drugs that target this pathway. An important step of the peptidoglycan synthesis in bacterial cell wall is transpeptidation, a reaction that results in the cross-linking of two glycan-linked peptide chain [183,184,185,186,187,188,189]. The enzymes involved in this step are transpeptidases that are able to bind to penicillin or other β -lactams. Thus, these transpeptidases are called penicillin-binding proteins (PBPs). There are a large number of PBPs, usually several in each organism and they are found as both membrane-bound and cytoplasmic proteins. This family of enzymes includes the low-molecular-weight PBPs, high-molecular-weight PBPs and peptidoglycan hydrolases (PGH) [190,191]. The interaction of β -lactams in Gram-negative bacteria consists of diffusing through the porin channels in the outer wall, resisting inactivation of β -lactamases and then binding to the PBPs. As a result of that binding, the transpeptidation in the peptidoglycan synthesis is inhibited but the cell wall synthesis continues. Consequently, a newly synthesized bacterial cell wall is no longer cross-linked and cannot maintain its strength. In addition, the antibiotic-PBP complex stimulates the release of autolysins – the enzymes that can digest the existing cell wall [192]. Because the cell wall and its synthesis mechanisms only exist in bacteria, the β -lactam antibiotics are highly selective and are not toxic to host cells.



Gram-positive



Gram-negative



Peptidoglycan

Figure 16: Cell wall structure of Gram-positive, Gram-negative bacteria and chemical bonds in peptidoglycan layer [173]

I.3.1.4 Mechanisms of resistance to β -lactams

Resistance is the term referred to as the insensitivity of a micro-organism to an antimicrobial drug when compared with other isolates of the same species. Micro-organisms have developed a multitude of mechanisms to overcome the effectiveness of antibiotics such as inactivation of antibiotics by enzymes, altered drug target, increased drug efflux, altered membrane permeability and thereby surviving exposure to the antimicrobial agents [193,194,195]. Different mechanisms of resistance to antibiotics are shown in Figure 17.

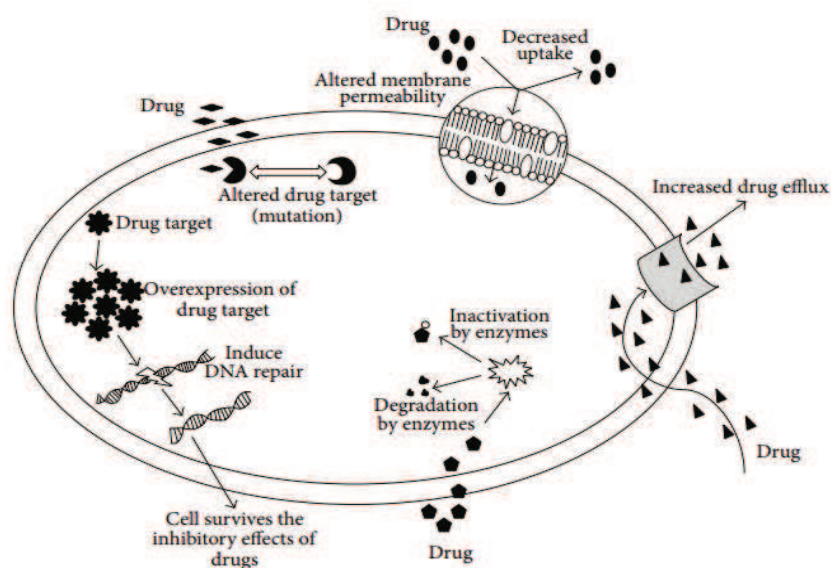


Figure 17: Mechanisms of resistance to antibiotics in bacteria [1]

Resistance to β -lactams is on the rise among clinical isolates of Gram-negative bacteria [196]. To inactivate the bactericidal effects of β -lactam antibiotics, Gram-negative bacteria have evolved multiple strategies such as production of β -lactamase enzymes, production of altered PBPs with reduced affinity to β -lactam antibiotics, prevention of access of β -lactam antibiotics to the target by way of altered permeability or forced efflux pumps (Figure 18). Among these mechanisms, the production of β -lactamases, the enzymes that catalyze the hydrolysis of the β -lactam ring, is the most efficient strategy [180,197]. Beta-lactamases were first identified in *Staphylococcus aureus* strains in the late 1940s and more than 470 β -lactamases are known to date. According to the Ambler classification based on the primary sequence similarity and catalytic mechanism, there are four different classes of β -lactamases: class A, B, C and D. Class A includes narrow-spectrum β -lactamases, extended-spectrum β -lactamases (ESBLs) and serine carbapenemases. Class B enzymes are metallo- β -lactamases. Class C enzymes are cephalosporinases and produced by Gram-negative bacteria. The overuse of third-generation cephalosporins has been associated with the selection and promotion of these β -lactamases. Finally, class D enzymes are oxacillinases [198,199,200]. All Gram-negative bacteria contain β -lactamases in the periplasmic space. Therefore, the rate at which the antibiotics can pass through the porin channels of the outer membrane into the cytoplasmic space is an important factor for its activity against bacteria. For instance, a β -lactam compound that diffuses through the outer membrane into the periplasm and binds to the PBPs in concentrations that can inhibit

peptidoglycan synthesis will lead to the bacterial cell death. Conversely, if the β -lactam drugs pass slowly and are either trapped or inactivated by β -lactamases, the cell will survive [188,201].

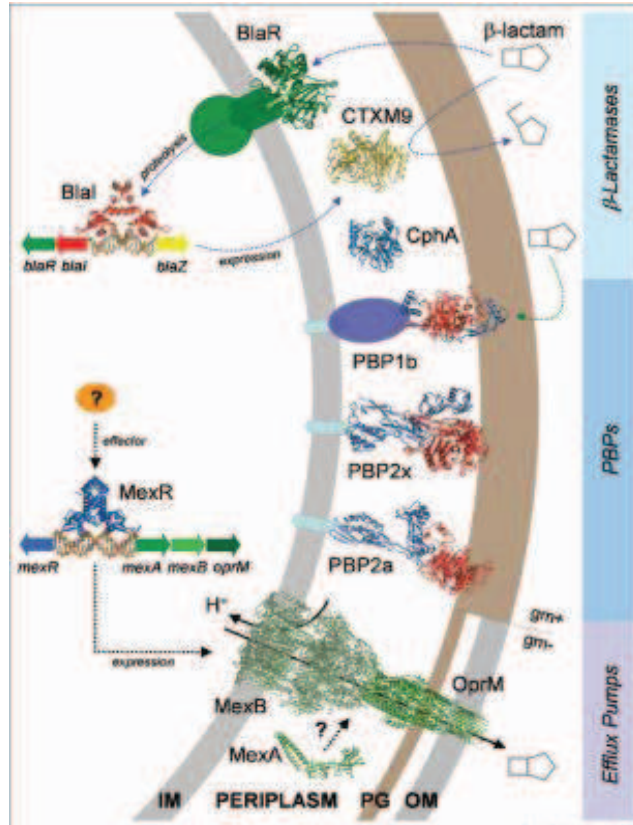


Figure 18: Three primary mechanisms of resistance to β -lactams [202]

I.3.2 Tetracyclines

I.3.2.1 History and structure

Tetracyclines that were discovered in the late 1940s are a family of broad spectrum antibiotics, exhibiting activity against a wide range of Gram-positive and Gram-negative bacteria, atypical organisms such as chlamydiae, mycoplasmas, rickettsiae and protozoan parasites [203]. The original tetracyclines were produced by several species of *Streptomyces* genus, but the newer derivatives are semi-synthetic. The basic structure of the tetracyclines consists of a naphthacene ring system. Substitution in the naphthacene ring leads to formation of new tetracycline analogs (Figure 19) [173].

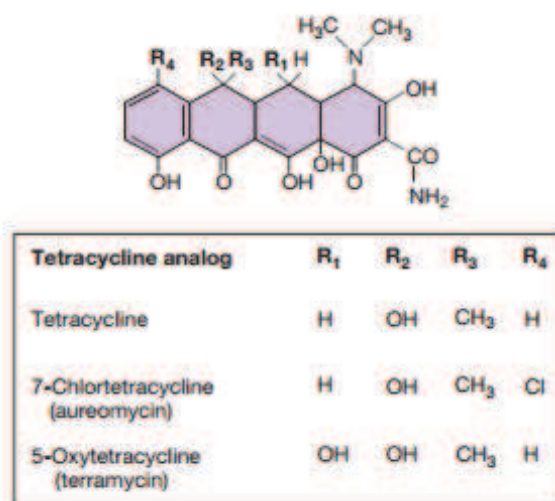


Figure 19: Structure of tetracycline and its semi-synthetic analogs [173]

I.3.2.2 Applications of tetracyclines

These drugs are mainly used to treat respiratory infections, bowel and genital infections in humans. In veterinary medicine, the tetracyclines are used for the treatment of infections in poultry, cattle, sheep, swine and domestic pets. Tetracyclines are used in aquaculture to control infections in salmon, catfish and lobsters farming. In the United States, the drugs are added in animal feed at low concentrations as growth promoters to improve growth and feed efficiency. In addition, tetracyclines have a wide range of non-antibacterial effects including anti-inflammation, immuno-suppression, inhibition of lipase and collagenase, enhancement of gingival fibroblast cell attachment and wound healing [173,204,205].

I.3.2.3 Mechanism of action

Tet inhibits bacterial protein synthesis by binding to the ribosomal complex, preventing the attachment of aminoacyl-tRNA to the A site of the 30S ribosomal subunit. The mode of action of Tet is presented in Figure 20. Association of tetracyclines with the ribosome is reversible, providing an explanation of their bacteriostatic effects. Therefore, to interact with their biological targets these molecules need to pass through one in Gram-positive bacteria or more membrane systems in Gram-negative bacteria under lipophilic form by an electroneutral mechanism. These drugs traverse the outer membrane of Gram-negative bacteria through the OmpF and OmpC porin channels and accumulate in the periplasmic space [173,203,204,206].

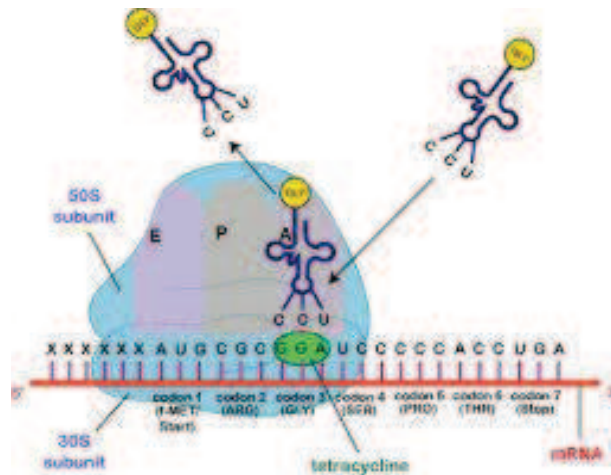


Figure 20: Mechanism of action of tetracyclines

I.3.2.4 Mechanisms of resistance to tetracyclines:

Three different bacterial strategies of resistance to tetracyclines have been identified [205,207]:

1- Protection of the ribosome as the antibiotic target by cytoplasmic proteins (Tet M, O-Q, S, OtrA). The ribosomal protection mechanism was firstly discovered in *Streptococci*.

2- Reduction of the intracellular concentration of Tet in the cytoplasm which can be achieved by two means: lowering the permeability of the cell envelope or pumping Tet out of the cytoplasm (efflux pumps). Efflux genes are found in both Gram-positive and Gram-negative bacteria. Both mechanisms reduce the intracellular drug concentration and thus protect the ribosome in the cell.

3- Production of tetracycline-inactivating enzymes. The tetracycline resistance gene (*tet* (X)) was first identified in *E.coli*. The gene product is a 44-kDa cytoplasmic protein that can chemically modify Tet and thus inactivate it.

I.3.3 Fluoroquinolones: ciprofloxacin

I.3.3.1 History and structure

Since the discovery of nalidixic acid for the treatment of Gram-negative urinary tract infections in 1962, several new groups of quinolones were introduced in order to increase the potency of these antibiotics, targeting broader class of pathogens, better pharmacodynamics and pharmacokinetics. Nowadays they are potent antibiotics against Gram-positive and Gram-

negative bacteria. Fluoroquinolones made up 24% of the antibiotics produced and used worldwide [173]. The common structural element of the fluoroquinolones is the central quinolone unit (Figure 21). The non-fluorinated compounds are grouped into the first generation and the fluorinated compounds are grouped into the latter generations. First generation quinolone antibiotics (nalidixic acid, cinoxacin, piperimdic acid) are typically active against Gram-negative bacteria.

Ciprofloxacin, a second generation of quinolone (fluorinated derivative of nalidixic acid), having a broad-spectrum activity, is more soluble than the parent compound, allowing it to reach therapeutic levels in blood, tissues and to enhance antibacterial activity mainly against Gram-negative pathogens and pneumococci [208].

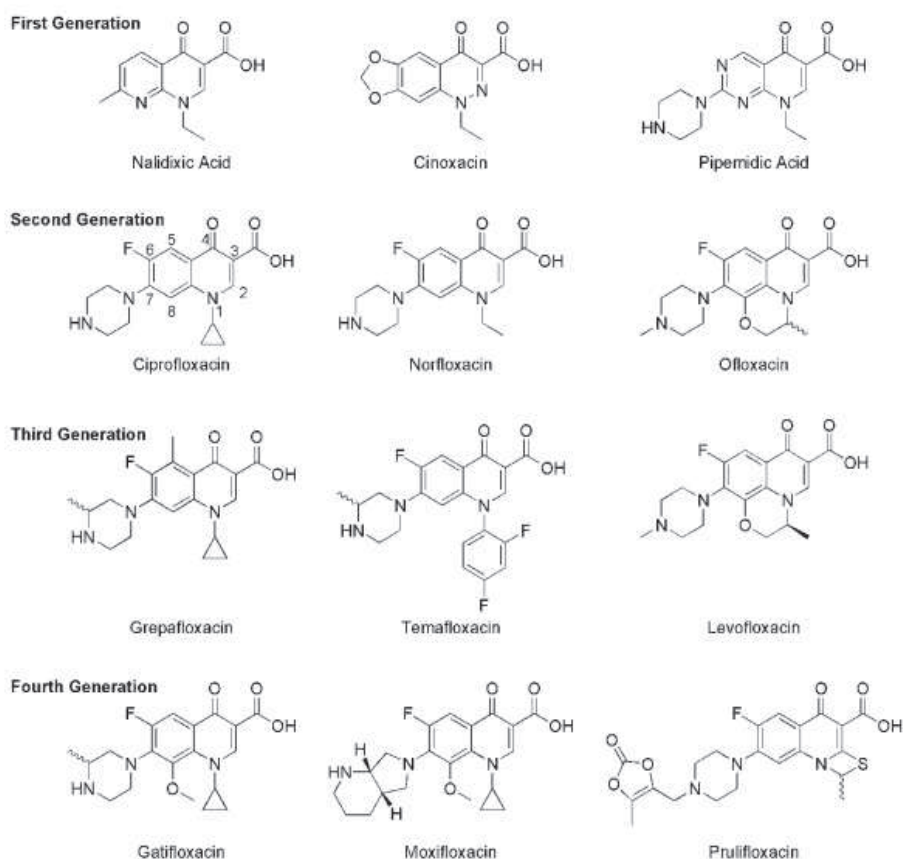


Figure 21: Selected examples representing each of the four fluoroquinolone generations [174]

I.3.3.2 Applications of fluoroquinolones

The first generation quinolone antibiotics (nalidixic acid, cinoxacin, pipemidic acid) have been used for treatment of uncomplicated urinary tract infections. The second generation fluoroquinolones (ciprofloxacin, norfloxacin, ofloxacin) have been prescribed for treatment of urinary tract infections, pyelonephritis, sexually transmitted diseases, prostatitis, localized skin and soft tissue infections. The third generation fluoroquinolones (grepafloxacin, temafloxacin, levofloxacin) are used against respiratory infections. The fourth generation fluoroquinolones are employed to treat similar conditions as third generation drugs but also have activity against the pelvis, abdomen and nosocomial pneumonia. The fluoroquinolones have been widely used in the beef, poultry industries for prevention and treatment of respiratory diseases in animals [174].

I.3.3.3 Mechanisms of action

The general mechanism of action employed by the fluoroquinolone antibiotics is inhibition of type II topoisomerase DNA gyrase or topoisomerase IV. These enzymes are responsible for the relaxing of supercoiled DNA and inducing supercoiling after replication. In Gram-positive bacteria topoisomerase IV is the biological target of fluoroquinolones. In Gram-negative bacteria fluoroquinolones act by inhibiting bacterial DNA gyrase, preventing the supercoiling of DNA, blocking DNA synthesis and ultimately resulting in bacterial cell death (Figure 22) [174,209,210,211,212,213].

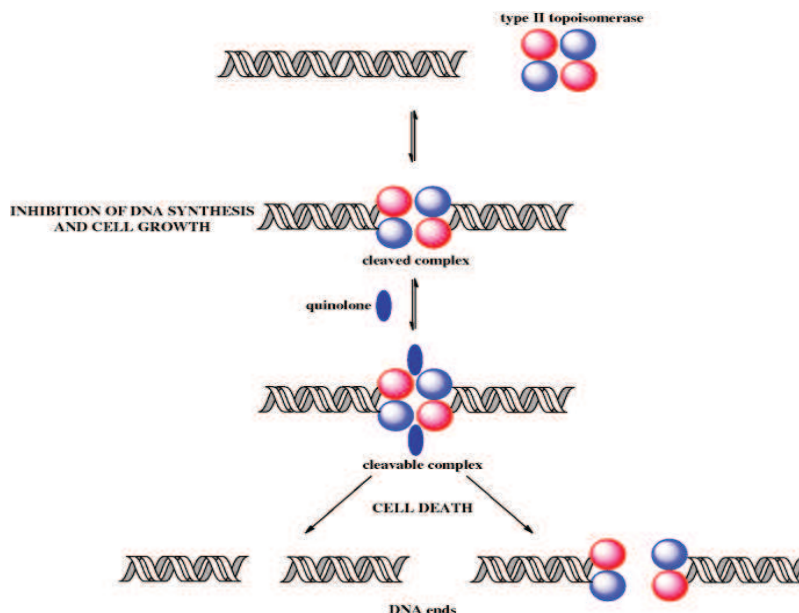


Figure 22: Mechanism of action of quinolones

I.3.3.4 Mechanisms of resistance to fluoroquinolones

Two main mechanisms of resistance to fluoroquinolones have been identified: alterations of the biological target of the drugs (DNA gyrase in Gram-negative bacteria and topoisomerase IV in Gram-positive bacteria) and expression of efflux pumps. Alterations in DNA gyrase occur most commonly in fluoroquinolone-resistant Gram-negative bacteria. The second mechanism of resistance is the expression of efflux pumps that can actively pump antibacterial agents out of the cell at a rate equal to or greater than its uptake [211].

CHAPTER II: MATERIAL AND METHODS

II.1 Spectroscopic instrumentation

II.1.1 Raman spectroscopy

Raman spectra were obtained in the range from 400 cm^{-1} to 1800 cm^{-1} with an excitation wavelength of 638 nm from a HeNe-laser, using a confocal Raman XploRA ONE™ spectrometer (Jobin Yvon, Horiba) with approximately 4 cm^{-1} resolution. The laser light was focussed on the sample by means of a $100\times$ microscope objective. The nominal power of the laser was 5 mW which allows avoiding damage to the bacterial cells. Each day before starting the experiments the system was calibrated and monitored by using a silicon sample wafer having a spectral band at 520.2 cm^{-1} . The accumulation time for each acquisition was 40 seconds and 3 accumulations were collected for a single measurement.

II.1.2 IR absorption spectroscopy

IR absorption spectra were recorded in the range $400 - 4000\text{ cm}^{-1}$ using Bruker Vertex 70v spectrometer with 4 cm^{-1} resolution. The accumulation time for each acquisition was about 9 seconds and 20 accumulations were collected for a single measurement. The IR absorption spectra were measured in ATR mode (Attenuated Total Reflectance). From a general description the ATR accessory consists of a highly refractive element (in our case diamond crystal) which contacts the sample and allows the IR beam to reflect, leaving the evanescent wave to penetrate into the sample [38]. The ATR accessory was purchased from Bruker company (Platinum ATR diamond F. vacuum – type A225/Q). This tool works in single reflection mode and samples are fixed using one-finger clamp mechanism. The bacterial cells were filtered by the anodisc membrane. Afterward, this filter was placed between IR source and in contact with diamond crystal.

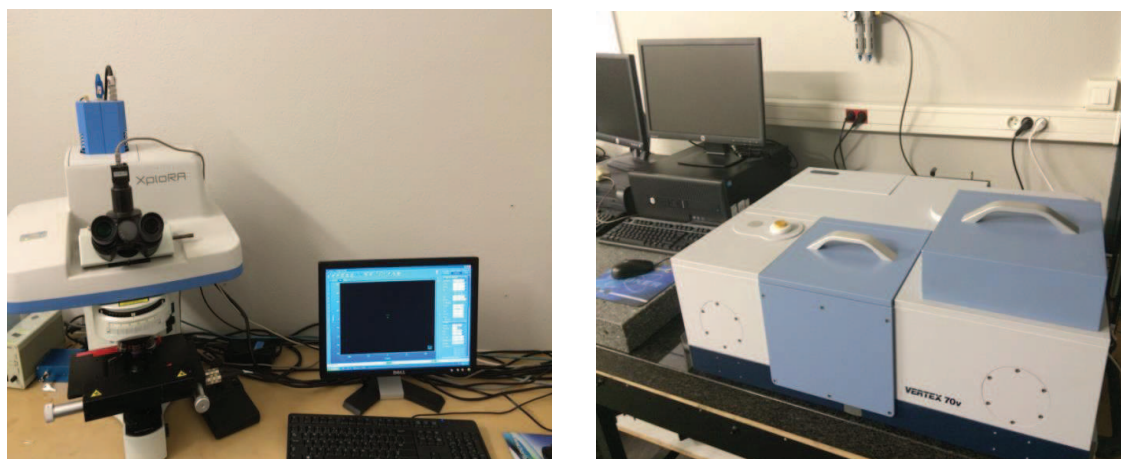


Figure 23: Confocal Raman (Horiba) and IR (Bruker) spectrometers used in the study

II.2 Growth conditions of bacteria

II.2.1 Bacterial strains

In this study the following bacterial strains have been investigated by confocal Raman and IR absorption spectroscopies:

Escherichia coli TOP10 (provided by CBAC research group GEPEA –
University of Nantes - La Roche/Yon, France)

Vibrio parahaemolyticus CIP 73.30 (purchased at Institute of Pasteur Paris, France)

II.2.2 Growth conditions of *E. coli*

E. coli was grown overnight on NA plate at 37°C. Isolated colonies were transferred to 5 ml of sterile saline water in order to obtain a bacterial suspension with an OD₆₀₀ close to 0.1 (~10⁸ CFU/ml). This suspension was then transferred into MHB (1% in volume) and incubated at 37°C with orbital shaking at 200 rpm. This protocol was used to prepare *E. coli* initial culture for all experiments performed below. MHB, which consists of basic nutrients and no additives that could significantly influence the spectral pattern, is proven to be the best medium for Raman spectroscopy and bacterial culture with antibiotics [214,215]. Consequently, this medium has been used in several studies. The different growth phases (lag, exponential and stationary phases) of *E. coli* were determined by measuring the OD₆₀₀ value.

II.2.3 Growth conditions of *V. parahaemolyticus*

V. parahaemolyticus was grown overnight on Zobell agar at 38°C. Isolated colonies were transferred to 5 ml of sterile saline water in order to obtain a bacterial suspension with an OD₆₀₀ close to 0.2 (~ 10⁸ CFU/ml). This suspension was transferred into MHB (1% in volume) and incubated at 38°C without shaking. This protocol was used to prepare *V. parahaemolyticus* initial culture for all experiments performed below. The different growth phases (lag, exponential and stationary phases) of *V. parahaemolyticus* were determined by measuring the OD₆₀₀ value.

II.3 Antibacterial activities of antibiotics against bacteria

II.3.1 Antibacterial activities of antibiotics against *E. coli*

The MIC and MBC values of Amp, Ctx, Tet and Cip against *E. coli* were determined by tube dilution technique. The MIC is defined as the lowest concentration of an antibiotic that inhibits the visible growth of a micro-organism after overnight incubation and the MBC as the lowest concentration that will prevent the growth of a micro-organism after subculture onto antibiotic-free agar. In order to determine MIC and MBC values, *E. coli* culture was prepared as mentioned in II.2.2. When the OD₆₀₀ value reached a range between 1.5 and 2.0 (~ 10⁷ - 10⁸ CFU/ml), the bacterial culture was transferred into MHB (1% in volume) in order to obtain a bacterial suspension containing 10⁵ – 10⁶ CFU/ml. All tested antibiotics (Amp, Ctx, Tet and Cip) were purchased as dehydrated powder from Sigma Aldrich (France). The antibiotic was dissolved and diluted in series in sterile water in order to obtain the required concentrations and were stocked at 4°C until use. Then 0.2 ml of each antibiotic solution were mixed with 1.8 ml of the bacterial culture being in the exponential phase and yielding approximately 10⁵ – 10⁶ CFU/ml and then incubated at 37°C for 24 h. The positive (0.2 ml of sterile water and 1.8 ml of the bacterial culture) and negative (0.2 ml of sterile water and 1.8 ml of sterile MHB) controls were prepared in similar conditions. Each tube was checked for visible growth (turbidity). The MIC was noted as the lowest concentration that completely inhibited the bacterial growth. All concentrations not showing visible growth were subcultured onto NA plates (0.1 ml per plate), incubated at 37°C for 24 h. The MBC was determined as the lowest concentration of antibiotic at which no cell growth occurred on the agar plates.

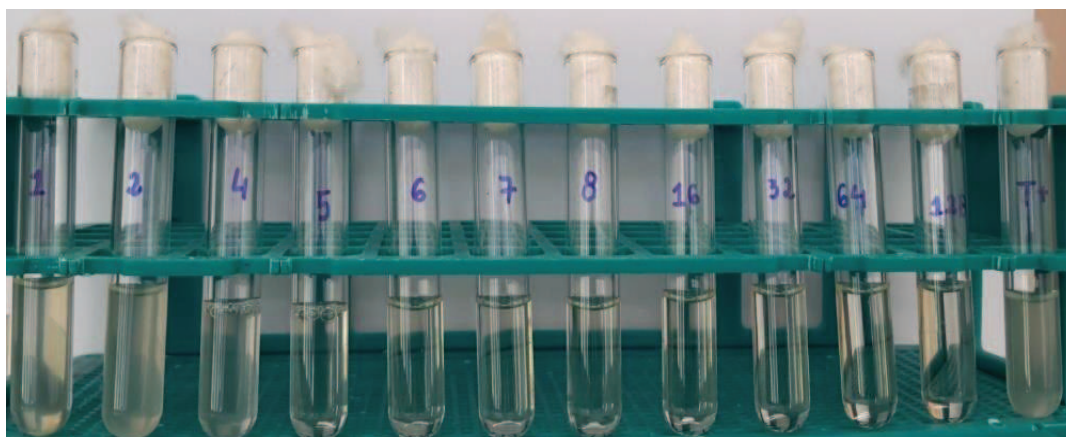


Figure 24: Determination of MIC value of Amp against *E. coli*

II.3.2 Antibacterial activities of antibiotics against *V. parahaemolyticus*

Because *V. parahaemolyticus* is resistant to Amp and can grow at concentration up to 50 µg/ml. A different experiment was designed for this antibiotic to test whether Raman and IR spectroscopies can be applied to differentiate Amp-resistant *V. parahaemolyticus* without (Control) and in the presence of Amp. The MIC and MBC values of Ctx, Tet and Cip against *V. parahaemolyticus* were determined according to the procedure described for *E. coli* with a few differences in culture medium and culture conditions. *V. parahaemolyticus* culture was prepared as previously described in II.2.3. When the OD₆₀₀ value reached a range between 1.0 and 1.2 (~ 10⁷ – 10⁸ CFU/ml), the bacterial culture was transferred into MHB (1% in volume) in order to obtain 10⁵ – 10⁶ CFU/ml. The positive and negative controls were prepared as described for *E. coli*. All concentrations not showing visible growth were subcultured onto Zobell plates (0.1 ml per plate), incubated at 38°C for 24 h to determine MBC value.

II.4 Raman and IR spectroscopy investigations

II.4.1 Bacterial growth monitoring

In order to explore metabolic changes occurring during bacterial growth of *E. coli*, the bacterial culture was prepared as described above. Raman and IR spectra were recorded at various growth time points, mainly during the exponential phase (3, 6, 8 h of incubation) and stationary phase (24 h of incubation). During the lag phase the bacterial cells prepare their metabolism for the upcoming growth phase and no net-increase of the biomass is observed. Therefore, no spectra were recorded in this phase since the bacterial concentration was too low to harvest a sufficient amount of cells. The bacterial cells were harvested after centrifugation at

8,000 rpm for 5 min at room temperature. In order to completely remove components of the culture medium, the cells were washed three times with sterile deionized water. The precipitate was then suspended in sterile deionized water for Raman and IR analysis. Deionized water is a suitable option for Raman analysis because it evaporates, leaving clean bacterial cells on the glass slide without residue [52].

For Raman spectroscopy, the precipitate was suspended in 100 μ l of sterile deionized water and dropped onto a glass microscope slide (10 droplets/sample) and then air-dried for 5 – 10 min at room temperature ($\sim 20^{\circ}\text{C}$) with air humidity of 70% to form a homogeneous film. The experiments were performed in triplicate and twenty to twenty-five measurements were recorded for each sample.

For IR spectroscopy, 3 ml of sterile deionized water were added to the precipitate. The bacterial suspension was then filtered through an aluminum oxide membrane filter (0.2 μm pore size, 25 mm diameter, Anodisc, Whatman) using a Whatman vacuum glass membrane filter holder to collect bacterial cells. The anodisc membrane filter does not contribute to spectral features between the wavenumber of 400 to 4000 cm^{-1} and provides a smooth, flat surface onto which the bacterial film can form. The experiments were performed in triplicate and fifty measurements were obtained for each sample.

In case of *V. parahaemolyticus*, the culture was prepared as described in II.2.3. Raman and IR spectra were recorded at various growth time points (8, 10 and 24 h of incubation). In order to collect Raman spectra of *V. parahaemolyticus*, CaF_2 slide was used like a substrate. In fact, CaF_2 was found to be an ideal substrate for the Raman spectroscopy because it gives no background signal, has a single Raman band at 322 cm^{-1} and therefore does not interfere with the bacterial Raman bands [216].

II.4.2 Effects of antibiotics against bacteria

II.4.2.1 Effects of antibiotics against *E. coli*

The experiments were performed by adding the different classes of antibiotics to the culture during the exponential phase. Indeed, the largest effects on the growth of the bacterial culture were observed during this phase, as the cells were found to be the most susceptible to changes in their environment.

In order to detect molecular changes induced by antibiotics, *E. coli* culture was prepared as described in II.2.2. Amp, Ctx and Tet were added to the culture at an OD₆₀₀ value comprised between 1.5 and 2.0 (5h30 – 6h of incubation) (~ 10⁷ – 10⁸ CFU/ml) achieving a final concentration of 40 µg/ml, 1.6 µg/ml and 40 µg/ml, respectively (8MIC). In case of Cip, this antibiotic was added at the final concentration of 0.8 µg/ml (8MIC) when the OD₆₀₀ value of the bacterial culture ranged from 0.5 to 0.8 (4h – 4h30 of incubation) (~ 10⁶ CFU/ml). At the end of each treatment, samples were prepared as described above for Raman and IR spectroscopy. The control (antibiotic-free culture) was prepared in similar conditions for comparison. The experiments were performed in triplicate. The experimental protocol is presented in Figure 25. The cell inactivation after antibiotic treatments was calculated as the formula below using the standard plate counts (CFU/ml) at the end of the exposure time for the control and the treated samples (2 h after Amp, Ctx, Tet additions and 1h30 after Cip addition), expressed as percentage (%) of bacterial count reduction as the formula below and performed in triplicate.

$$(1 - N_T/N_C) \times 100$$

where N_T is the bacterial count for treated sample (CFU/ml)

N_C is the bacterial count of the control (CFU/ml)

II.4.2.2 Effects of antibiotics against *V. parahaemolyticus*

Regarding the experiment designed for Amp, firstly *V. parahaemolyticus* culture was prepared as described in II.2.3. When the OD₆₀₀ value ranged from 1.0 – 1.2 (after 6h – 6h30 of incubation) (~ 10⁷ – 10⁸ CFU/ml), the bacterial suspension was transferred into MHB (1% in volume) (~ 10⁵ – 10⁶ CFU/ml). Amp was added at 20 µg/ml and incubated at 38°C for 15 h – 18 h without shaking. Although the bacterial strain can grow in the presence of Amp up to 50 µg/ml, the bacterial concentration was too low to harvest a sufficient amount of cells for Raman and IR spectroscopies. The concentration of 20 µg/ml was chosen because it was high enough for bacterial growth and collection of cells after 15 h – 18 h of incubation. The control contained the bacterial culture with no antibiotic was prepared under the similar conditions. The experiment was performed in duplicate. The experimental protocol is shown in Figure 25.

In order to explore the effects of antibiotics against *V. parahaemolyticus*, firstly the bacterial culture was prepared as previously described. Then, Ctx and Tet were added to the culture at an OD₆₀₀ value comprised between 1.0 and 1.2 (6h – 6h30 of incubation) (~ 10⁷ – 10⁸

CFU/ml) at the final concentration of 0.72 $\mu\text{g/ml}$ (12MIC), 0.8 $\mu\text{g/ml}$ (8MIC) respectively. In case of Cip, this antibiotic was added at the final concentration of 0.9 $\mu\text{g/ml}$ (18MIC) when the OD_{600} value of the bacterial culture ranged from 0.6 to 0.8 (5h30 – 6h of incubation) ($\sim 10^6$ CFU/ml). At the end of each treatment, samples were prepared as described above for Raman and IR spectroscopy. The control (antibiotic-free culture) was prepared in similar conditions. The experiment was performed in triplicate. The detailed protocol is shown in Figure 26. The cell inactivation after antibiotics treatments was calculated using the standard plate count (CFU/ml) at the end of the exposure time for the control and treated samples (2 h after antibiotic addition), expressed as percentage (%) of bacterial count reduction as the formula previously mentioned above and performed in triplicate.

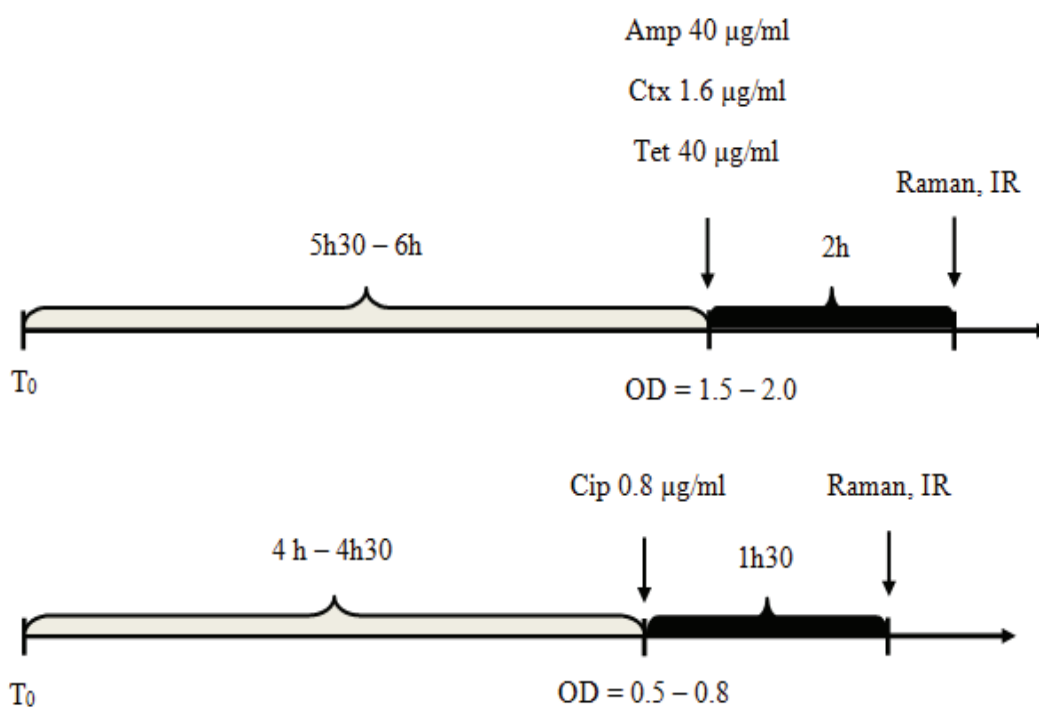


Figure 25: Experimental protocol for detection of molecular changes induced by different classes of antibiotics (Amp, Ctx, Tet and Cip) against *E. coli*

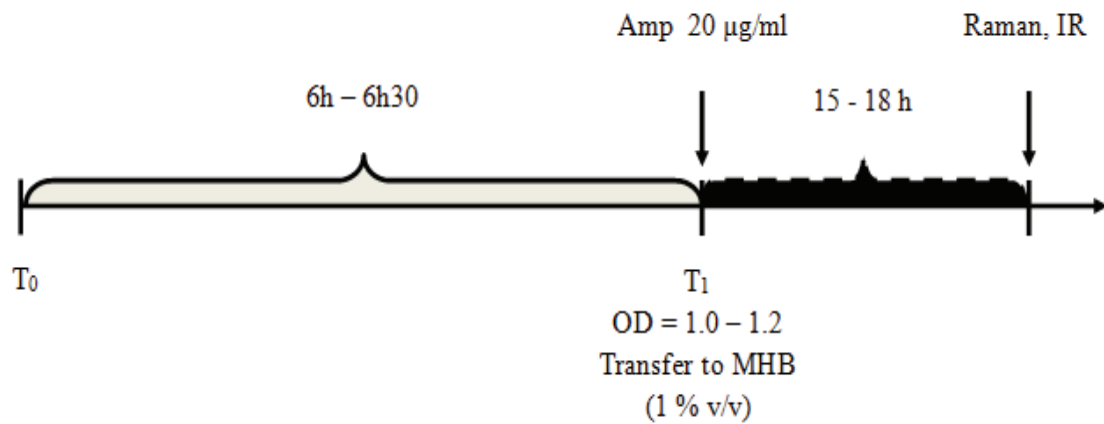


Figure 26: Experimental protocol for differentiation Amp-resistant *V. parahaemolyticus* culture (Control) and culture with Amp at 20 µg/ml

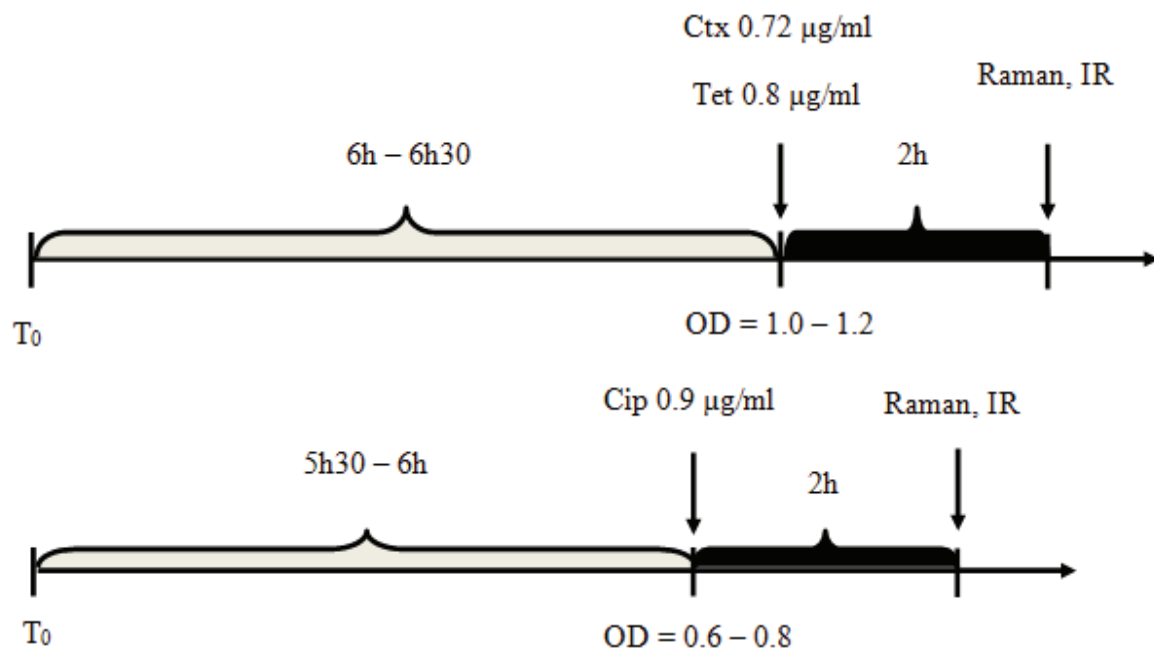


Figure 27: Experimental protocol for detection of molecular changes induced by different classes of antibiotics (Ctx, Tet and Cip) against *V. parahaemolyticus*

II.5 Data analysis

Spectral processing included baseline removal and normalization using Labspec 6 for Raman spectra and Opus for IR spectra. For Raman spectra, the polynomial baseline correction and the vector normalization were applied. For IR spectra, the elastic baseline correction and the vector normalization were performed. Raman and IR spectral graphs were done by Origin 8.5.1 software. Statistic calculations using PCA method were managed with the help of The Unscrambler 10.2 software (CAMO). The mean-centered data were analyzed by calculating the PCs, creating score plots for the first and second PCs. With PCA, it is possible to identify patterns in the dataset and to highlight similarities and differences according to similarities and differences in the samples and group together the variables that are highly correlated. Through linear transformation of the data to a new coordinate system, the largest variance will be positioned as the first coordinate (PC1), the second largest variance, orthogonal to the first one, will be the second coordinate (PC2) and so on. Each principal component has a weight score, which is the intensity of each principal component to recover the original data. From the loadings of the principal component analysis the wavenumbers having the highest variance can be identified. The spectral region of interest from 400 to 1800 cm^{-1} for Raman and 900 to 2000 cm^{-1} for IR were analyzed by PCA.

CHAPTER III: RESULTS AND DISCUSSION

Part III.1 Vibrational spectroscopic study of bacterial growth

III.1.1 Growth curve of bacteria

The growth curve of bacteria is mainly composed of four major phases [173,217]:

- ✓ Lag phase: during this phase, there is no increase in cell number. Bacterial cells increase in size to prepare for reproduction, synthesis of DNA and various inducible enzymes required for cell division.
- ✓ Log phase (exponential phase): in this phase, the bacteria become extremely active and begin the process of dividing. This phase starts with a rapid increase in bacterial biomass as a function of time. The bacterial cells in the exponential phase are the most susceptible to changes in their environment.
- ✓ Stationary phase: the stationary phase occurs at the end of cell division. After that the density of bacteria population has become too high and the biological mass does not increase anymore. Thus, the growth rate is exactly equal to the death rate. A bacterial population may enter the stationary phase when the essential nutrients required for bacterial growth are exhausted and metabolic inhibitory byproducts accumulate. The cells start to die and the lysis of the biomass occurs.
- ✓ Death phase: the number of viable bacterial cells begins to decline. No further divisions occur in this phase. The bacterial cells are broken down due to the additional accumulation of inhibitory byproducts, depletion of cellular energy and pH changes.

III.1.2 *Escherichia coli*

III.1.2.1 Raman spectrum of *E. coli*

Raman and IR spectra provide the overall vibrational and chemical information of the bacteria. Due to the different selection rules, Raman and IR spectra often give complementary information. Raman and IR absorption spectra of *E. coli* are presented in Figure 28. The important spectral bands related to the major constituents of biological samples are summarized in Table 5.

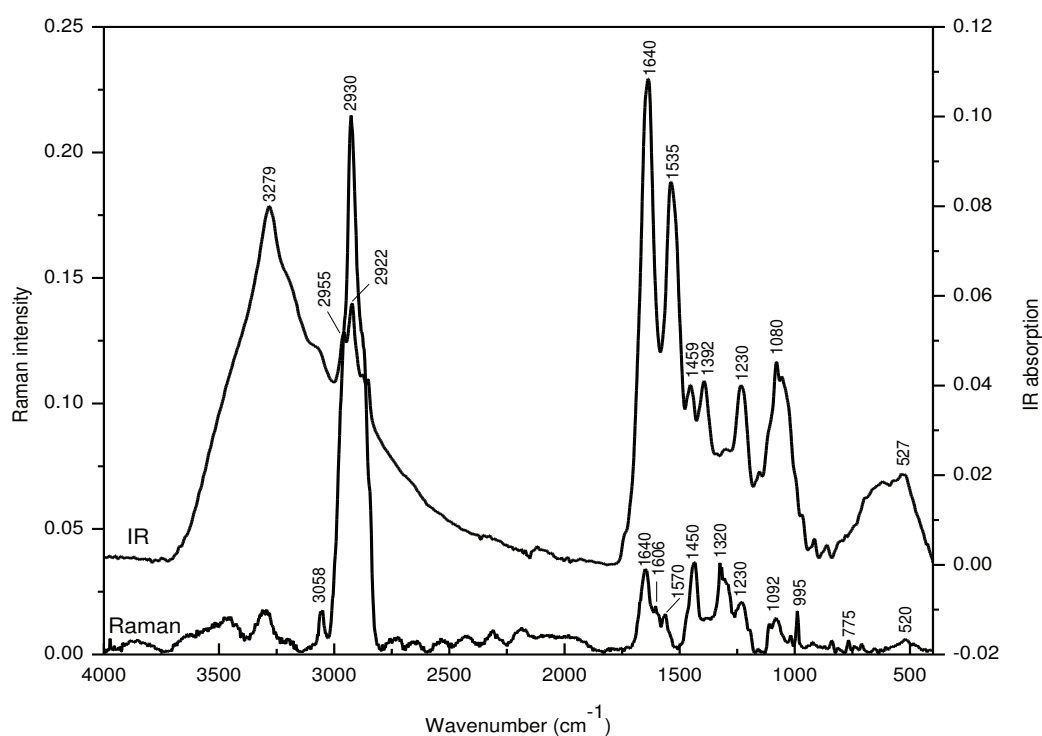


Figure 28: Raman and IR absorption spectra of *E. coli* recorded 8h of incubation

The most prominent feature in the Raman spectrum (lower spectrum in Figure 28) is the strong band around 2930 cm^{-1} which is a superposition from the symmetric and antisymmetric C-H stretching vibrations of the CH_2 and CH_3 groups from lipids, proteins and carbohydrates [17,32,218]. Another prominent band is around 1450 cm^{-1} which is attributed to the deformation of the C-H bond. The amide bands can be found around 1660 cm^{-1} (the amide I) and 1230 cm^{-1} (the amide III). The amino acid contribution can be observed at 995 cm^{-1} assigned to the aromatic ring of phenylalanine. The bands around 775 cm^{-1} , 1570 cm^{-1} are assigned to the nucleic acids, especially to contributions from cytosine and uracil, guanine and adenine, respectively [17,32,219].

Table 5: Assignment of some bands frequently found in FT-IR and Raman spectra in biological samples [32]

FT-IR		Raman	
Frequency (cm ⁻¹)	Assignment	Frequency (cm ⁻¹)	Assignment
3500	O-H str of hydroxyl groups	3059	(C=C-H) _(aromatic) str
3200	N-H str (amide A) of proteins	2975	CH ₃ str
2955	C-H str (asym) of -CH ₃ in fatty acids	2935	CH ₃ and CH ₂ str
2930	C-H str (asym) of >CH ₂	2870-2890	CH ₂ str
2918	C-H str (asym) of >CH ₂ in fatty acids	1735	>C=O ester str
2898	C-H str of C-H in methane groups	1650-1680	amide I
2870	C-H str (sym) of -CH ₃	1614	tyrosine
2850	C-H str (sym) of >CH ₂ in fatty acids	1606	phenylalanine
1740	>C=O str of esters	1575	guanine, adenine (ring stretching)
1715	>C=O str of carbonic acid	1440-1460	C-H ₂ def
1680-1715	>C=O in nucleic acids	1295	CH ₂ def
1695, 1685, 1675	amide I band components resulting from antiparallel pleated sheets and β-turns of proteins	1230-1295	amide III
1655	amide I of α-helical structures	1129	C-N and C-C str
1637	amide I of β-pleated sheet structures	1102	>PO ₂ ⁻ str (sym)
1550-1520	amide II	1098	CC skeletal and COC str from glycosidic link
1515	“tyrosine” band	1085	C-O str
1468	C-H def of >CH ₂	1061	C-N and C-C str
1400	C=O str (sym) of COO ⁻	1004	Phenylalanine
1310-1240	amide III band components of proteins	897	COC str
1250-1220	P=O str (asym) of >PO ₂ ⁻ phosphodiester	858	CC str, COC 1,4 glycosidic link
1200-900	C-O, C-C str, C-O-H, C-O-C def of carbohydrates	852	“buried” tyrosine
1090-1085	P=O str (sym) of >PO ₂ ⁻	829	“exposed” tyrosine
720	C-H rocking of >CH ₂	785	cytosine, uracil (ring, str)
900-600	“fingerprint region”	720	adenine
		665	guanine
		640	tyrosine (skeletal)
		620	phenylalanine (skeletal)
		540	COC glycosidic ring def
		520-540	S-S str

str: stretching, def: deformation, sym: symmetric, asym: antisymmetric

III.1.2.2 IR absorption spectrum of *E.coli*

Due to the different selection rules the vibrational pattern of the IR absorption spectrum is quite different from the one of the Raman spectrum as can be seen in Figure 28. In the IR absorption spectrum of *E.coli* (upper spectrum in Figure 28), a strong band resulting from N-H stretching vibrations is noticed around 3279 cm^{-1} . Two spectral peaks around 2955 cm^{-1} and 2922 cm^{-1} are due to the asymmetric C-H stretching vibration of methyl- and methylene groups. In almost bacterial samples the most prominent features in the IR absorption spectrum are the amide I band at 1640 cm^{-1} , the amide II band at 1535 cm^{-1} . Another protein contribution with less intensity is the amide III at 1230 cm^{-1} [38]. The weak band at 1459 cm^{-1} results from the CH_2 deformation vibration. The band at 1080 cm^{-1} can be assigned to the symmetric PO stretching vibration of PO_2^- as it is found in nucleic acids. The spectral region below 900 cm^{-1} contains very poor resolved features, therefore an assignment is difficult to achieve.

III.1.2.3 Characterization of *E. coli* growth curve

In order to assess metabolic changes occurring during the bacterial growth, Raman and IR absorption spectra were recorded at different growth time points, mainly during the exponential and stationary phases. Figure 29 presents the growth curve of *E. coli* in MHB at 37°C , shaking at 200 rpm. During the lag phase (0 – 2 h of incubation) no spectra were measured since the bacterial concentration was too low to harvest a sufficient amount of cells. During the exponential phase (3, 6 and 8 h of incubation) and the stationary phase (24 h of incubation), bacterial cells were harvested for Raman and IR absorption spectroscopies.

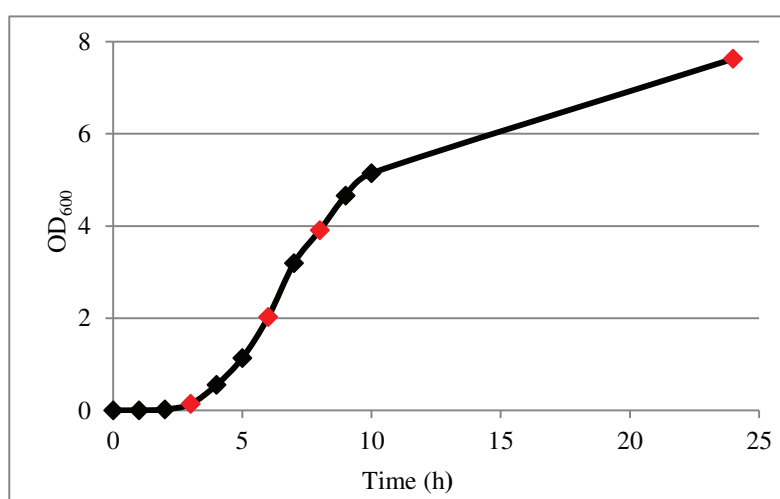


Figure 29: Growth curve of *E.coli* in MHB at 37°C , shaking at 200 rpm ($n = 3 \pm \text{SD}$)

Figure 30 shows the average Raman and IR spectra of *E. coli* at different growth time points (3, 6, 8 and 24 h of incubation). Metabolic changes within bacteria according to the growth time were reflected in changes in intensity of some spectral bands. According to the loading plot of the first PC accounting for 63% of the total variance for Raman and 66% for IR spectra (results not shown) the Raman spectral bands around 775 cm^{-1} (uracil and cytosine), 1571 cm^{-1} (guanine and adenine), 995 cm^{-1} (phenylalanine), 1087 cm^{-1} (DNA), 1445 cm^{-1} (lipid) and 1660 cm^{-1} (protein) were identified to have the major contributions to the spectral variances during bacterial growth. Minor contributions resulted from the vibrational bands at 1230 cm^{-1} , 1533 cm^{-1} and 1636 cm^{-1} (the amide III, amide II and amide I bands of protein), 1080 cm^{-1} (phosphor-esters in DNA/RNA backbone) in IR spectra [26,32,59,220,221,222,223].

Raman spectroscopy provides the chemical information of a variety of constituents within bacterial cells: DNA/RNA, carbohydrates, proteins, lipids. During the exponential phase (3, 6 and 8h of incubation) an increase in lipids, nucleic acids (DNA, RNA), proteins are necessary for the cell division and replication [50,173]. IR spectroscopy provides the overall chemical composition of the bacteria, with special focus on the protein components (especially due to intense peptide bond variations). It was found that during the exponential phase, the protein content of the bacterial cells increased due to an enhanced synthesis of ribosomes for the translation and later due to an augmented synthesis of enzymes and other functional proteins. These findings are in agreement with other studies [17,50,52,217,224]. Clear discrimination of the different growth time points (3, 6, 8 and 24 h of incubation) by analyzing the score plot of the first and second PC was also observed in Figure 31.

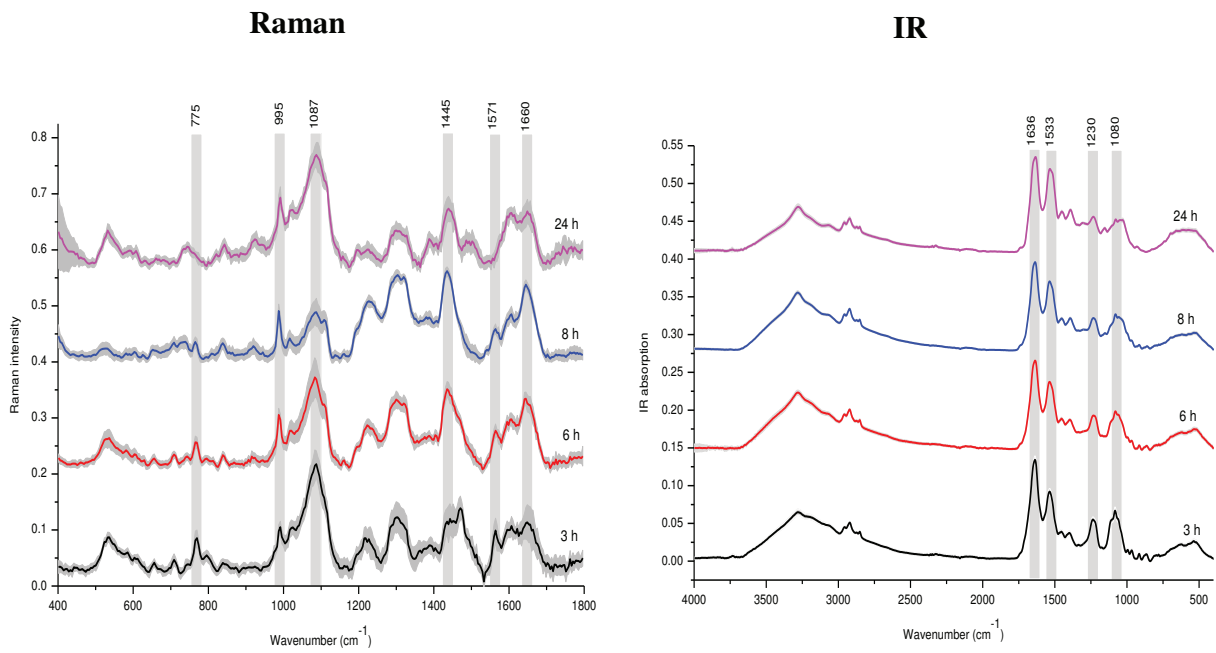


Figure 30: Average Raman and IR absorption spectra of *E. coli* with double standard deviation as grey corona at different growth time points (3, 6, 8 and 24 h of incubation)

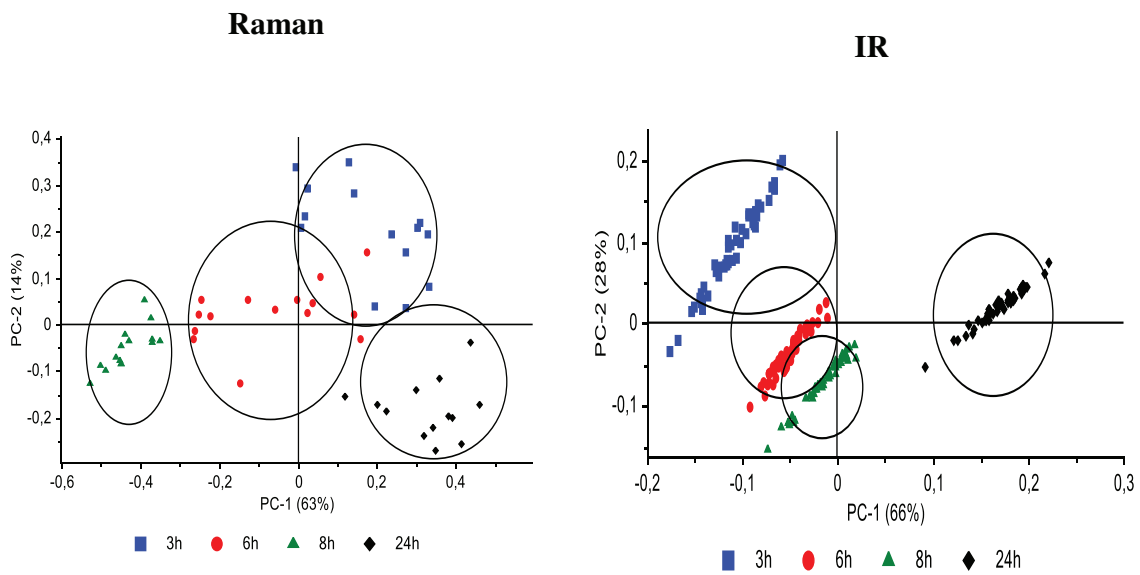


Figure 31: Scores plot of Raman and IR absorption spectra of *E. coli* at different growth time points (3, 6, 8 and 24 h of incubation)

III.1.3 *Vibrio parahaemolyticus*

III.1.3.1 Raman spectrum of *V. parahaemolyticus*

Like the Raman spectrum of *E. coli*, the spectral bands around 2930 cm^{-1} (CH_2 and CH_3 groups from lipids, proteins and carbohydrates), 1450 cm^{-1} (C-H bond in lipids), 1640 cm^{-1} , 1230 cm^{-1} (the amide I and amide III of proteins), 995 cm^{-1} (phenylalanine), 775 cm^{-1} (cytosine, uracil), 720 cm^{-1} (adenine) were detected in the one of *V. parahaemolyticus* (lower spectrum in Figure 32) [17,32,218,219]. In addition, three spectral bands around 930 cm^{-1} , 840 cm^{-1} and 1118 cm^{-1} which are assigned to polysaccharides were observed [85,91,221,225,226].

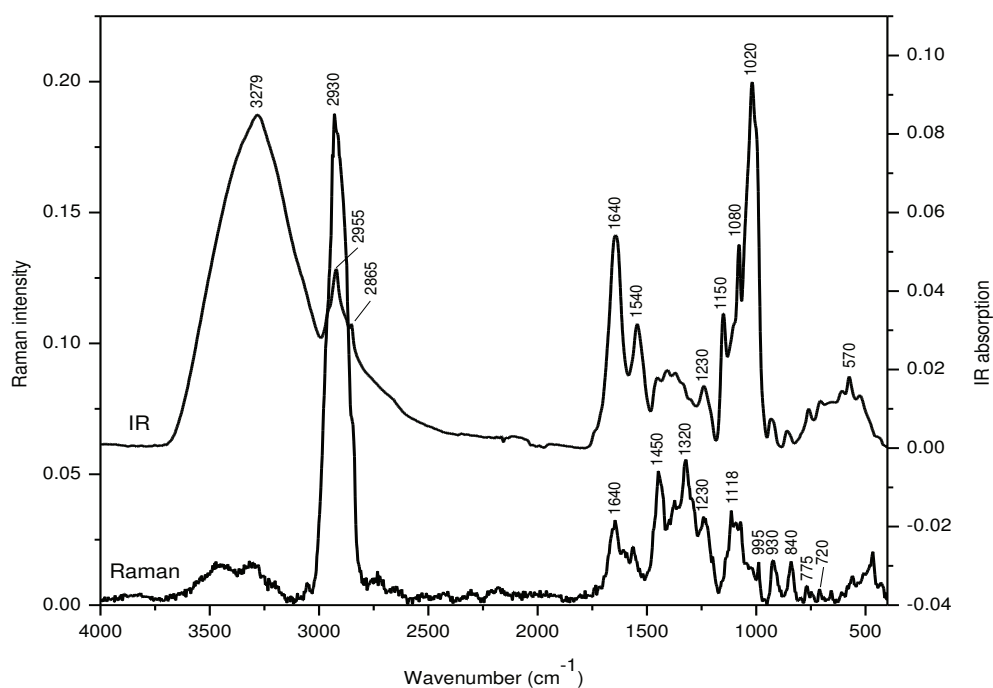


Figure 32: Raman and IR absorption spectra of *V. parahaemolyticus* recorded 8 h of incubation

III.1.3.2 IR absorption spectrum of *V. parahaemolyticus*

As mentioned above, similar and in part complementary information on the chemical composition of the bacteria can be revealed by Raman and IR absorption spectroscopies. In the IR absorption spectrum of *V. parahaemolyticus* (upper spectrum in Figure 32), the spectral bands around 3279 cm^{-1} (N-H stretching vibrations), 2955 cm^{-1} (C-H stretch of methyl group), 2865 cm^{-1} (C-H stretching vibration), 1640 cm^{-1} , 1540 cm^{-1} , 1230 cm^{-1} (the amide I, II and III of proteins), 1080 cm^{-1} (DNA/RNA backbone) [17,217,227], 1150 cm^{-1} and 1020 cm^{-1} (polysaccharides) [227] were observed.

III.1.3.3 Characterization of *V. parahaemolyticus* growth curve

Like the case of *E. coli*, Raman and IR absorption spectra of *V. parahaemolyticus* were recorded at different growth time points: 8, 10 and 24 h of incubation. Figure 33 shows growth curve of *V. parahaemolyticus* in MHB at 38°C without shaking. During the lag phase (0 – 2 h of incubation) no spectra were measured since the bacterial concentration was too low to harvest a sufficient amount of cells. After 8, 10 and 24 h of incubation, bacterial cells were harvested for Raman and IR spectroscopies.

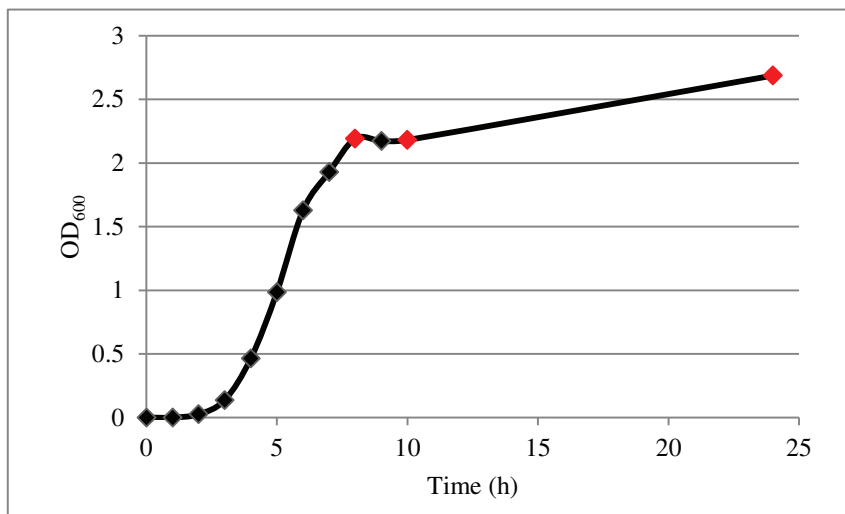


Figure 33: Growth curve of *V. parahaemolyticus* in MHB at 38°C without shaking (n = 3 ± SD)

Figure 34 shows the average Raman and IR spectra of *V. parahaemolyticus* at different growth time points (8, 10 and 24 h of incubation). Metabolic changes within bacteria *versus* time were reflected in changes in intensity of some spectral bands. According to the loading plot of the first PC accounting for 33% of the total variance (result not shown), the Raman spectral bands around 995 cm⁻¹ (phenylalanine), 1073 cm⁻¹ (DNA), 1446 cm⁻¹ (lipid), 1230 cm⁻¹ and 1656 cm⁻¹ (the amide III and amide I of proteins) were identified to have major contributions to the spectral variances during bacterial growth [26,32,59,84,220,221,222,228]. In particular, three intense spectral bands around 841 cm⁻¹, 925 cm⁻¹ were detected in Raman spectra of *V. parahaemolyticus*. According to the study carried out by Kusic *et al.* [91], these peaks are assigned to polysaccharides resulting from biofilm formation in some bacterial strains. Our findings are in agreement with other studies [85,221,225,226]. In fact, *V. parahaemolyticus* can

form a mature biofilm on food and food contact surfaces during food processing [133]. A biofilm is an accumulation of microorganisms embedded in a matrix of polysaccharides. Biofilm formation constitutes a protected mode of growth that allows survival of bacteria in hostile conditions [85,155,169,229]. The temperatures in the range of 25 - 37°C result in significant biofilm formation as well as exoprotease and AI-2 production. Indeed, a positive correlation was reported between protease production, biofilm-forming ability and AI-2 production [168,230]. Biofilm formation is considered as a drawback for harvesting bacterial cells and for the antibiotic penetration [87]. From this point of view, a temperature of 38°C was chosen in this study as an optimal temperature for growth and in order to limit the biofilm formation of *V. parahaemolyticus*. In the IR spectra of *V. parahaemolyticus*, some prominent spectral peaks around 1656 cm^{-1} and 1532 cm^{-1} (the amide I and amide II of proteins) [17,26,32], 1072 cm^{-1} (DNA backbone) [17,217,227], 1145 cm^{-1} and 1017 cm^{-1} (polysaccharides) [227] were observed. According to the loading plot of the second PC accounting for 39% of the total variance (result not shown), the spectral bands around 1656 cm^{-1} and 1532 cm^{-1} , 1017 cm^{-1} were determined to have the highest contributions to the spectral variances during the bacterial growth. The scores plot of the first two principal components which describe together 53% for Raman and 97% for IR of the data are shown in Figure 35. The figure indicated that the spectra recorded at 8 and 10 h were not clearly grouped but well separated with the one at 24 h in both Raman and IR.

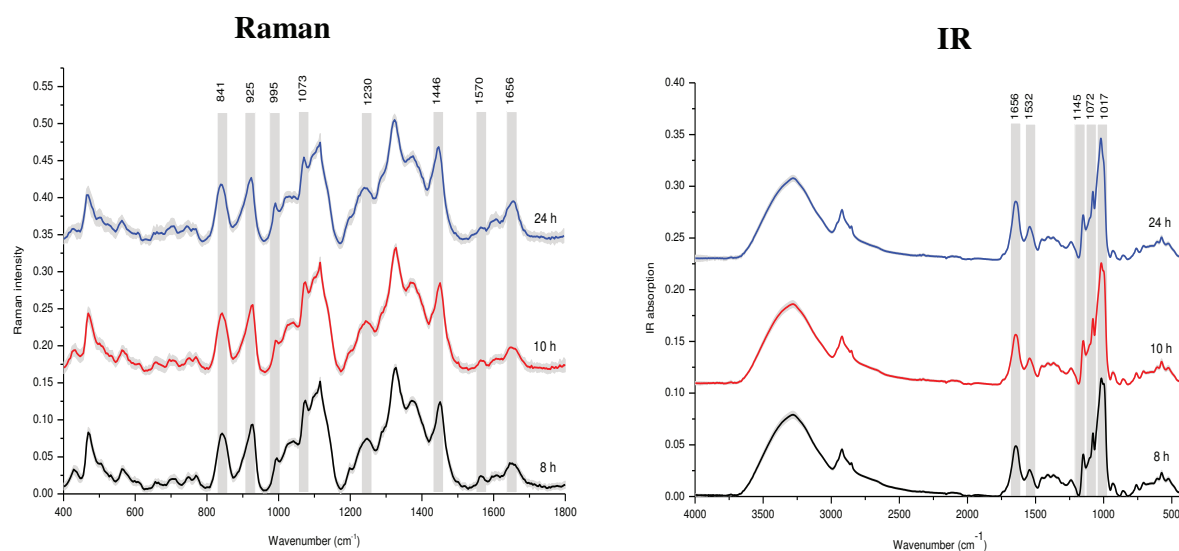


Figure 34: Raman and IR absorption spectra of *V. parahaemolyticus* with double standard deviation as grey corona at different growth time points (8, 10 and 24 h of incubation)

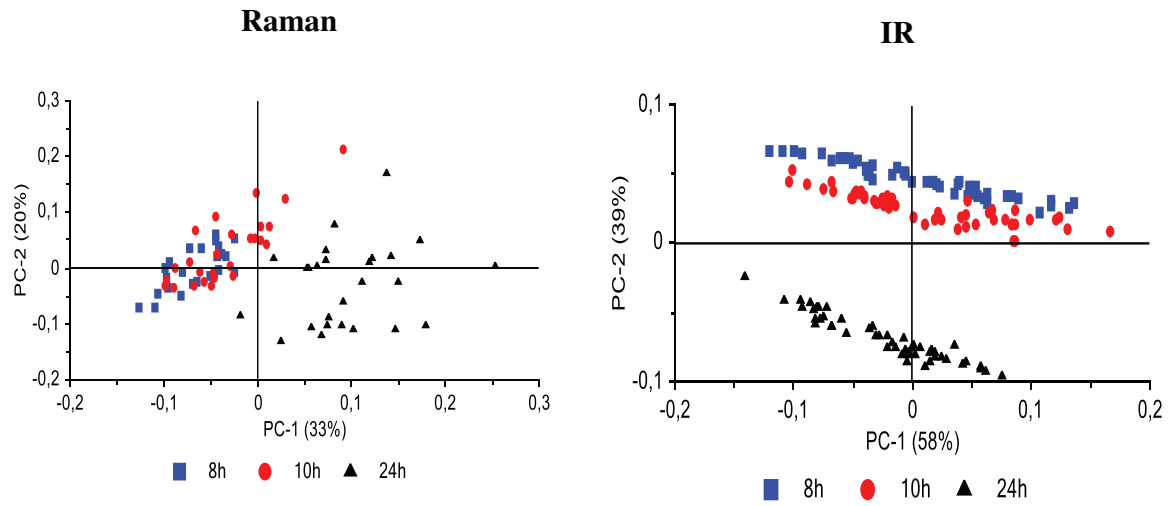


Figure 35: Scores plot of Raman and IR absorption spectra of *V. parahaemolyticus* at different growth time points (8, 10 and 24 h of incubation)

Part III.2: Effects of antibiotics against *Escherichia coli*

Within this chapter Raman and IR absorption spectroscopies will be used to gain a deeper insight into the mechanisms of action of antibiotics against *E. coli*. Different classes of antibiotics were investigated, such as β -lactams (Amp, Ctx – cell wall inhibitors), tetracyclines (Tet – protein synthesis inhibitor), fluoroquinolones (Cip – DNA replication inhibitor) [173,204,206,207,231,232]. Spectra were recorded from the antibiotic-treated samples and the control (antibiotic-free culture). With the help of statistical method (PCA) the spectral changes due to the action of the drug were pointed out and assigned to biological features within the cell.

III.2.1 Effects of ampicillin and cefotaxime

Raman spectra

The MIC and MBC values were equivalent for Amp and Ctx against *E. coli* and corresponded to 5 $\mu\text{g/ml}$ and 0.2 $\mu\text{g/ml}$, respectively, showing that these antibiotics are bactericidal. Several antibiotic concentrations corresponding to 2MIC, 4MIC, 6MIC and 8MIC were tested. In order to produce significant inactivation of bacterial cells, the antibiotic concentration used in this study corresponded to 8MIC (40 $\mu\text{g/ml}$, 1.6 $\mu\text{g/ml}$ for Amp and Ctx, respectively). High percentage of inactivated cells (> 90%) were necessary to observe spectral differences between the antibiotic-treated samples and the control [104]. The concentrations of 2MIC, 4MIC and 6MIC did not provide significant molecular modifications in *E. coli* cells (data not shown). Finally, the concentration of 8MIC was chosen to perform the experiments. Compared to the control, the inactivation of bacterial cells after the antibiotic addition was approximately 99.99% for both Amp and Ctx. As a consequence, it is likely that the cells were significantly injured or dead, showing important changes in their chemical composition that will be detected in Raman and IR absorption spectra.

Figure 36 shows the average Raman spectra of *E. coli* control and culture with Amp 8MIC or Ctx 8MIC. On a first view all spectra look very similar. However, clear discrimination of the antibiotic-treated samples compared to the control was recorded in both Amp and Ctx treatments. The scores plots of the first two PCs which describe together 90% and 83% of the explained variance for Amp, Ctx, respectively are shown in Figure 37A and 38A. According to the loading plots of the first PC presented in Figure 37B and 38B, the most important spectral changes were identified. A decrease in proteins (the amide III at 1230 cm^{-1} and the amide I at

1660 cm^{-1}) was detected in the antibiotic-treated samples compared to the control. In addition, an increase around 1083 cm^{-1} assigned to DNA/RNA and a decrease at 1445 cm^{-1} assigned to lipid were detected as well [12,52,59,213,219,220].

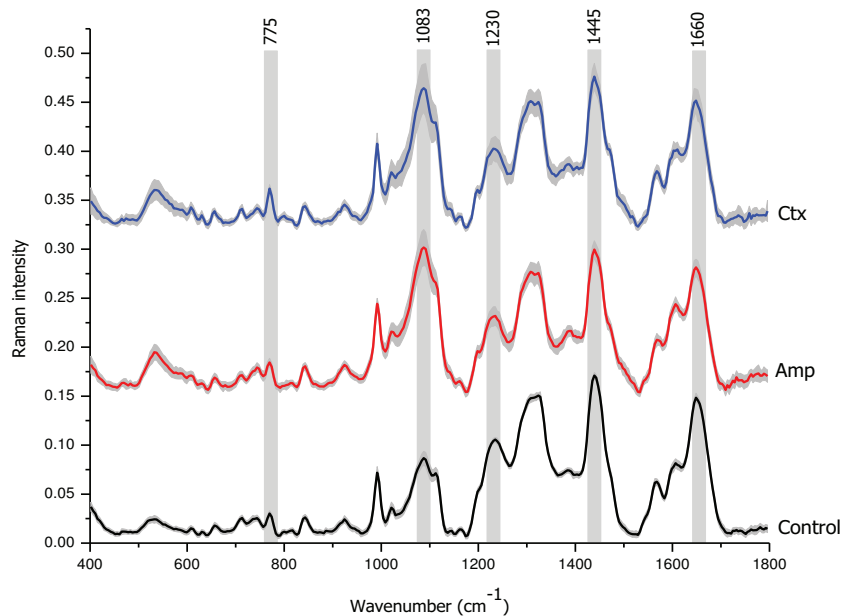


Figure 36: Average Raman spectra with double standard deviation as grey corona of *E. coli* control (black line) and culture with Amp 8MIC (40 $\mu\text{g/ml}$) (red line), or with Ctx 8MIC (1.6 $\mu\text{g/ml}$) (blue line) recorded 120 min after the antibiotic addition

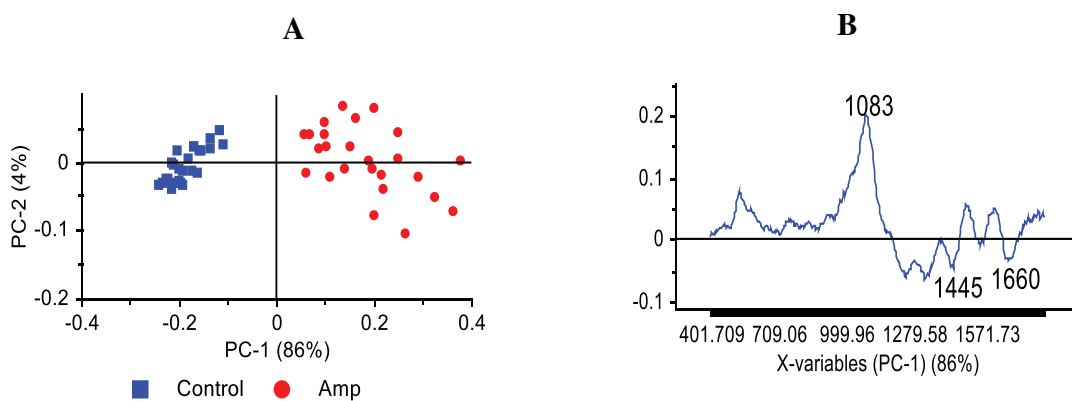


Figure 37: **A)** Scores plot of the first two PC of Raman spectra of *E. coli* control (blue points) and culture with Amp 8MIC (40 $\mu\text{g/ml}$) (red points) recorded 120 min after the antibiotic addition. **B)** Loading plot for the first PC from A

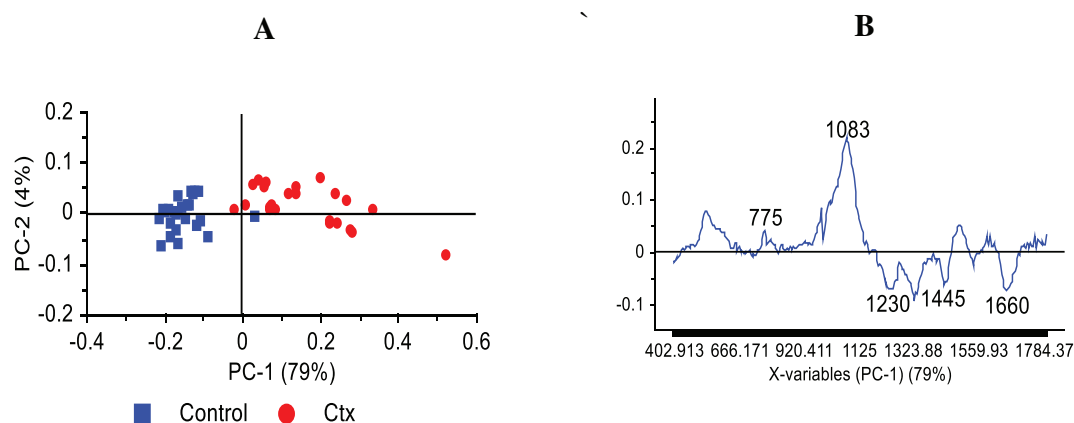


Figure 38: **A)** Scores plot of the first two PC of Raman spectra of *E. coli* control (blue points) and culture with Ctx 8MIC (16 µg/ml) (red points) recorded 120 min after the antibiotic addition. **B)** Loading plot for the first PC from A

IR absorption spectra

Figure 39 shows the average IR absorption spectra of *E. coli* control and culture with Amp 8MIC or with Ctx 8MIC. The scores plots of the first two PCs which describe together 98% and 88% of the explained variance for Amp and Ctx respectively are presented in Figure 40A, 41A. The antibiotic-treated samples were distinguished from the control (antibiotic-free culture). The loading plot of the second PC identifies the wavenumbers that show the largest variation associated with the action of the drugs (Figure 40B and 41B). Like in the Raman spectra, a decrease in proteins (the amide III band – 1230 cm⁻¹, amide II – 1540 cm⁻¹ and amide I – 1640 cm⁻¹) was observed and confirmed. In addition, an increase in carbohydrates (1150 cm⁻¹, 1017 cm⁻¹) were detected for both Amp and Ctx treatments [3,36,227,233].

In conclusion, Amp and Ctx treatments caused a decrease in protein bands in both Raman and IR absorption spectra, an increase in carbohydrates in IR spectra. The spectral perturbation seems to be correlated with the mode of action of these drugs. Ampicillin and cefotaxime belong to β-lactams that are inhibitors of cell wall synthesis. These drugs inhibit transpeptidation, the reaction that results in the cross-linking of two glycan-linked peptide chain. As a result, a newly synthesized bacterial cell wall is no longer cross-linked and cannot maintain its strength, leading to cell death [173,234,235,236,237]. This can probably explain the decrease of the protein content observed for both Amp and Ctx treatments. Additionally, in order to repair damages of the cell wall induced by antibiotics, the bacteria may enhance the synthesis of precursors of

peptidoglycan – N-acetyl glucosamine and N-acetyl muramic acid, generally amino-sugar. Consequently, the accumulation of these precursors inside the cells has led to the increase of the carbohydrate bands in IR spectra [71].

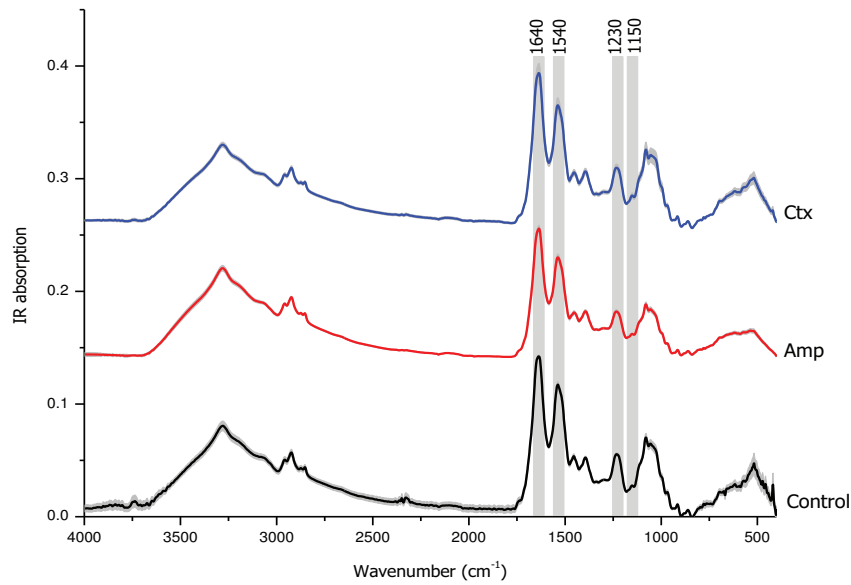


Figure 39: Average IR absorption spectra with double standard deviation as grey corona of *E. coli* control (black line) and culture with Amp 8MIC (40 µg/ml) (red line), or with Ctx 8MIC (1.6 µg/ml) (blue line) recorded 120 min after the antibiotic addition

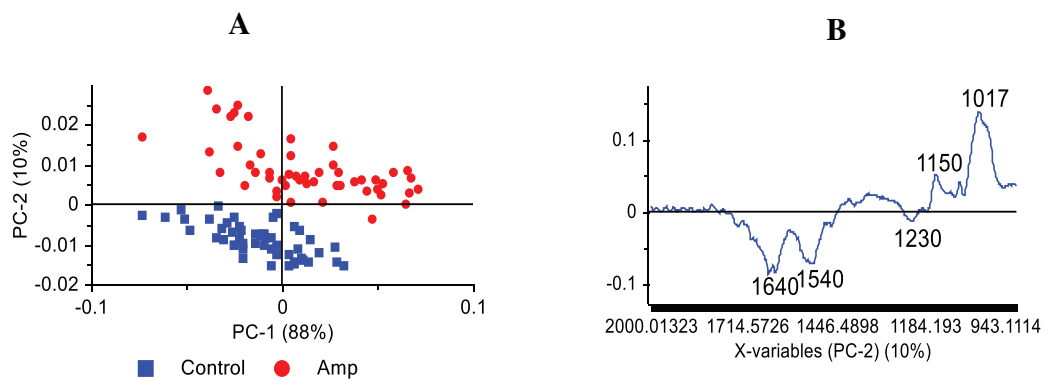


Figure 40: A) Scores plot of the first two PCs of IR absorption spectra of *E. coli* control (blue points) and culture with Amp 8MIC (40 µg/ml) (red points) recorded 120 min after the antibiotic addition. B) Loading plot for the second PC from

A

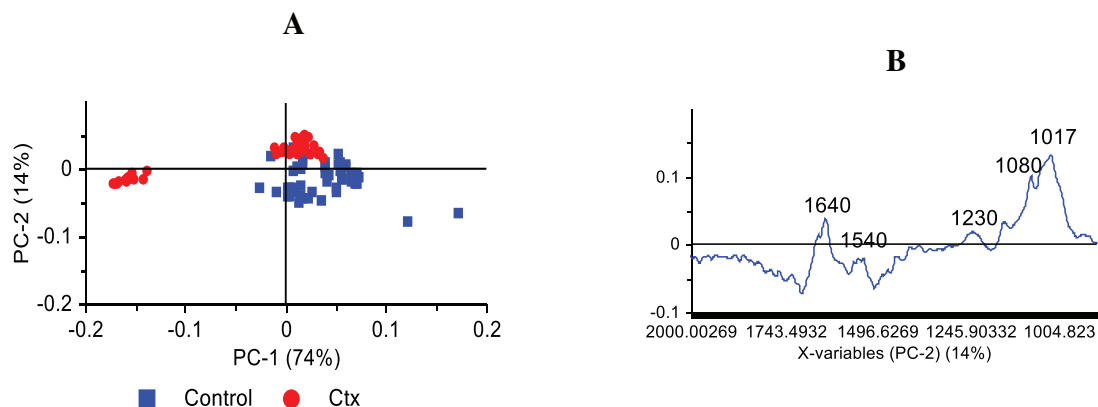


Figure 41: **A)** Scores plot of the first two PCs of IR absorption spectra of *E. coli* control (blue points) and culture with Ctx 8MIC (1.6 µg/ml) (red points) recorded 120 min after the antibiotic addition. **B)** Loading plot for the second PC from A

III.2.2 Effects of tetracycline

Raman spectra

The MIC and MBC values of Tet against *E. coli* were 5 µg/ml and 40 µg/ml, respectively, indicating that Tet is a bacteriostatic antibiotic. The concentration of 8MIC (40 µg/ml) was also chosen to detect molecular changes induced by Tet against *E. coli* cells. Compared to the control, the inactivation of viable cells after Tet addition was approximately 90%. Figure 42A shows the average Raman spectra of *E. coli* control and culture with Tet 8MIC (40 µg/ml). The scores plot of the first two PCs which represents 80% of the explained variance is shown in Figure 42B. Clear discrimination of Tet-treated sample compared to the control was recorded. Thanks to the loading plot of the first PC in Figure 42C, the most different spectral changes were identified including [17,32,104,220,222,224,238]:

- ✓ An increase of nucleic bands around 775 cm⁻¹ (uracil, cytosine), 1475 cm⁻¹ and 1570 cm⁻¹ (guanine, adenine)
- ✓ An increase in the spectral band at 1083 cm⁻¹ which is assigned to the symmetric PO stretching vibration of PO₂⁻ as it is found in nucleic acids (DNA/RNA)
- ✓ A decrease of the amide I band at 1660 cm⁻¹
- ✓ In particular, a sharp decrease at 995 cm⁻¹ (phenylalanine) was noticed

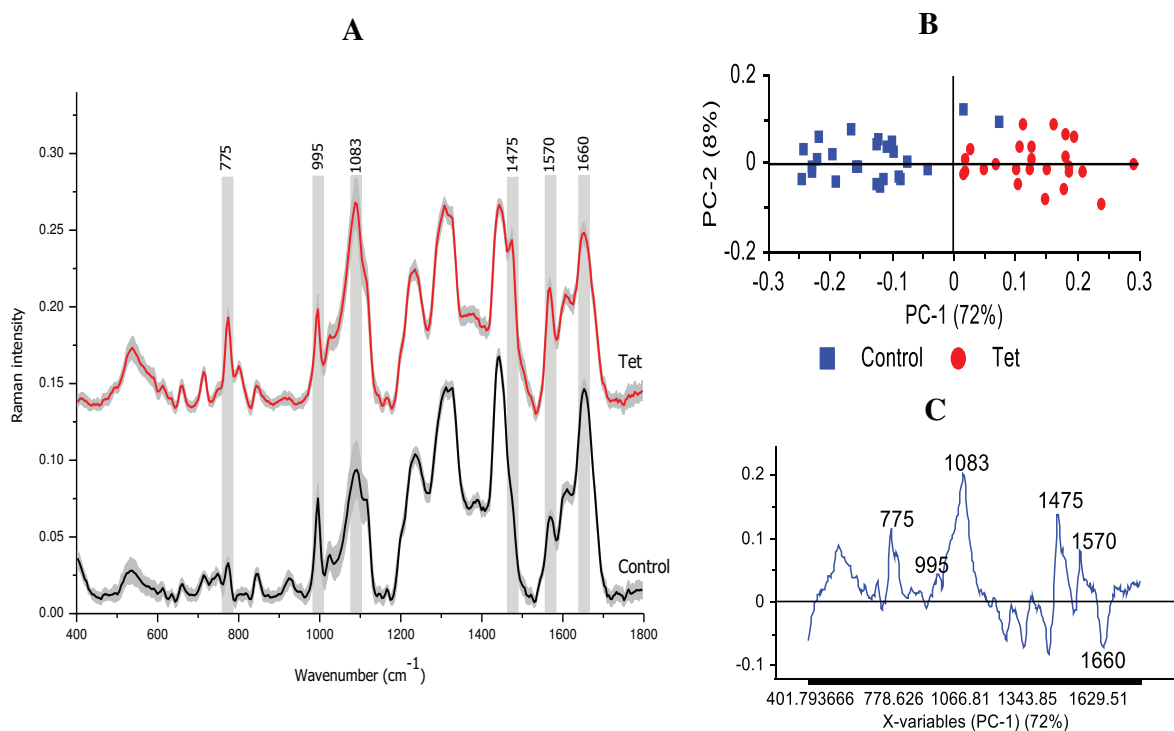


Figure 42: **A)** Average Raman spectra with double standard deviation as grey corona of *E. coli* control (black line) and culture with Tet 8MIC (40 µg/ml) (red line) recorded 120 min after the antibiotic addition. **B)** Scores plot of the first two PCs. **C)** Loading plot of the first PC from B

IR absorption spectra

The average IR absorption spectra of *E. coli* control and culture with Tet and the control are presented in Figure 43A. The most prominent spectral changes were determined by the loading plot of the first PC (Figure 43C) including [217]:

- ✓ An increase in the amide II band at 1540 cm⁻¹ (proteins)
- ✓ An increase in the spectral band at 1080 cm⁻¹ (DNA/RNA)
- ✓ A decrease in the amide III band (1230 cm⁻¹)

The scores plot of the first two PCs which accounts for 99% of the spectral variance is shown in Figure 43B. Distinct segregation between the Tet-treated sample and the control was recorded as well.

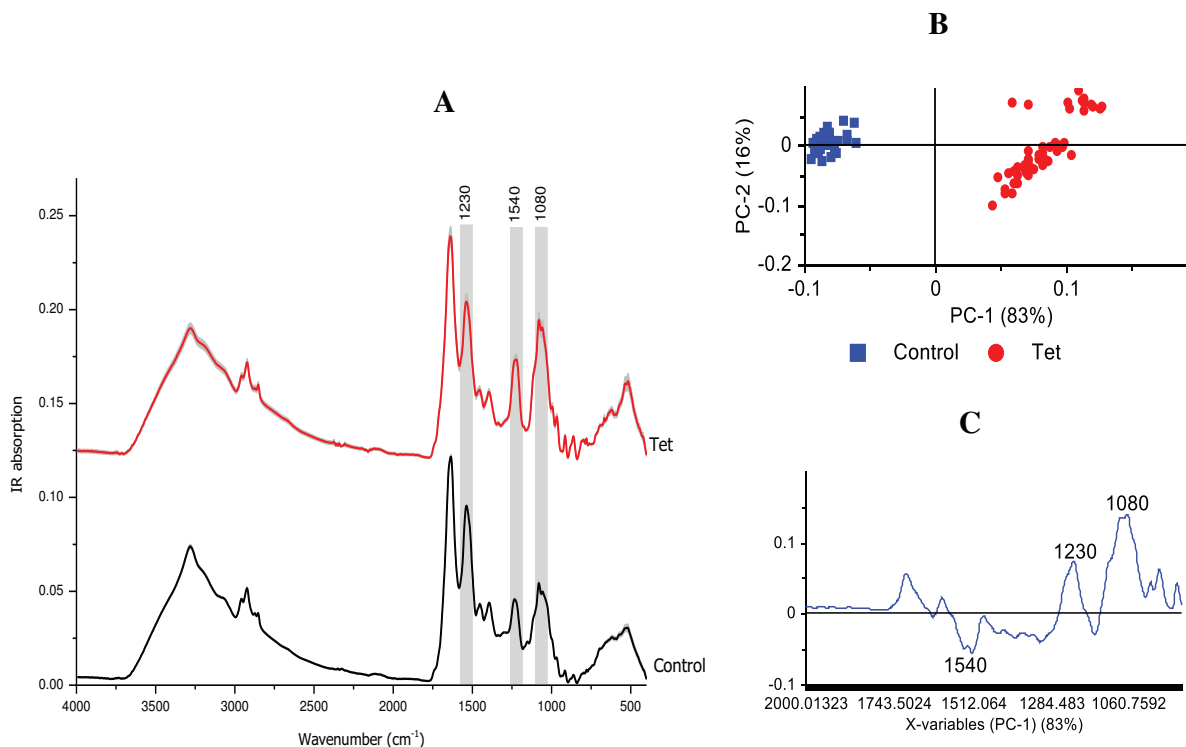


Figure 43: **A)** Average IR absorption spectra with double standard deviation as grey corona of *E. coli* without (black line) and with Tet 8MIC (40 $\mu\text{g/ml}$) (red line) recorded 120 min after the antibiotic addition. **B)** Scores plot of the first two PCs. **C)** Loading plot of the first PC from B

Tetracyclines are broad-spectrum agents, exhibiting activity against a wide range of Gram-positive and Gram-negative bacteria, chlamydiae, mycoplasmas, rickettsiae and protozoan parasites. Tetracycline reversibly inhibits bacterial protein synthesis by preventing the association of aminoacyl-tRNA with the ribosomal acceptor (A) site [204,206,207]. When Tet attaches to the site A of ribosome, the protein synthesis is blocked which has led to a sharp increase of nucleic acids (775 , 1475 and 1570 cm^{-1}) in Raman spectra and a decrease of the amide III bands (1230 cm^{-1}) in IR absorption spectra. Besides, an increase of the amide II at 1540 cm^{-1} in IR could result from enhanced synthesis of transport proteins such as efflux pump that are involved in the extrusion of antibiotics [128,239]. In addition, Tet could influence the synthesis of phenylalanine in animals and micro-organisms [204,207,240,241,242]. Consequently, a dramatic decrease of phenylalanine band (995 cm^{-1}) in Raman was observed after the drug treatment.

III.2.3 Effects of ciprofloxacin

Raman spectra

The MIC and MBC values of Cip against *E. coli* were equivalent and corresponded to 0.1 $\mu\text{g/ml}$, showing that this antibiotic is bactericidal. The concentration of 8MIC (0.8 $\mu\text{g/ml}$) was chosen to assess molecular changes caused by Cip treatment. Compared to the control, the inactivation of viable cells after the Cip addition were approximately 99.99%. The average Raman spectra of *E. coli* control and culture with Cip 8MIC are shown in Figure 44A. The scores plot of the first two PCs which describes together 81% of the explained variance is presented in Figure 44B. Clear discrimination between the Cip-treated sample and the control was recorded. Due to the loading plot of the first PC (Figure 44C), the largest spectral changes identified in the wavenumber regions around 775 cm^{-1} (uracil, cytosine), 1578 cm^{-1} (guanine, adenine) and 1087 cm^{-1} (DNA/RNA).

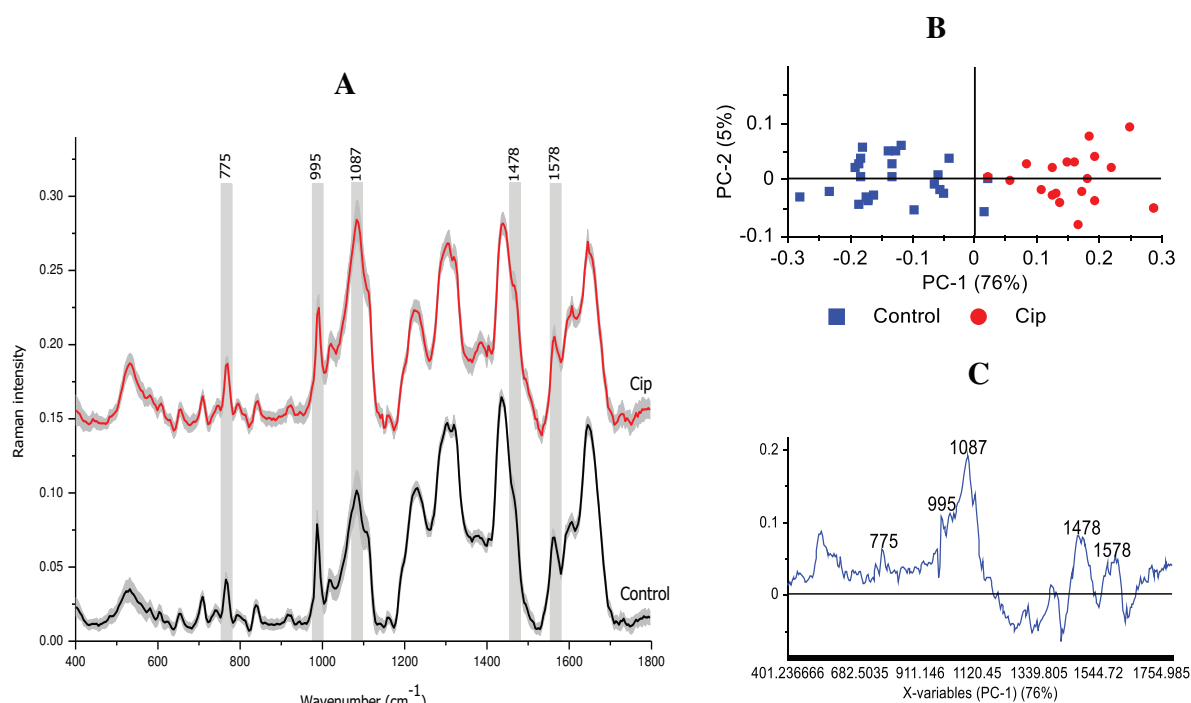


Figure 44: **A)** Average Raman spectra with double standard deviation as grey corona of *E. coli* control (black line) and culture with Cip 8MIC (0.8 $\mu\text{g/ml}$) (red line) recorded 90 min after the antibiotic addition. **B)** Scores plot of the first two PCs.

C) Loading plot of the first PC from B

IR absorption spectra

Figure 45A shows the average IR absorption spectra of *E. coli* control and culture with Cip 8MIC. The scores plot of the first two PCs which describes together 100% of the explained variance is shown in Figure 45B. The Cip-treated sample and the control were grouped. Like previously mentioned, IR absorption spectrum provides mainly the chemical composition of proteins. In case of Cip treatment, the most important spectral changes were the amide III (1230 cm^{-1}), the amide II (1520 cm^{-1}) and the amide I (1640 cm^{-1}) bands of proteins. Additionally, the spectral band at 1080 cm^{-1} (DNA/RNA backbone) increased as well (Figure 45C) [26,32].

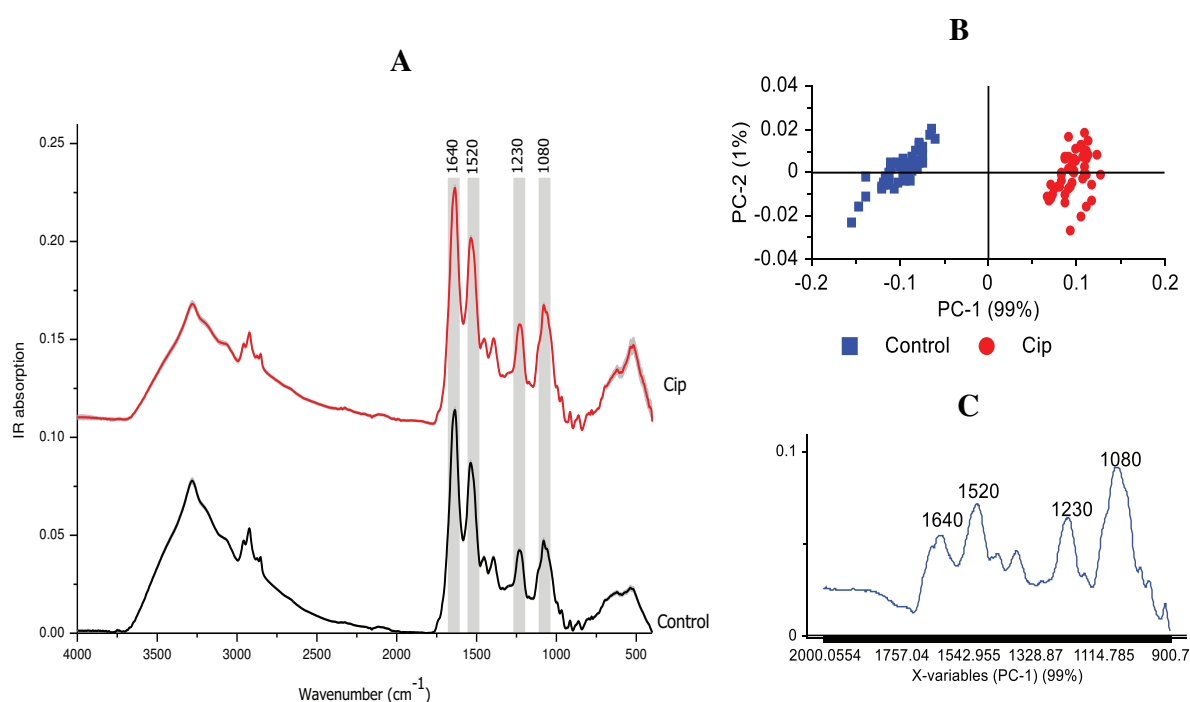


Figure 45: **A)** Average IR absorption spectra with double standard deviation as grey corona of *E. coli* control (black line) and culture with Cip 8MIC (0.8 $\mu\text{g}/\text{ml}$) (red line) recorded 90 min after the antibiotic addition. **B)** Scores plot of the first two PCs. **C)** Loading plot of the first PC from B

Ciprofloxacin belongs to the second generation of quinolone analogues of nalidixic acid that show greater potency, lower toxicity and a broader antibacterial spectrum. Cip inhibits DNA gyrase in Gram-negative bacteria or topoisomerase IV in Gram-positive bacteria. DNA gyrase introduces negative superhelical twists into DNA. Negatively super-twisted DNA is important for initiation of DNA replication and allows for binding of initiation proteins. Inhibition of DNA

gyrase results in impaired DNA replication (at lower concentrations) and cell death (at lethal concentrations) [173,237,243,244,245,246,247,248]. As a result, a sharp increase in nucleic acid bands was recorded after Cip treatment. Furthermore, the spectral bands of proteins increased as well. This finding indicates that interactions of Cip with its cell targets and the subsequent reactions mainly involve changes of the DNA but also proteins [17,211,244,249].

III.2.4 Conclusion

Raman and IR absorption spectra were recorded to detect molecular modifications induced by different classes of antibiotics, such as Amp, Ctx – cell wall synthesis inhibitors, Tet – protein synthesis inhibitor and Cip – DNA replication inhibitor. The MIC, MBC values of the antibiotics against *E. coli* were determined by tube dilution method and counting viable cells on agar plate. The MIC and MBC were equivalent for Amp, Ctx, Cip and corresponded to 5 µg/ml, 0.2 µg/ml and 0.1 µg/ml, respectively, showing that these antibiotics are bactericidal. In case of Tet, the MIC, MBC were 5 µg/ml and 40 µg/ml, respectively, indicating that the antibiotic is bacteriostatic. In order to produce significant inactivation of cells, the concentration of 8MIC was chosen to carry out all experiments. Raman and IR absorption spectra were measured 120 min after Amp, Ctx, Tet additions and 90 min after Cip addition. With the help of principal component analysis, it was possible to discriminate between the antibiotic-treated samples and the control (antibiotic-free culture) and identify the most important spectral changes in the variance of samples. For Amp and Ctx treatments, a decrease of protein bands in both Raman and IR absorption spectra, an increase of carbohydrates in IR absorption spectra were noticed. Tet addition led to an increase of nucleic acids and a sharp decrease of phenylalanine in Raman spectra. In IR absorption spectra, a decrease of the amide III of proteins and an increase in the amide II were obtained. In case of Cip, an increase of nucleic acids in Raman spectra and an increase of proteins in IR spectra were detected. Molecular changes in Raman and IR absorption spectra resulted mainly from the mechanisms of action of antibiotics. Clear discrimination of the antibiotic-treated sample and the control was well obtained for the three classes.

This chapter demonstrates that Raman and IR absorption spectroscopies in conjunction with statistical analysis (PCA) can be applied to detect molecular changes caused by different classes of antibiotics against *E. coli*. Raman spectroscopy allows to detect changes in nucleic acids, proteins, amino acid. IR absorption spectroscopy mainly reveals changes in proteins, carbohydrates. Consequently, combination of these two techniques is indispensable to obtain the

overall modifications related to the cell biochemical composition. The findings of this chapter demonstrates that using Raman and IR spectroscopies to detect molecular modifications induced by different classes of antibiotics is feasible. This study could be the basis for future investigations for understanding the mechanisms involved in bacterial resistance to antibiotics using resistant strains.

Part III.3 Effects of antibiotics against *Vibrio parahaemolyticus*

In this chapter Raman and IR absorption spectroscopies will be explored to understand the mechanisms of action of antibiotics against *V. parahaemolyticus*. Like the case of *E. coli* in Part III.2, different classes of antibiotics as β -lactams (Amp, Ctx), tetracyclines (Tet) and fluoroquinolones (Cip) were tested to investigate molecular changes that they induce in the cell by Raman and IR absorption spectroscopies. In conjunction with statistical method (PCA) the spectral changes due to the action of the drug were pointed out and assigned to biological features within the cell.

III.3.1 Effects of ampicillin

Raman spectra

V. parahaemolyticus strain used in the study is resistant to Amp up to 50 $\mu\text{g/ml}$. A number of studies reported that most *V. parahaemolyticus* isolates were resistant to Amp [152,153,250,251]. The mechanism of resistance toward Amp is due to β -lactamase activity (penicillinases) that catalyzes the hydrolysis of the β -lactam ring [171,251,252]. On the other hand, Ctx (third generation cephalosporine) possesses a strong affinity with penicillin binding proteins (PBPs) compared to the first and second generation, protecting this drug from β -lactamase activity [253]. Consequently, *V. parahaemolyticus* strain used in this work is resistant to Amp and sensitive to Ctx.

The average Raman spectra of *V. parahaemolyticus* control and culture with Amp at 20 $\mu\text{g/ml}$ are shown in Figure 46A. Clear segregation of Amp-treated sample compared to the Amp-free culture is observed (Figure 46B). According to the loading plot of the second PC shown in Figure 46C, an increase of protein (1230 cm^{-1} , 1650 cm^{-1}), nucleic acids (775 and 1570 cm^{-1}) and lipid (1450 cm^{-1}) bands were detected in Raman spectra.

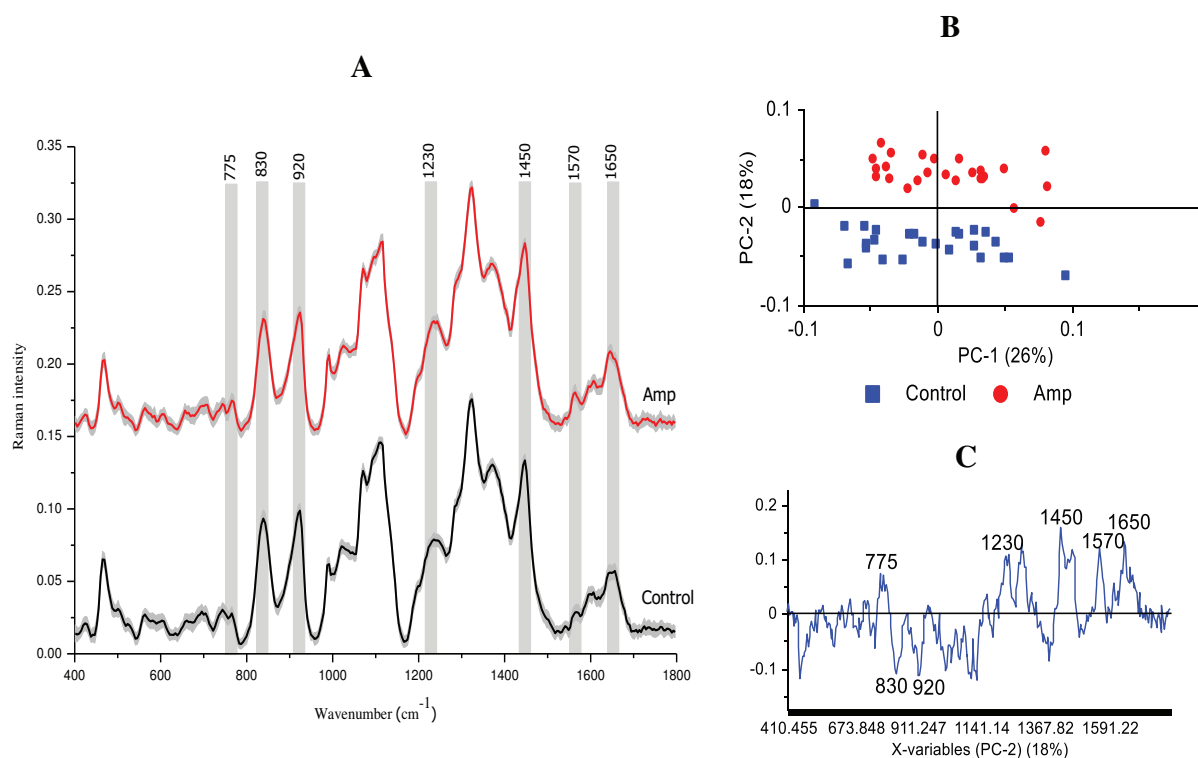


Figure 46: **A)** Average Raman spectra with double standard deviation as grey corona of *V. parahaemolyticus* control (black line) and culture with Amp at 20 $\mu\text{g/ml}$ (red line) recorded 17h after the antibiotic addition. **B)** Scores plot of the first two PCs. **C)** Loading plot of the second PC from B

IR absorption spectra

Figure 47A shows the average IR absorption spectra of *V. parahaemolyticus* control and culture with Amp at 20 $\mu\text{g/ml}$. The scores plot of the first two PCs which describes together 99% of the explained variance is presented in Figure 47B. Clear segregation of the Amp-treated sample compared to the Amp-free culture (control) was recorded. The loading plot of the first PC identified an increase in proteins (the amide I at 1640 cm^{-1} , the amide II at 1540 cm^{-1}) and a decrease in polysaccharides (1150 cm^{-1} , 1017 cm^{-1}) as the most important spectral changes in IR absorption spectra (Figure 47C).

Among four known ways of resistance to β -lactam antibiotics, such as production of β -lactamase enzymes, production of altered penicillin binding proteins, alteration of porin channels, initiation of efflux exporter proteins, the production of β -lactamases is considered as the most efficient strategy [199,254,255,256]. In this regards, *V. parahaemolyticus* strain used in the study

may produce β -lactamase enzymes to inactivate antibacterial activity of Amp and thus the protein content in both Raman and IR spectra increased markedly.

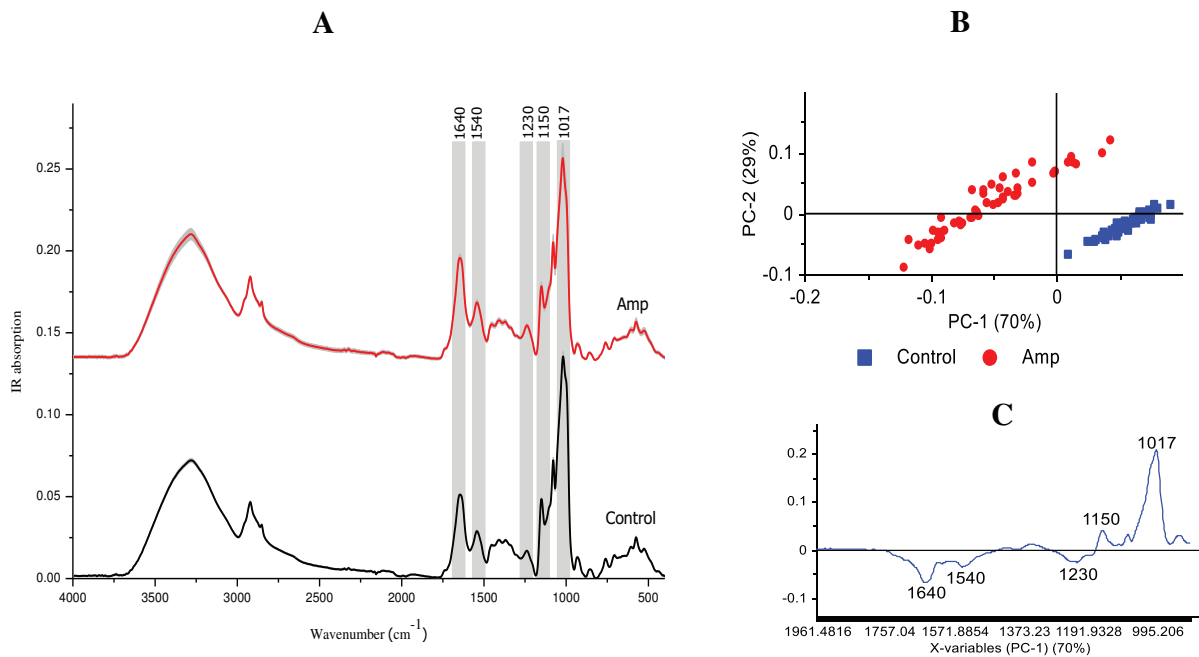


Figure 47: **A)** Average IR absorption spectra with double standard deviation as grey corona of *V. parahaemolyticus* control (black line) and culture with Amp at 20 $\mu\text{g/ml}$ (red line) recorded 17 h after the antibiotic addition. **B)** Scores plot of the first two PCs. **C)** Loading plot of the first PC from B

III.3.2 Effects of cefotaxime

Raman spectra

The MIC and MBC values of Ctx against *V. parahaemolyticus* were equivalent and corresponded to 0.06 $\mu\text{g/ml}$. In order to produce significant inactivation of bacterial cells, several antibiotic concentrations were tested and finally the concentration of 12MIC (0.72 $\mu\text{g/ml}$) was selected to perform experiments. Compared to the control, the inactivation of viable cells after Ctx treatment was approximately 98%.

The average Raman spectra of *V. parahaemolyticus* control and culture with Ctx 12MIC (0.72 $\mu\text{g/ml}$) are presented in Figure 48A. Ctx-treated sample and the control were significantly discriminated as shown in Figure 48B. The loading plot of the second PC (Figure 48C) determined the largest spectral changes caused the differences between the antibiotic-treated

sample and the control. The Raman spectra of Ctx-treated cells shows a decreased production of proteins (1230 cm^{-1} , 1650 cm^{-1}), lipid (1440 cm^{-1}) and an increase in polysaccharide (922 cm^{-1}) compared to the control

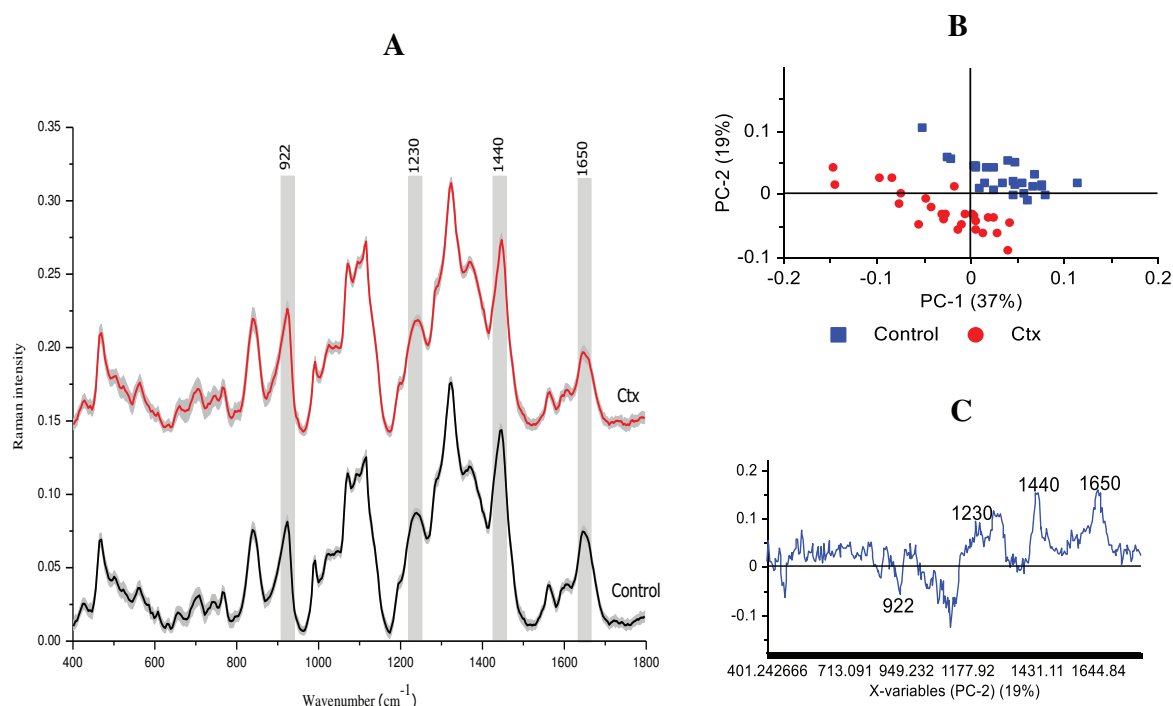


Figure 48: **A)** Average Raman spectra with double standard deviation as grey corona of *V. parahaemolyticus* control (black line) and culture with Ctx 12MIC (0.72 $\mu\text{g/ml}$) (red line) recorded 120 min after the antibiotic addition. **B)** Scores plot of the first two PCs. **C)** Loading plot of the second PC from B

IR absorption spectra

The average IR absorption spectra of *V. parahaemolyticus* control and culture with Ctx 12MIC (0.72 $\mu\text{g/ml}$) are presented in Figure 49A. Figure 49B presents the scores plot of the first two PCs that represents 99 % of the explained variance. Clear discrimination of Ctx-treated sample compared to the control was observed. The most important spectral changes were determined by the loading plot of the second PC (Figure 49C). A decrease in protein bands (1230 cm^{-1} , 1540 cm^{-1} and 1640 cm^{-1}) and an increase in polysaccharide content (1150 cm^{-1} and 1017 cm^{-1}) were detected. The spectral perturbation seems to be correlated with the mode of action of the antibiotic. Cefotaxime (third generation cephalosporine) belongs to β – lactam groups that are

inhibitors of the cell wall synthesis. The drug inhibits transpeptidation - the reaction that results in the cross-linking of two glycan-linked peptide chain. Consequently, a newly synthesized bacterial cell wall is no longer cross-linked and cannot maintain its strength, leading to the cell death [234,235,252]. This can probably explain the decrease of the protein content detected in both Raman and IR absorption spectra.

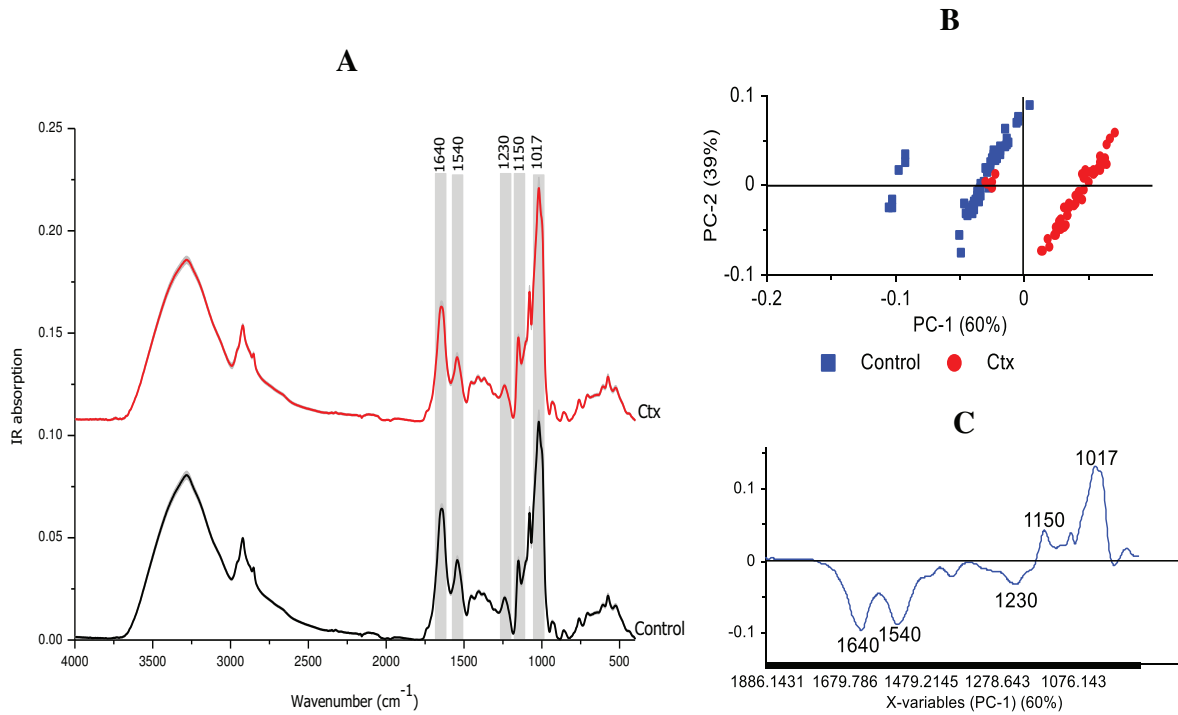


Figure 49: **A)** Average IR absorption spectra with double standard deviation as grey corona of *V. parahaemolyticus* control (black line) and culture with Ctx 12MIC (0.72 $\mu\text{g/ml}$)(red line) recorded 120 min after the antibiotic addition. **B)** Scores plot of the first two PCs. **C)** Loading plot of the second PC from B

Despite the fact that the experiments for detection of molecular changes caused by Ctx and Amp additions were differently designed, comparison of Raman and IR absorption spectra will be performed to test whether it is possible to discriminate between Ctx-sensitive and Amp-resistant samples. The average Raman spectra of *V. parahaemolyticus* population grown in the presence of Amp at 20 $\mu\text{g/ml}$ recorded 17 h after the antibiotic addition and with Ctx 12MIC (0.72 $\mu\text{g/ml}$) recorded 120 min after the drug addition are shown in Figure 50A. According to the loading plot of the first PC in Figure 50C, the spectral changes in polysaccharides at 830, 930 cm^{-1} were observed.

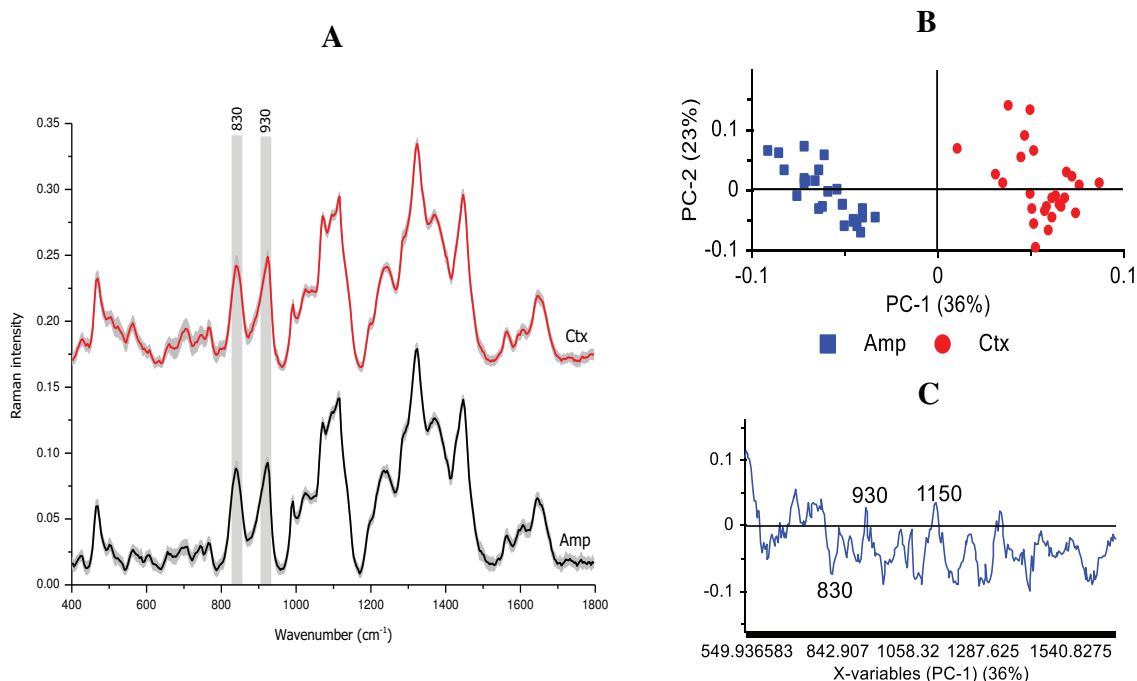


Figure 50: **A)** Average Raman spectra with double standard deviation as grey corona of *V. parahaemolyticus* culture with Amp (20 μg/ml) (black line) recorded 17 h after the antibiotic addition and with Ctx 12MIC (0.72 μg/ml) (red line) recorded 120 min after the antibiotic addition. **B)** Scores plot of the first two PCs. **C)** Loading plot of the first PC from B

Figure 51A presents the average IR absorption spectra of *V. parahaemolyticus* population grown in the presence of Amp at 20 μg/ml recorded 17 h after the antibiotic addition and with Ctx 12MIC (0.72 μg/ml) recorded 120 min after the drug addition. According to the loading plot of the first two PCs in Figure 51C, an increase in proteins was detected (the amide I band at 1640 cm⁻¹, the amide II at 1540 cm⁻¹ and the amide III band at 1230 cm⁻¹) in Amp-treated samples compared to Ctx-treated. Additionally, an increase in polysaccharide content (1150 cm⁻¹, 1017 cm⁻¹) was recorded as well. Distinct segregation of Ctx-treated and Amp-treated samples was noticed in both Raman and IR absorption spectra (Figure 50B and 51B).

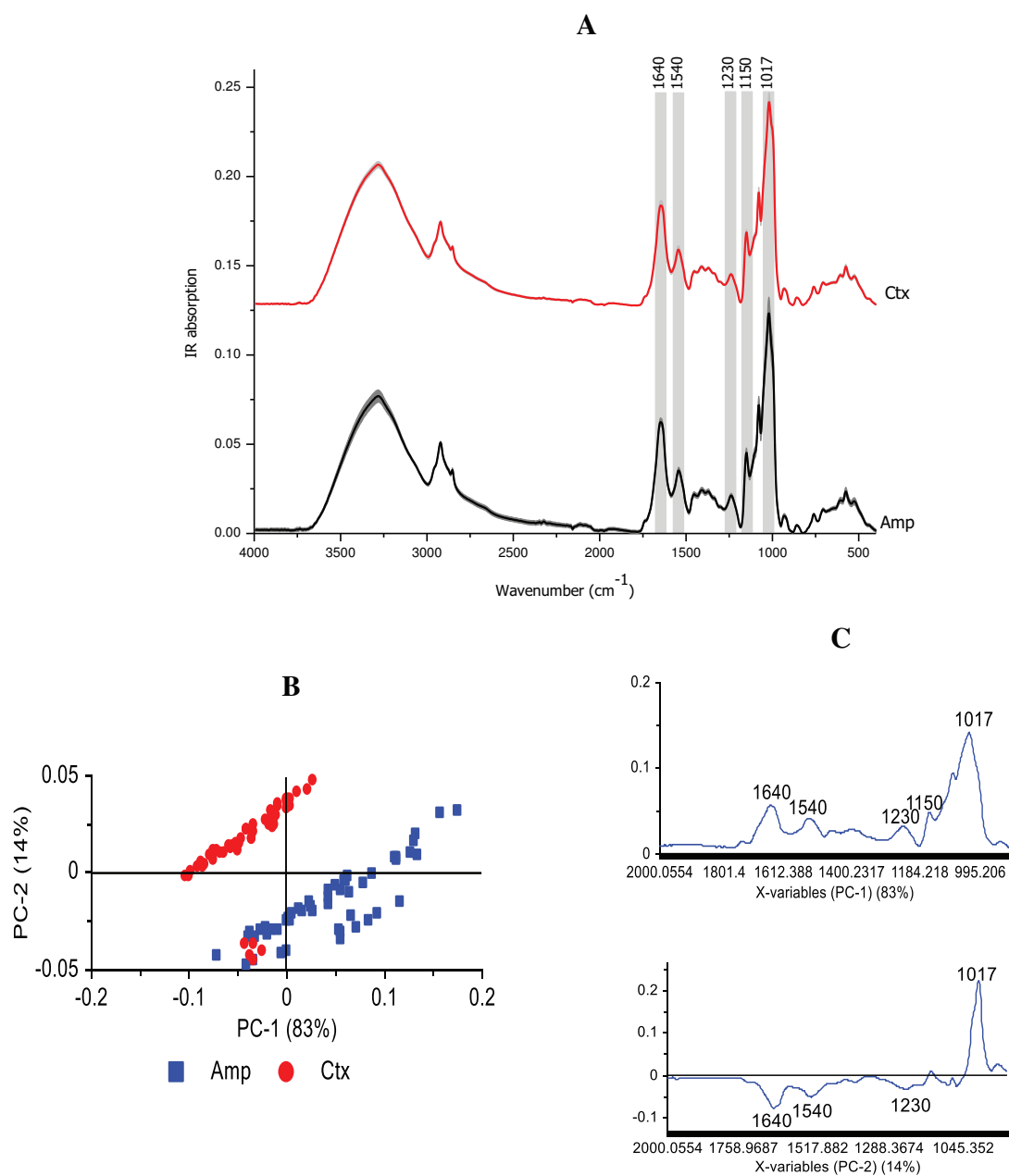


Figure 51: **A)** Average IR absorption spectra with double standard deviation as grey corona of *V. parahaemolyticus* with Amp (20 $\mu\text{g/ml}$) (black line) recorded 17 h after the antibiotic addition and with Ctx 12MIC (0.72 $\mu\text{g/ml}$) (red line) recorded 120 min after the antibiotic addition. **B)** Scores plot of the first two PCs. **C)** Loading plot of the first and second PCs from B

III.3.3 Effects of tetracycline

Raman spectra

The MIC and MBC values of Tet against *V. parahaemolyticus* were 0.1 $\mu\text{g/ml}$ and 0.2 $\mu\text{g/ml}$, respectively. In order to produce significant inactivation of bacterial cells, the concentration of 8MIC (0.8 $\mu\text{g/ml}$) was chosen to carry out experiments for Tet treatment. Compared to the control, the inactivation of viable cells after Tet addition was approximately 99%.

The average Raman spectra of *V. parahaemolyticus* control and culture with Tet 8MIC are presented in Figure 52A. The scores plot of the first two PCs which describes together 61% of the explained variance is shown in Figure 52B. The loading plot of the first PC (Figure 52C) indicated the most prominent spectral differences including:

- ✓ A decrease of protein bands (the amide III at 1230 cm^{-1} , the amide I at 1660 cm^{-1})
- ✓ A sharp decrease around 995 cm^{-1} band assigned to phenylalanine
- ✓ A decrease of lipid band at 1430 cm^{-1}

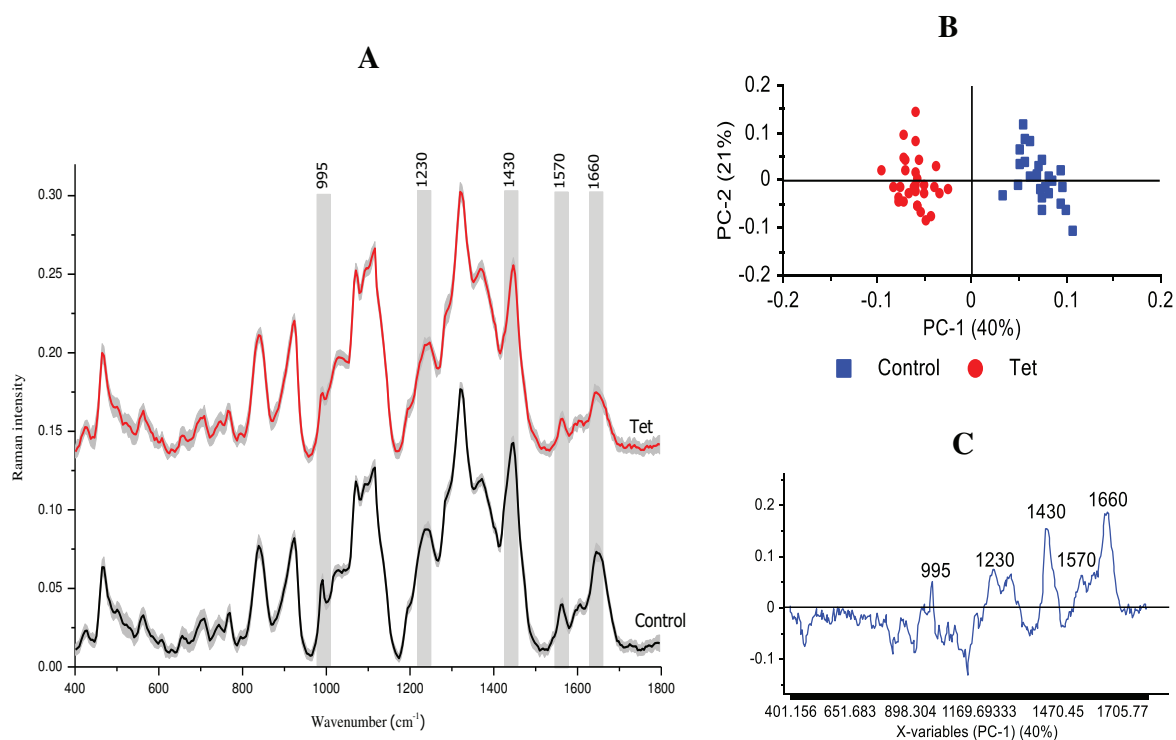


Figure 52: **A)** Average Raman spectra of *V. parahaemolyticus* control (black line) and culture with Tet 8MIC (0.8 $\mu\text{g/ml}$) (red line) recorded 120 min after the antibiotic addition. **B)** Scores plot of the first two PCs. **C)** Loading plot of the first PC from B

IR absorption spectra

The average IR absorption spectra of *V. parahaemolyticus* control and culture with Tet 8MIC are shown in Figure 53A. The scores plot of the first two PCs which accounts for 99% of the spectral variance is presented in Figure 53B. According to the loading plot of the first PC (Figure 53C), a decrease of the spectral bands at 1650 cm^{-1} , 1540 cm^{-1} and 1230 cm^{-1} (the amide I, the amide II and the amide III of proteins) was detected. In addition, an increase around 1150 cm^{-1} and 1017 cm^{-1} (polysaccharides) was noticed. The Tet-treated sample and the control were grouped in both Raman and IR absorption spectra (Figure 52B and 53B).

The Raman and IR spectral changes may be explained by the mechanisms of action of Tet towards *V. parahaemolyticus*. Tetracyclines are broad-spectrum agents, exhibiting activity against a wide range of Gram-positive and Gram-negative bacteria, chlamydiae, mycoplasma, rickettsiae and protozoan parasites. Tetracycline reversibly inhibits bacterial protein synthesis by preventing the association of aminoacyl-tRNA with the ribosomal acceptor (A) site [204,206,207]. When Tet attaches to the site A of ribosome, the protein synthesis is blocked, which leads to a noticeable decrease of the protein content in both Raman and IR absorption spectra. Besides, Tet could influence the synthesis of phenylalanine in animals and microorganisms [240,241,242]. Consequently, an observable decrease of phenylalanine band (995 cm^{-1}) was detected after the drug treatment in Raman spectra.

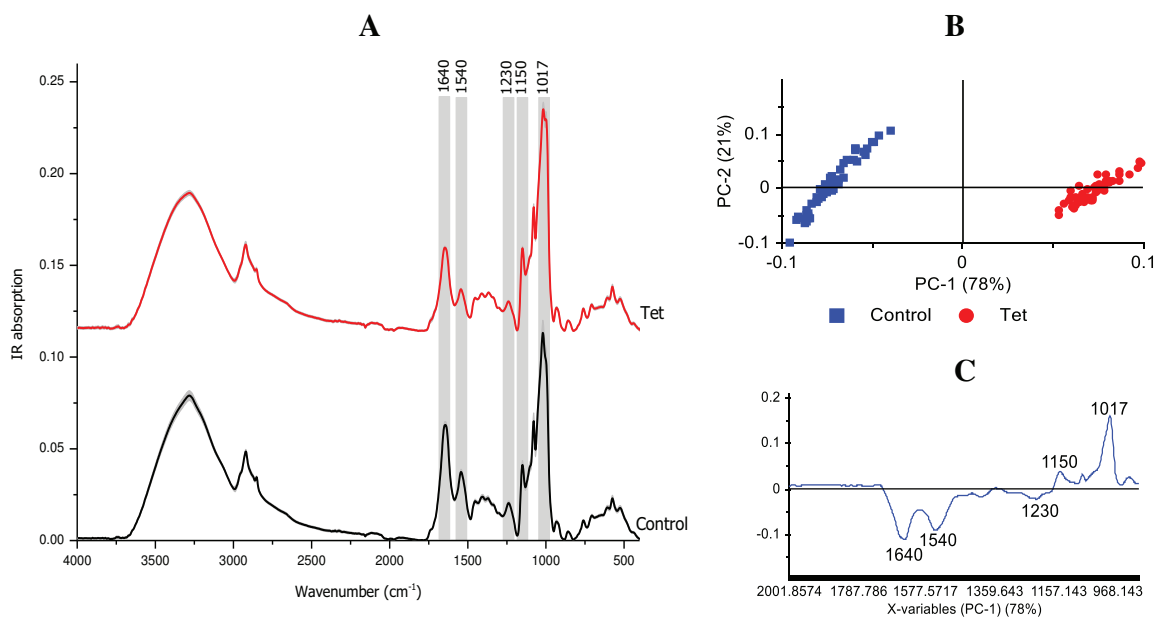


Figure 53: **A)** Average IR absorption spectra of *V. parahaemolyticus* control (black line) and culture with Tet 8MIC (0.8 $\mu\text{g/ml}$) (red line) recorded 120 min after the antibiotic addition. **B)** Scores plot of the first two PCs. **C)** Loading plot of the first PC from B

III.3.4 Effects of ciprofloxacin

Raman spectra

The MIC and MBC values of Cip against *V. parahaemolyticus* were equivalent and corresponded to 0.05 $\mu\text{g/ml}$. Experiments for the detection of molecular changes induced by Cip were performed with the concentration of 18MIC (0.9 $\mu\text{g/ml}$). Compared to the control, the inactivation of viable cells after Cip addition was approximately 99%.

The average Raman spectra of *V. parahaemolyticus* control and culture with Cip 18MIC (0.9 $\mu\text{g/ml}$) is shown in Figure 54A. According to the loading plot of the second PC in Figure 54C, the spectral changes occurred in the wavenumber regions around 840 cm^{-1} and 923 cm^{-1} . In addition, the wavenumbers around 1230 cm^{-1} and 1660 cm^{-1} (proteins), 1440 cm^{-1} (lipids), 1570 cm^{-1} (guanine, adenine) also contributed with markedly weight to the variance of Raman spectra.

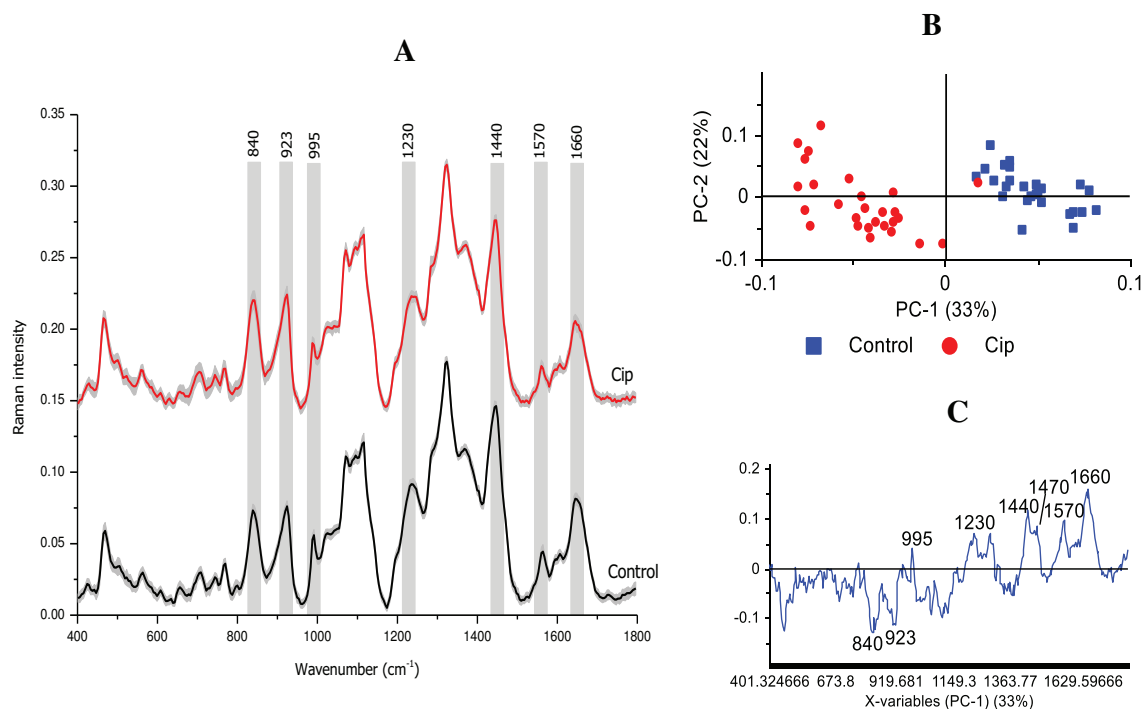


Figure 54: **A)** Average Raman spectra of *V. parahaemolyticus* control (black line) and culture with Cip 18MIC (0.9 $\mu\text{g/ml}$) (red line) recorded 120 min after the antibiotic addition. **B)** Scores plot of the first two PCs. **C)** Loading plot of the second PC from B

IR spectra

Figure 55A presents the average IR absorption spectra of *V. parahaemolyticus* control and culture with Cip 18MIC (0.9 $\mu\text{g/ml}$). The scores plot of the first two PCs which describes together 98% of the spectral variance is shown in Figure 55B. The most important changes were observed around 1230 cm^{-1} , 1540 cm^{-1} and 1640 cm^{-1} for proteins; 1150 cm^{-1} and 1017 cm^{-1} for polysaccharides (Figure 55C). *V. parahaemolyticus* control and Cip-treated sample were significantly discriminated in both Raman and IR absorption spectra (Figure 54B and 55B).

The spectral changes in Cip-treated sample compared to the control can be explained by the mode of action of Cip against *V. parahaemolyticus*. Ciprofloxacin (fluoroquinolone) belongs to the second generation of quinolone analogues of nalidixic acid that shows greater potency, lower toxicity and a broader antibacterial spectrum. In Gram-negative bacteria, Cip interferes with bacterial DNA gyrase and inhibits the DNA replication. Therefore, the process of synthesis of RNA from DNA (transcription) and initiation of translation (protein synthesis) are inhibited as

well [173,237,244,245,246,247,249]. As a result, it was found in both Raman and IR spectra that the protein content of *V. parahaemolyticus* treated with Cip decreased in comparison with the control.

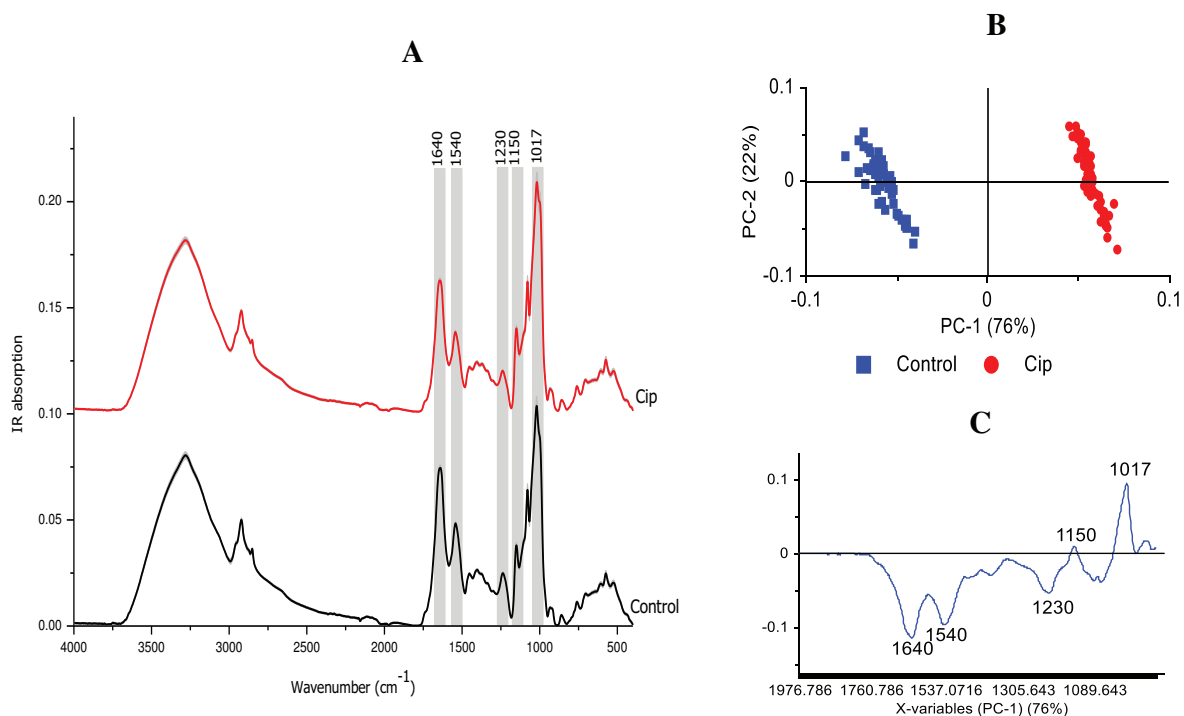


Figure 55: **A)** Average IR absorption spectra of *V. parahaemolyticus* control (black line) and culture with Cip 18MIC (0.9 $\mu\text{g/ml}$) (red line) recorded 120 min after the antibiotic addition. **B)** Scores plot of the first two PCs. **C)** Loading plot of the first PC from B

After the antibiotic addition (Amp, Ctx, Tet and Cip), it was found that the spectral bands around 840 cm^{-1} and 923 cm^{-1} for Raman spectra, 1150 cm^{-1} and 1017 cm^{-1} for IR spectra which are assigned to polysaccharides increased noticeably. These modifications may result from the biofilm formation in *V. parahaemolyticus*. The antibiotic treatment is considered as a stressful factor for the bacterial growth. Therefore, *V. parahaemolyticus* may enhance biofilm formation in order to limit penetration of antibiotics inside the bacterial cells and thus the micro-organism can survive in harsh conditions [87,156,169,230].

III.3.5 Conclusion

Raman and IR absorption spectra were measured to detect molecular changes induced by different classes of antibiotics, such as Amp, Ctx – cell wall inhibitors, Tet – protein synthesis inhibitor and Cip – DNA replication inhibitor. The MIC and MBC values of the antibiotics

against *V. parahaemolyticus* were determined by tube dilution method and counting viable cells on agar plate. *V. parahaemolyticus* strain used in the study is resistant to Amp up to 50 µg/ml. The MIC and MBC were equivalent for Ctx, Cip and corresponded to 0.06 µg/ml and 0.05 µg/ml, respectively, showing that these antibiotics are bactericidal. Concerning Tet, the MIC and MBC corresponded to 0.1 µg/ml and 0.2 µg/ml, respectively, indicating that the drug is bacteriostatic. A different experiment was designed for only Amp to test whether Raman and IR spectroscopies can be used to differentiate Amp-resistant *V. parahaemolyticus* without (Control) and in the presence of Amp up to 20 µg/ml. Raman and IR absorption spectra were recorded after 17 h of incubation. In order to cause significant inactivation of cells, the antibiotic concentrations of 12MIC (0.72 µg/ml) for Ctx, 8MIC (0.8 µg/ml) for Tet and 18MIC (0.9 µg/ml) for Cip were chosen to perform all experiments. Raman and IR absorption spectra were recorded 120 min after the antibiotic addition. With the help of Principal Components Analysis (PCA), it was possible to discriminate between the antibiotic-treated samples and the control (antibiotic-free culture) and identify the most important spectral changes in the variance of samples. Compared to the control (antibiotic-free culture), Raman and IR absorption of *V. parahaemolyticus* in the presence of Amp at 20 µg/ml indicated an increase in proteins and lipids, a decrease in polysaccharides. For Ctx treatment, a decrease in protein bands in both Raman and IR absorption spectra, an increase in polysaccharides in IR absorption spectra were detected. Compared to Ctx-treated sample, the addition of Amp in the culture resulted in an increase of protein bands and polysaccharides in IR spectra. Tet treatment caused a decrease in protein bands in both Raman and IR spectra, a dramatic decrease in phenylalanine in Raman and an increase in polysaccharides in IR. Cip addition led to a decrease in protein bands, an increase in polysaccharides in both Raman and IR spectra, a decrease in nucleic acids and lipids in Raman. Molecular changes in Raman and IR absorption spectra were mainly explained by the mechanisms of action of antibiotics against *V. parahaemolyticus*.

This chapter indicates that Raman and IR spectroscopies combined with principal component analysis can be used to detect molecular changes caused by different classes of antibiotics against *V. parahaemolyticus*. Both Raman and IR showed spectral changes in proteins and polysaccharides. In addition, changes in phenylalanine, lipids and nucleic acids were observed in Raman spectra. Moreover, Amp – resistant mechanism can be determined due to an increase of protein content in both Raman and IR spectroscopies. Therefore, it was clearly shown that both Raman and IR spectroscopies can contribute efficiently to the understanding of the

mechanisms of action of antibiotics against *V. parahaemolyticus* or those involved in its resistance as was shown in our study for Amp. This work paved the way for future investigations to differentiate resistant and sensitive strains and to further understand the mechanisms involved in bacterial resistance to antibiotics by applying Raman and IR spectroscopies.

CHAPTER IV: SUMMARY AND OUTLOOK

IV.1 Summary

This work has shown how vibrational spectroscopic techniques (Raman and IR) detect metabolic changes occurring during the bacterial growth and molecular modifications induced by different classes of antibiotics against two bacterial models, *E. coli* and *V. parahaemolyticus*. Raman spectroscopy provides the overall biochemical composition of the bacteria, like phenylalanine, nucleic acids, proteins, lipids, carbohydrates. Likewise, IR absorption spectroscopy also reveals the biochemical composition of the bacteria, with special focus on the protein components (especially due to intense peptide bond variations). Raman and IR spectra will be coupled to Principal Components Analysis to determine the important spectral changes in the variance, allowing comprehensive interpretation of the results. It was found that during the bacterial growth the protein content increased in both Raman and IR spectra due to an enhanced synthesis of ribosomes for the translation and later due to an augmented synthesis of enzymes and other functional proteins. In addition, changes in phenylalanine, lipids and carbohydrates were also noticed. These metabolic changes allowed a classification of the bacterial spectra according to the different growth time points (3, 6, 8, 24 h of incubation in *E. coli* and 8, 10, 24 h of incubation in *V. parahaemolyticus*).

In order to detect molecular modifications induced by antibiotics using Raman and IR spectroscopies, three classes of drugs were used in the study, such as β -lactams (Amp, Ctx – cell wall inhibitors), tetracyclines (Tet – protein synthesis inhibitor) and fluoroquinolones (Cip – DNA replication inhibitor). The MIC and MBC values of Amp, Ctx, Cip against *E. coli* were equivalent and corresponded to 5 $\mu\text{g/ml}$, 0.2 $\mu\text{g/ml}$ and 0.1 $\mu\text{g/ml}$, respectively, showing that these antibiotics are bactericidal. The MIC and MBC values of Tet against *E. coli* were 5 $\mu\text{g/ml}$ and 40 $\mu\text{g/ml}$, respectively, indicating that the antibiotic is bacteriostatic. The antibiotic concentration of 8 MIC (40 $\mu\text{g/ml}$ for Amp, 1.6 $\mu\text{g/ml}$ for Ctx, 40 $\mu\text{g/ml}$ for Tet and 0.8 $\mu\text{g/ml}$ for Cip) was chosen to perform the experiments. Compared to the control (antibiotic-free culture), the inactivation of viable cells after the antibiotic addition was approximately 99.99% for Amp, Ctx and Cip (bactericidal drugs); 90% for Tet (bacteriostatic drug). Raman and IR absorption spectra were recorded 120 min after Amp, Ctx, Tet addition and 90 min after Cip addition. Amp and Ctx additions led to a decrease of protein bands in both Raman and IR absorption spectra, an increase of carbohydrates in IR absorption spectra. After Tet treatment, an increase of nucleic acids and a dramatic decrease of phenylalanine in Raman, a decrease of the amide I and the amide II of proteins, an increase of the amide III in IR were detected. In case of

Cip, an increase of nucleic acids in Raman spectra, an increase of proteins in IR spectra were noticed. Molecular changes in Raman and IR spectra were mainly explained by the mechanisms of action of antibiotics and allowed a classification between the antibiotic-treated samples and the control for the three classes.

V. parahaemolyticus strain used in the study is resistant to Amp up to 50 µg/ml. The concentration of 20 µg/ml was used to differentiate Amp-resistant cells without and in the presence of Amp. The MIC and MBC values of Ctx, Cip against *V. parahaemolyticus* were equivalent and corresponded to 0.06 µg/ml and 0.05 µg/ml, respectively. The MIC and MBC values of Tet against *V. parahaemolyticus* were 0.1 µg/ml and 0.2 µg/ml, respectively. The antibiotic concentrations of 12MIC for Ctx (0.72 µg/ml), 8MIC for Tet (0.8 µg/ml) and 18MIC for Cip (0.9 µg/ml) were chosen to carry out the experiments. Compared to the control, the inactivation of viable cells after the antibiotic treatment was approximately 98% for Ctx, 99% for both Tet and Cip. Compared with the control (Amp-free culture) the presence of Amp at 20 µg/ml caused an increase of protein bands in both Raman and IR, an increase of lipids in Raman, a decrease of polysaccharides in IR. Clear segregation between the Amp-added sample and the Amp-free culture was observed. The mechanisms involved in antibiotic resistance can be used to explain the findings. For cefotaxime, a decrease of protein bands in both Raman and IR, an increase of polysaccharides in IR were detected. Tetracycline addition led to a decrease of phenylalanine in Raman, a decrease of protein in both Raman and IR and an increase of polysaccharides in IR. Cip treatment resulted in an increase of polysaccharides and a decrease of proteins in both Raman and IR. Clear discrimination of antibiotic-treated samples compared to the control was recorded for the three classes. Like *E. coli*, molecular modifications in Raman and IR spectra can be interpreted by the mechanisms of action of antibiotics against *V. parahaemolyticus*. In particular, an increase of polysaccharides detected in the three classes of antibiotics can be interpreted by the enhanced biofilm formation against harmful factors in environment (antibiotics in this case), allowing the survival of the bacterium in unfavorable life conditions.

In brief, the experiments performed in this work demonstrated how Raman and IR spectroscopies can be used in combination with Principal Components Analysis to detect metabolic changes during the bacterial growth and molecular modifications induced by different classes of antibiotics against *E. coli* and *V. parahaemolyticus*. The results encourage the

continuation of the research in this field and further investigations will be presented in the next paragraph.

IV.2 Outlook: Further experiments

It was shown that the effects of antibiotics against *E. coli* and *V. parahaemolyticus* can be detected via Raman and IR spectroscopies. Three different classes of antibiotics were chosen to carry out the experiments (β -lactams: Amp, Ctx – cell wall synthesis inhibitor; tetracyclines: Tet – protein synthesis inhibitor and fluoroquinolones: Cip – DNA replication inhibitor) in two Gram-negative bacteria (*E. coli* and *V. parahaemolyticus*). In further investigations, other classes of antibiotics and other bacteria (Gram-positive, spore-forming bacteria, pathogenic bacteria) should be tested to comprehensively assess molecular changes induced by antibiotics against bacteria. In addition, the concentration of 8MIC was chosen for Amp, Ctx, Tet and Cip in case of *E. coli*. In *V. parahaemolyticus*, the different concentrations were applied like 12MIC for Ctx, 8MIC for Tet and 18MIC for Cip. In further experiments more different concentrations of antibiotics, like below, around and above MIC should be incorporated to assess molecular changes as a function of antibiotic concentrations.

In addition to two bacterial models (*E. coli* and *V. parahaemolyticus*) studied in this work, other species can be chosen to evaluate molecular changes caused by antibiotics, such as *Staphylococcus aureus*, *Streptococcus pneumoniae*, *Salmonella* spp., *Pseudomonas*, pathogenic *E. coli* strains, spore-forming bacteria (*Clostridium* spp., *Bacillus* spp.)...

Furthermore, it was clearly indicated that the mechanisms involved in antibiotic resistance can be determined by means of Raman and IR spectroscopies as was shown in our study for Amp in *V. parahaemolyticus*. The result paves the way for future investigations to discriminate resistant (especially multidrug resistant strains) and sensitive strains and to further understand the mechanisms related to bacterial resistance to antibiotics. Such research could facilitate the detection and the discrimination of bacteria isolated from reservoirs of resistance in the environment or in the food chain.

REFERENCES

1. Tanwar J., Das S., Fatima Z., Hameed S. (2014). Multidrug resistance: An emerging crisis. *Interdiscip. Perspect. Infect. Dis.*, 2014. Article ID 541340.
2. Nikaido H. (2009). Multidrug resistance in bacteria. *Annu. Rev. Biochem.*, 78, 119-146.
3. Naumann D., Keller S., Helm D., Schultz Ch., Schrader B. (1995). FT-IR spectroscopy and FT-Raman spectroscopy are powerful analytical tools for the non-invasive characterization of intact microbial cells. *J. Mol. Struct.*, 347, 399-406.
4. Kastanos E., Kyriakides A., Hadjigeorgiou K., Pitris C. (2011). Identification and antibiotic sensitivity of UTI pathogens using Raman spectroscopy. InTech. *Urinary Tract Infections*. Chapter 12, 207-226
5. Guibet F., Amiel C., Cadot P., Cordevant C., Desmonts M. H., Lange M., Marecat A., Travert J., Denis C., Mariey L. (2003). Discrimination and classification of *Enterococci* by Fourier transform infrared (FT-IR) spectroscopy. *Vib. Spectrosc.*, 33, 133-142.
6. Vossenbergh J., Tervahauta H., Maquelin K., Blokker-Koopmans C. H. W., Uytewaal-Aarts M., Kooij D., Wezel A. P., Gaag B. (2013). Identification of bacteria in drinking water with Raman spectroscopy. *Anal. Methods*, 5, 2679-2687.
7. Goeller L. J., Riley M. R. (2007). Discrimination of bacteria and bacteriophages by Raman spectroscopy and surface-enhanced Raman spectroscopy. *Appl. Spectrosc.*, 61, 7, 679-685.
8. Al-Holy M. A., Lin M., Al-Qadiri H., Cavinato A. G., Rasco B. A. (2006). Classification of foodborne pathogens by fourier transform infrared spectroscopy and pattern recognition techniques. *J. Rapid Methods Autom. Microbiol.*, 14, 189-200.
9. Ngo-Thi N. A., Kirschner C., Naumann D. (2003). Characterization and identification of microorganisms by FT-IR microspectrometry. *J. Mol. Struct.*, 661 - 662, 371-380.
10. Meisel S., Stockel S., Rosch P., Popp J. (2014). Identification of meat-associated pathogens via Raman microspectroscopy. *Food Microbiol.*, 38, 36-43.
11. Filip Z., Hermann S., Demnerova K. (2008). FT-IR spectroscopic characteristics of differently cultivated *Escherichia coli*. *Czech J. Food Sci.*, 26, 6, 458-463.
12. Singh B., Gautam R., Kumar S., Vinay Kumar B. N., Nongthomba U., Nandi D., Mukherjee G., Santosh V., Somasundaram K., Umopathy S. (2012). Application of vibrational microspectroscopy to biology and medicine. *Current Science*, 102, 2, 232-244.

13. Lu X., Al-Qadiri H. M., Lin M., Rasco B. A. (2011). Application of mid-infrared and Raman spectroscopy to the study of bacteria. *Food Bioprocess Technol.*, 4, 919-935.
14. Ferraro J. R., Nakamoto K., Brown C. W. (2003). Introductory Raman spectroscopy. Elsevier, 2nd edition.
15. Stuart B. (2004). Infrared spectroscopy: Fundamentals and applications. John Wiley and Sons.
16. Nawrocka A., Lamorska J. (2013). Determination of food quality by using spectroscopic methods. *Advances in Agrophysical Research*. Intech. Chapter 14, 347-367.
17. Neugebauer U. (2007). Characterization of bacteria, antibiotics of the fluoroquinolone type and their biological targets DNA and gyrase utilizing the unique potential of vibrational spectroscopy. Ph.D dissertation of Friedrich-Schiller-Universität Jena
18. Vankeirsbilck T., Vercauteren A., Baeyens W., Van der Weken G., Verpoort F., Vergote G., Remon J. P. (2002). Applications of Raman spectroscopy in pharmaceutical analysis. *Trends Analyt. Chem.*, 21, 12, 869-877.
19. Goodwin J. R. (2006). Vibrational microspectroscopy of bacterial colonies. Ph.D dissertation of Queensland University..
20. Huang W. E., Li M., Jarvis R. M., Goodacre R., Banwart S. A. (2010). Shining light on the microbial world: The application of Raman microspectroscopy. Burlington, 153-186.
21. Bommel J. H. (2002). Confocal Raman microspectroscopy a novel diagnostic tool in medical microbiology. Ph.D dissertation of Rotterdam University.
22. Clarke S. J., Littleford R. E., Smith W. E., Goodacre R. (2005). Rapid monitoring of antibiotics using Raman and surface enhanced Raman spectroscopy. *Analyst*, 130, 1019-1026.
23. Kerr L. T., Byrne H. J., Hennelly B. M. (2015). Optimal choice of sample substrate and laser wavelength for Raman spectroscopic analysis of biological specimen. *Analytical Methods*, 7, 5041-5952, 1-14.
24. Puppels G. J., Mul F. F. M., Otto C., Greve J., Robert-Nicoud M., Arndt-Jovin D. J., Jovin T. M. (1990). Studying single living cells and chromosomes by confocal Raman microspectroscopy. *Nature*, 347, 20, 301-303.
25. Premasiri W. R., Moir D. T., Klempner M. S., Krieger N. G., Jones I. I. G., Ziegler L. D. (2005). Characterization of the surface enhanced Raman scattering (SERS) of bacteria. *J.*

Phys. Chem., 109, 1, 312-320.

26. Harz M., Rosch P., Popp J. (2009). Vibrational spectroscopy - a powerful tool for the rapid identification of microbial cells at the single-cell level. *Cytometry*, 75A, 104-113.
27. Sivanesan A., Witkowska E., Adamkiewicz W., Dziewit L., Kaminska A., Waluka J. (2014). Nanostructured silver-gold bimetallic SERS substrates for selective identification of bacteria in human blood. *Analyst*, 139, 1037-1043.
28. Efrima S., Zeiri L. (2009). Understanding SERS of bacteria. *J. Raman Spectrosc.*, 40, 277-288.
29. Kairyte K., Luksiene Z., Pucetaite M., Sablinskas V. (2012). Differentiation of bacterial strains by means of surface enhanced FT-Raman spectroscopy. *Lith. J. Phys.*, 52, 3, 276-283.
30. Lee P. C., Meisel D. (1982). Adsorption and surface-enhanced Raman of dyes on silver and gold sols. *J. Phys. Chem.*, 86, 17, 3391-3395.
31. Sharma B., Frontiera R. R., Henry A.-I., Ringe E., Van Duyne R. P. (2012). SERS: Materials, applications, and the future. *Mater. Today*, 15, 1-2.
32. Maquelin K., Kirschner C., Choo-Smith L.-P., Braak N., Endtz H. Ph., Naumann D., Puppels G. J. (2002). Identification of medically relevant microorganisms by vibrational spectroscopy. *J. Microbiol. Methods*, 51, 255-271.
33. Jarvis R. M., Goodacre R. (2004). Discrimination of bacteria using surface-enhanced Raman spectroscopy. *Anal. Chem.*, 76, 1, 40-47.
34. Jarvis R. M., Goodacre R. (2008). Characterisation and identification of bacteria using SERS. *Chem. Soc. Rev.*, 37, 5, 931-936.
35. Doris C. S. (2014). Comparative evaluation of the ascorbic acid content of mineral ascorbate and ascorbic acid tablets marketed in Zaria. Ph.D dissertation of Ahmadu Bello University.
36. Alvarez-Ordóñez A., Mouwen D. J. M., Lopez M., Prieto M. (2011). Fourier transform infrared spectroscopy as a tool to characterize molecular composition and stress response in foodborne pathogenic bacteria. *J. Microbiol. Methods*, 84, 369-378.
37. Davis R., Mauer L. J. (2011). Fourier transform infrared (FT-IR) spectroscopy: A rapid tool for detection and analysis of foodborne pathogenic bacteria. *Current Research, Technology and Education Topics in Applied Microbiology and Microbial Biotechnology*.

38. Barth A. (2007). Infrared spectroscopy of proteins. *Biochim. Biophys. Acta*, 1767, 1073-1101.
39. Ashton L., Lau K., Winder C. L., Goodacre R. (2011). Raman spectroscopy: Lighting up the future of microbial identification. *Future Microbiol.*, 6, 9, 991-997.
40. Moen B., Janbu A. O., Langsrud S., Langsrud Ø., Hobman J. L., Constantinidou C., Kohler A., Rudi K. (2009). Global responses of *Escherichia coli* to adverse conditions determined by microarrays and FT-IR spectroscopy. *Can. J. Microbiol.*, 55, 714–728.
41. AlRabiah H. (2014). Advanced metabolomics for the discrimination of uropathogenic *Escherichia coli* and their response to antibiotics. Ph.D dissertation of Manchester University .
42. Stöckel S., Kirchhoff J., Neugebauer U., Rösch P., Popp J. (2016). The application of Raman spectroscopy for the detection and identification of microorganisms. *J. Raman Spectrosc.*, 47, 89-109.
43. Paret M. L., Sharma S. K., Green L. M., Alvarez A. M. (2010). Biochemical characterization of Gram-positive and Gram-negative plant-associated bacteria with micro-Raman spectroscopy. *Appl. Spectrosc.*, 64, 4, 433-441.
44. Wallach D. F. H., Verma S. P., Fookson J. (1979). Application of laser Raman and infrared spectroscopy to the analysis of membrane structure. *Biochim. Biophys. Acta*, 559, 153-208.
45. Serban D., Benevides J. M., Thomas Jr. G. J. (2002). DNA secondary structure and Raman markers of supercoiling in *Escherichia coli* plasmid pUC19. *Biochemistry*, 41, 3, 847-853.
46. Jiang W., Saxena A., Song B., Ward B. B., Beveridge T. J. ,Myneni S. C. B. (2004). Elucidation of functional groups on Gram-positive and Gram-negative bacterial surfaces using Infrared spectroscopy. *Langmuir*, 20, 11433-11442.
47. Helm D., Naumann D. (1995). Identification of some bacterial cell components by FT-IR spectroscopy. *FEMS Microbiol. Lett.*, 126, 75-80.
48. Naumann D., Barnickel G., Bradaczek H., Labischinski H., Giesbrecht P. (1982). Infrared spectroscopy, a tool for probing bacterial peptidoglycan. Potentialities of infrared spectroscopy for cell wall analytical studies and rejection of models based on crystalline chitin. *Eur. J. Biochem.*, 125, 505-515.
49. Arrondo J. L. R., Goni F. M. (1999). Structure and dynamics of membrane proteins as studied by infrared spectroscopy. *Prog. Biophys. Mol. Biol.*, 72, 367-405.

50. Strola S. A., Marcoux P. R., Schultz E., Perenon R., Simon A.-C., Espagnon I., Allier C. P., Dinten J.-M. (2014). Differentiating the growth phases of single bacteria using Raman spectroscopy. *Proc. SPIE 8939 Biomedical Vibrational Spectroscopy VI: Advances in Research and Industry*, 8939, 893905, 1-9.
51. Al-Qadiri H. M., AL-Alami N. I., Al-Holy M. A., Rasco B. A. (2008). Using Fourier Transform Infrared (FT-IR) absorbance spectroscopy and multivariate analysis to study the effect of chlorine-induced bacterial injury in water. *J. Agric. Food Chem.*, 56, 8992-8997.
52. Escoriza M. F., Vanbriesen J. M., Stewart S., Maier J. (2006). Studying bacterial metabolic states using Raman spectroscopy. *Appl. Spectrosc.*, 60, 9, 971-976.
53. Choo-Smith L.-P., Maquelin K., Van Vreeswijk T., Bruining H. A., Puppels G. J., Ngo Thi N. A., Kirschner C., Naumann D., Ami D., Villa A. M., Orsini F., Doglia S. M., Lamfarraj H., Sockalingum G. D., Manfait M., Allouch P., Endtz H. P. (2001). Investigating microbial (Micro) colony heterogeneity by vibrational spectroscopy. *Appl. Environ. Microbiol.*, 67, 4, 1461-1469.
54. Kemmler M., Rodner E., Rosch P., Popp J., Denzler J. (2013). Automatic identification of novel bacteria using Raman spectroscopy and Gaussian processes. *Anal. Chim. Acta*, 794, 29-37.
55. Espagnon I., Ostrovskii D., Mathey R., Dupoy M., Joly P. L., Novelli-Rousseau A., Pinston F., Gal O., Mallard F., Leroux D. F. (2014). Direct identification of clinically relevant bacterial and yeast microcolonies and macrocolonies on solid culture media by Raman spectroscopy. *J Biomed Opt*, 19, 2.
56. Maquelin K., Choo-Smith L.-P., Vreeswijk T., Endtz H. Ph., Smith B., Bennett R., Bruining H. A., Puppels G. J. (2000). Raman spectroscopic method for identification of clinically relevant microorganisms growing on solid culture medium. *Anal. Chem.*, 72, 1.
57. Almarashi J. F. M., Kapel N., Wilkinson T. S., Telle H. H. (2012). Raman spectroscopy of bacterial species and strains cultivated under reproducible conditions. *Int. J. Spectrosc.*, 27, 361-365.
58. Ciobota V., Burkhardt E.-M., Schumacher W., Rosch P., Kusel K., Popp J. (2010). The influence of intracellular storage material on bacterial identification by means of Raman spectroscopy. *Anal. Bioanal. Chem.*, 397, 2929-2937.
59. Huang W. E., Griffiths R. I., Thompson I. P., Bailey M. J., Whiteley A. S. (2004). Raman microscopic analysis of single microbial cells. *Anal. Chem.*, 76, 15, 4452-4458.
60. Rosch P., Harz M., Schmitt M., Peschke K.-D., Ronneberger O., Burkhardt H., Motzkus H.-W., Lankers M., Hofer S., Thiele H., Popp J. (2005). Chemotaxonomic identification of

- single bacteria by micro-Raman spectroscopy: Application to clean-room-relevant biological contaminations. *Appl. Environ. Microbiol.*, 71, 3, 1626-1637.
61. Muhamadali H., Chisanga M., Subaihi A., Goodacre R. (2015). Combining Raman and FT-IR spectroscopy with quantitative isotopic labeling for differentiation of *E. coli* cells at community and single cell levels. *Anal. Chem.*, 87, 4578-4586.
 62. Schmid U., Rosch P., Krause M., Harz M., Popp J., Baumann K. (2009). Gaussian mixture discriminant analysis for the single-cell differentiation of bacteria using micro-Raman spectroscopy. *Chemometr Intell Lab Syst*, 96, 159-171.
 63. Mobili P., Londero A., Antoni G., Gomez-Zavaglia A., Araujo-Andrade C., Avila-Donoso H., Ivanov-Tzonchev R., Moreno I., Frausto-Reyes C. (2010). Multivariate analysis of Raman spectra applied to microbiology: Discrimination of microorganisms at the species level. *Revista Mexicana de Fisica*, 56, 5, 378-385.
 64. Schuster K. C., Urlaub E., Gapes J. R. (2000). Single-cell analysis of bacteria by Raman microscopy: spectral information on the chemical composition of cells and on the heterogeneity in a culture. *J. Microbiol. Methods*, 42, 29-38.
 65. Kastanos E., Kyriakides A., Hadjigeorgiou K., Pitris C. (2011). A novel method for bacterial UTI diagnosis using Raman spectroscopy. *Inter. J. Spectrosc.*, 2012. Article ID 195317.
 66. Forrester J. B., Valentine N. B., Su Y.-F., Johnson T. J. (2009). Chemometric analysis of multiple species of *Bacillus* bacterial endospores using infrared spectroscopy: Discrimination to the strain level. *Anal. Chim. Acta*, 651, 24-30.
 67. Davis R., Paoli G., Mauer L. J. (2012). Evaluation of Fourier transform infrared (FT-IR) spectroscopy and chemometric as a rapid approach for sub-typing *Escherichia coli* O157:H7 isolates. *Food Microbiol.*, 31, 181-190.
 68. Davis R., Deering A., Burgula Y., Mauer L. J., Reuhs B. L. (2011). Differentiation of live, dead and treated cells of *Escherichia coli* O157:H7 using FT-IR spectroscopy. *J. Appl. Microbiol.*, 112, 743-751.
 69. Maquelin K., Kirschner C., Choo-Smith L.-P., Ngo-Thi N. A., Vreeswijk T., Stammler M., Endtz H. P., Bruining H. A., Naumann D., GPuppels G. J. (2003). Prospective study of the performance of vibrational spectroscopies for rapid identification of bacterial and fungal pathogens recovered from blood cultures. *J. Clin. Microbiol.*, 41, 1, 324-329.
 70. Filip Z., Hermann S. (2001). An attempt to differentiate *Pseudomonas* spp. and other soil bacteria by FT-IR spectroscopy. *Eur. J. Soil Biol.*, 37, 137-143.

71. Zeroual W., Manfait M., Choisy C. (1995). FT-IR spectroscopy study of perturbations induced by antibiotic on bacteria (*Escherichia coli*). *Pathologie Biologie*, 43, 4, 300-305.
72. Athamneh A. I. M., Alajlouni R. A., Wallace R. S., Seleem M. N., Senger R. S. (2014). Phenotypic profiling of antibiotic response signatures in *Escherichia coli* using Raman spectroscopy. *Antimicrob. Agents Chemother.*, 58, 3, 1302-1314.
73. Neugebauer U., Schmid U., Baumann K., Holzgrabe U., Ziebuhr W., Kozitskaya S., Kiefer W., Schmitt M., Popp J. (2006). Characterization of bacterial growth and the influence of antibiotics by means of UV resonance Raman spectroscopy. *Biopolymers*, 82, 306-311.
74. Moritz T. J., Polage C. R., Taylor D. S., Krol D. M., Lane S. M., Chan J. W. (2010). Evaluation of *Escherichia coli* cell response to antibiotic treatment by use of Raman spectroscopy with laser tweezers. *J. Clin. Microbiol.*, 48, 11, 4287-4290.
75. Sockalingum G. D., Bouhedja W., Pina P., Allouch D., Mandray C., Labia R., Millot J. M., Manfait M. (1997). ATR-FTIR spectroscopic investigation of imipenem-susceptible and -resistant *Pseudomonas aeruginosa* isogenic strains. *Biochem. Biophys. Res. Commun.*, 232, 240-246. Article RC976263.
76. Amiali M. N. (2003). Identification of antibiotic-resistant *Staphylococci* and epidemiological typing of methicillin-resistant *Staphylococcus aureus* by Fourier Transform Infrared spectroscopy. Ph.D dissertation of McGill University .
77. Torkabadi H. H. (2016). Raman microscopic studies of antimicrobial reactions in solution, crystals and bacterial cells. Ph.D dissertation of Case Western Reserve University.
78. Walter A., Reinicke M., Bocklitz T., Schumacher W., Rösch P., Kothe E., Popp J. (2011). Raman spectroscopic detection of physiology changes in plasmid-bearing *Escherichia coli* with and without antibiotic treatment. *Anal. Bioanal. Chem.*, 400, 2763-2773.
79. Bouhedja W., Sockalingum G. D., Pina P., Allouch P., Bloy C., Labia R., Millot J. M., Manfait M. (1997). ATR-FTIR spectroscopic investigation of *E.coli* transconjugants beta-lactams-resistance phenotype. *FEBS Lett.*, 412, 39-42.
80. Lechowicz L., Urbaniak M., Adamus-Białek W., Kaca W. (2013). The use of infrared spectroscopy and artificial neural networks for detection of uropathogenic *Escherichia coli* strains' susceptibility to cephalothin. *Acta ABP Biochimica Polonica*, 60, 4, 713-718.
81. Kirschner C., Ngo Thi N. A., Naumann D. (1999). FT-IR spectroscopic investigations of antibiotic sensitive and resistant microorganisms. Springer Netherlands, 561-526.
82. Schroder U.-Ch., Beleites C., Assmann C., Glaser U., Hubner U., Pfister W., Fritzsche W., Popp J., Neugebauer U. (2015). Detection of vancomycin resistances in *enterococci* within 3

1/2 hours. *Sci Rep*, 5, 8217.

83. Qi L., Li H., Zhang C., Liang B., Li J., Wang L., Du X., Liu X., Qiu S., Song H. (2016). Relationship between antibiotic resistance, biofilm formation, and biofilm-specific resistance in *Acinetobacter baumannii*. *Front. Microbiol.*, 7, 1-10. Article 483.
84. Chao Y., Zhang T. (2012). Surface-enhanced Raman scattering (SERS) revealing chemical variation during biofilm formation: From initial attachment to mature biofilm. *Anal. Bioanal. Chem.*, 404, 1465-1475.
85. Samek O., Al-Marashi J. F. M., Telle H. H. (2010). The potential of Raman spectroscopy for the identification of biofilm formation by *Staphylococcus epidermidis*. *Laser Phys. Lett.*, 7, 5, 378-383.
86. Delille A. (2007). Etude in situ, par spectroscopie infrarouge en mode ATR, des premières étapes de la formation d'un biofilm de *Pseudomonas fluorescens* et de sa réponse aux variations de la quantité de carbone organique dissous : application à la détection précoce du changement de la qualité microbiologique d'une eau de distribution. Thèse de l'Université de Henri Poincaré - Nancy I.
87. Anderl J. N., Franklin M. J., Stewart P. S. (2000). Role of antibiotic penetration limitation in *Klebsiella pneumoniae* biofilm resistance to ampicillin and ciprofloxacin. *Antimicrob. Agents Chemother.*, 44, 7, 1818-1824.
88. Mah T.-F. C., OToole G. A. (2001). Mechanisms of biofilm resistance to antimicrobial agents. *Trends Microbiol.*, 9, 1, 34-39.
89. Desai M., Buhler T., Weller P. H., Brown M. R. W. (1998). Increasing resistance of planktonic and biofilm cultures of *Burkholderia cepacia* to ciprofloxacin and ceftazidime during exponential growth. *J. Antimicrob. Chemother.*, 42, 153-160.
90. Paraje M. G. (2011). Antimicrobial resistance in biofilm. *Science against microbial pathogens*, 736-744.
91. Kusic D., Kampe B., Ramoji A., Neugebauer U., Rosch P., Popp J. (2015). Raman spectroscopic differentiation of planktonic bacteria and biofilms. *Anal. Bioanal. Chem.*, 407, 6803-6813.
92. Sandt C., Smith-Palmer T., Pink J., Brennan L., Pink D. (2007). Confocal Raman microspectroscopy as a tool for studying the chemical heterogeneities of biofilms in situ. *J. Appl. Microbiol.*, 103, 1808-1820.
93. Delille A., Quiles F., Humbert F. (2007). In situ monitoring of the nascent *Pseudomonas fluorescens* biofilm response to variations in the dissolved organic carbon level in low-

nutrient water by Attenuated Total Reflectance-Fourier Transform Infrared spectroscopy. *Appl. Environ. Microbiol.*, 73, 18, 5782-5788.

94. Assaf A., Cordella C. B. Y., Thouand G. (2014). Raman spectroscopy applied to the horizontal methods ISO 6579:2002 to identify *Salmonella* spp. in the food industry. *Anal. Bioanal. Chem.*, 406, 4899-4910.
95. Al-Qadiri H. M., Lin M., Cavinato A. G., Rasco B. A. (2006). Fourier transform infrared spectroscopy, detection and identification of *Escherichia coli* O157:H7 and *Alicyclobacillus* strains in apple juice. *Int. J. Food Microbiol.*, 111, 73-80.
96. Al-Holy M. A., Lin M., Cavinato A. G., Rasco B. A. (2006). The use of Fourier transform infrared spectroscopy to differentiate *Escherichia coli* O157:H7 from other bacteria inoculated into apple juice. *Food Microbiol.*, 23, 162-168.
97. Argyri A. A., Jarvis R. M., Wedge D., Xu Y., Panagou E. Z., Goodacre R., Nychas G.-J. E. (2013). A comparison of Raman and FT-IR spectroscopy for the prediction of meat spoilage. *Food Control*, 29, 461-470.
98. Sowoidnich K., Schmidt H., Kronfeldt H.-D., Schwagele F. (2012). A portable 671 nm Raman sensor system for rapid meat spoilage identification. *Vib. Spectrosc.*, 62, 70-76.
99. Papadopoulou O., Panagou E. Z., Tassou C. C., Nychas G.-J. E. (2011). Contribution of Fourier transform infrared (FTIR) spectroscopy data on the quantitative determination of minced pork meat spoilage. *Food Res. Int.*, 44, 3264-3271.
100. Whittaker P., Mossoba M. M., Al-Khaldi S., Fry F. S., Dunkel V. C., Tall B. D., Yurawecz M. P. (2003). Identification of foodborne bacteria by infrared spectroscopy using cellular fatty acid methyl esters. *J. Microbiol. Methods*, 55, 709-716.
101. Kusic D., Kampe B., Rosch P., Popp J. (2014). Identification of water pathogens by Raman microspectroscopy. *Water Res.*, 48, 179-189.
102. Tripathi A., Jabbour R. E., Treado P. J., Neiss J. H., Nelson M. P., Jensen J. L., Snyder A. P. (2008). Waterborne pathogen detection using Raman spectroscopy. *Appl. Spectrosc.*, 62, 1.
103. Escoriza M. F., VanBriesen J. M., Stewart S., Maier J., Treado P. J. (2006). Raman spectroscopy and chemical imaging for quantification of filtered waterborne bacteria. *J. Microbiol. Methods*, 66, 63-72.
104. Escoriza M. F., Vanbriesen J. M., Stewart S., Maier J. (2007). Raman spectroscopic discrimination of cell response to chemical and physical inactivation. *Appl. Spectrosc.*, 61, 8, 812-823.

105. Lin M., Al-Holy M., Al-Qadiri H., Kang D.-H., Cavinato A. G., Huang Y., Rasco B. A. (2004). Discrimination of intact and injured *Listeria monocytogenes* by Fourier Transform Infrared spectroscopy and principal component analysis. *J. Agric. Food Chem.*, 52, 5769-5772.
106. Al-Qadiri H. M., Lin M., Al-Holy M. A., Cavinato A. G., Rasco B. A. (2008). Detection of sublethal thermal injury in *Salmonella enterica* serotype typhimurium and *Listeria monocytogenes* using Fourier transform infrared (FT-IR) spectroscopy (4000 to 600 cm^{-1}). *J. Food Sci.*, 73, 2, M54-M61.
107. Lorin-Latxague C., Melin A.-M. (2005). Radical induced damage of *Micrococcus luteus* bacteria monitored using FT-IR spectroscopy. *Spectroscopy*, 19, 17-26.
108. Paudel A., Rajjada D., Rantanen J. (2015). Raman spectroscopy in pharmaceutical product design. *Adv. Drug Deliv. Rev.*, 89, 3-20.
109. Mak P. J., Denisov I. G., Grinkova Y. V., Sligar S. G., Kincaid J. R. (2011). Defining CYP3A4 structural responses to substrate binding. Raman spectroscopic studies of a nanodisc-incorporated mammalian Cytochrome P450. *J. Am. Chem. Soc.*, 133, 5, 1357-1366.
110. Farquharson S., Shende C., Inscore F. E., Maksymiuk P., Gift A. (2005). Analysis of 5-fluorouracil in saliva using surface-enhanced Raman spectroscopy. *J. Raman Spectrosc.*, 36, 208-212.
111. Torkabadi H. H., Bethel C. R., Papp-Wallace K. M., Boer P. A. J., Bonomo R. A., Carey P. R. (2014). Following drug uptake and reactions inside *Escherichia coli* by Raman microspectroscopy. *Biochemistry*, 53, 4113-4121.
112. Kuriyama A., Ozaki Y. (2014). Assessment of active pharmaceutical ingredient particle size in tablets by Raman chemical imaging validated using polystyrene microsphere size standards. *AAPS PharmSciTech*, 15, 2, 375-386.
113. Scoutaris N., Gellert P. R., Alexander M., Roberts C. J. (2011). Inkjet printing as a novel medicine formulation technique. *J. Control Release*, 156, 2, 179-185.
114. Sacré P.-Y., Lebrun P., Chavez P.-F., Bleye C., Netchacovitch L., Rozet E., Klinkenberg R., Streel B., Hubert P., Ziemons E. (2014). A new criterion to assess distributional homogeneity in hyperspectral images of solid pharmaceutical dosage forms. *Anal. Chim. Acta*, 818, 7-14.
115. Wartewig S., Neubert R. H. H. (2005). Pharmaceutical applications of Mid-IR and Raman spectroscopy. *Adv. Drug Deliv. Rev.*, 57, 1140-1170.

116. Armstrong C. L., Edwards H. G. M., Farwell D. W., Williams A. C. (1996). Fourier transform Raman microscopic study of drug distribution in a transdermal drug delivery device. *Vib. Spectrosc.*, 11, 105-113.
117. Chan K. L., Hammond S. V., Kazarian S. G. (2003). Applications of attenuated total reflection infrared spectroscopy imaging to pharmaceutical formulations. *Anal. Chem.*, 75, 9, 2140-2146.
118. Mariey L., Signolle J. P., Amiel C., Travert J. (2001). Discrimination, classification, identification of microorganisms using FTIR spectroscopy and chemometrics. *Vib Spectrosc.*, 26, 151-159.
119. Noor R., Islam Z., Munshi S. K., Rahman F. (2013). Influence of temperature on *Escherichia coli* growth in different culture media. *J. Pure Appl. Microbiol.*, 7, 2, 899-904.
120. Orskov I., Orskov F., Jann B., Jann K. (1977). Serology, chemistry, and genetics of O and K antigens of *Escherichia coli*. *Bacteriol. Rev.*, 41, 3, 667-710.
121. Clements A., Young J. C., Constantinou N., Frankel G. (2012). Infection strategies of enteric pathogenic *Escherichia coli*. *Gut Microbes*, 3, 2, 71-87.
122. Szmolka A., Nagy B. (2013). Multidrug resistant commensal *Escherichia coli* in animals and its impact for public health. *Front. Microbiol.*, 4. Article 258.
123. Bailey J. K., Pinyon J. L., Anantham S., Hall R. M. (2010). Commensal *Escherichia coli* of healthy humans: a reservoir for antibiotic-resistance determinants. *J. Med. Microbiol.*, 59, 1331-1339.
124. Ruy S. H., Lee J. H., Park S. H., Song M. O., Park S. H., Jung H. W., Park G. Y., Choi S. M., Kim M. S., Chae Y. Z., Park S. G., Lee Y. K. (2012). Antimicrobial resistance profiles among *Escherichia coli* strains isolated from commercial and cooked foods. *Int. J. Food Microbiol.*, 159, 3, 263-6.
125. Van T. T., Chin J., Chapman T., Tran L. T., Coloe P. J. (2008). Safety of raw meat and shellfish in Vietnam: an analysis of *Escherichia coli* isolations for antibiotic resistance and virulence genes. *Int. J. Food Microbiol.*, 124, 3, 217-23.
126. Su Y.-C., Liu C. (2007). *Vibrio parahaemolyticus*: A concern of seafood safety. *Food Microbiol.*, 24, 549-558.
127. Hassan Z. H., Zwartkruis-Nahuis J. T. M., Boer E. (2012). Occurrence of *Vibrio parahaemolyticus* in retailed seafood in The Netherlands. *Int. Food Res. J.*, 19, 1, 39-43.

128. Martinez J. L., Sanchez M. B., Martinez-Solano L., Hernandez A., Garmendia L., Fajardo A., Alvarez-Ortega C. (2009). Functional role of bacterial multidrug efflux pumps in microbial natural ecosystems. *FEMS Microbiol. Rev.*, 33, 430-449.
129. Lozano-Leon A., Torres J., Osorio C. R., Martinez-Urtaza J. (2003). Identification of tdh-positive *Vibrio parahaemolyticus* from an outbreak associated with raw oyster consumption in Spain. *FEMS Microbiol. Lett.*, 226, 281-284.
130. Martinez-Urtaza J., Lozano-Leon A., DePaola A., Ishibashi M., Shimada K., Nishibuchi M., Liebana E. (2004). Characterization of pathogenic *Vibrio parahaemolyticus* isolates from clinical sources in Spain and comparison with Asia and North American pandemic isolates. *J. Clin. Microbiol.*, 42, 10, 4672-4678.
131. Odeyemi O. A. (2016). Incidence and prevalence of *Vibrio parahaemolyticus* in seafood: a systematic review and meta-analysis. *Springerplus*, 5, 464, 1-17.
132. Bowers J., Dalsgaard A., DePaola A., Karunasagar I., McMeekin T., Nishibuchi M., Osaka K., Sumner J., Walderhaug M. (2011). Risk assessment of *Vibrio parahaemolyticus* in seafood. WHO and FAO. Microbiological Risk Assessment.
133. Yildiz F. H., Visick K. L. (2009). *Vibrio* biofilms: so much the same yet so different. *Trends Microbiol.*, 17, 3, 109-118.
134. Vongxay K., Wang S., Zhang X., Wu B., Hu H., Pan Z., Chen S. (2008). Pathogenetic characterization of *Vibrio parahaemolyticus* isolates from clinical and seafood sources. *Int. J. Food Microbiol.*, 126, 71-75.
135. McLaughlin J. B., DePaola A., Bopp C. A., Martinek K. A., Napolilli N. P., Allison C. G., Murray S. L., Thompson E. C., Bird M. M., Middaugh J. P. (2005). Outbreak of *Vibrio parahaemolyticus* gastroenteritis associated with Alaskan oysters. *N. Engl. J. Med.*, 353, 14, 1463-1470.
136. Wang L., Ling Y., Jiang H., Qiu Y., Qiu J., Chen H., Yang R., Zhou D. (2013). AphA is required for biofilm formation, motility, and virulence in pandemic *Vibrio parahaemolyticus*. *Int. J. Food Microbiol.*, 160, 245-251.
137. Wong H.-C., Liu S.-H., Wang T.-K., Lee C.-L., Chiou C.-S., Liu D.-P., Nishibuchi M., Lee B.-K. (2000). Characteristics of *Vibrio parahaemolyticus* O3:K6 from Asia. *Appl. Environ. Microbiol.*, 66, 9 (2000), 3981-3986.
138. Shinoda S. (2011). Sixty years from the discovery of *Vibrio parahaemolyticus* and some recollections. *Biocontrol Sci.*, 16, 4, 129-137.

139. Richards G. P., Fay J. P., Dickens K. A., Parent M. A., Soroka D. S., Boyd E. F. (2012). Predatory bacteria as natural modulators of *Vibrio parahaemolyticus* and *Vibrio vulnificus* in seawater and oysters. *Appl. Environ. Microbiol.*, 78, 20, 7455-7466.
140. Deepanjali A., Sanath Kumar H., Karunasagar I. (2005). Seasonal variation in abundance of total and pathogenic *Vibrio parahaemolyticus* bacteria in oysters along the Southwest coast of India. *Appl. Environ. Microbiol.*, 71, 7, 3575-3580.
141. DePaola A., Nordstrom J. L., Bowers J. C., Wells J. G., Cook D. W. (2003). Seasonal abundance of total and pathogenic *Vibrio parahaemolyticus* in Alabama oysters. *Appl. Environ. Microbiol.*, 69, 3, 1521-1526.
142. Kim Y. W., Lee S. H., Hwang I. G., Yoon K. S. (2012). Effect of temperature on growth of *Vibrio parahaemolyticus* and *Vibrio vulnificus* in flounder, salmon sashimi and oyster meat. *Int. J. Environ. Res. Public Health*, 9, 4662-4675.
143. Zhang L., Orth K. (2013). Virulence determinants for *Vibrio parahaemolyticus* infection. *Curr. Opin. Microbiol.*, 16, 70-77.
144. Cruz C. D., Hedderley D., Fletcher G. C. (2015). Long-term study of *Vibrio parahaemolyticus* prevalence and distribution in New Zealand shellfish. *Appl. Environ. Microbiol.*, 81, 7, 2320-2327.
145. Shimohata T., Takahashi A. (2010). Diarrhea induced by infection of *Vibrio parahaemolyticus*. *J. Med. Invest.*, 57.
146. Broberg C. A., Calder T. J., Orth K. (2011). *Vibrio parahaemolyticus* cell biology and pathogenicity determinants. *Microbes Infect.*, 13, 992-1001.
147. Letchumanan V., Chan K.-G., Lee L.-H. (2014). *Vibrio parahaemolyticus*: a review on the pathogenesis, prevalence, and advance molecular identification techniques. *Front. Microbiol.*, 5, 1-13. Article 705.
148. Cabello F. C. (2006). Heavy use of prophylactic antibiotics in aquaculture: A growing problem for human and animal health and for the environment. *Environ. Microbiol.*, 8, 7, 1137-1144.
149. Han J. E., Mohny L. L., Tang K. F. J., Pantoja C. R., Lightner D. V. (2015). Plasmid mediated tetracycline resistance of *Vibrio parahaemolyticus* associated with acute hepatopancreatic necrosis disease (AHPND) in shrimps. *Aquaculture Reports*, 2, 17-21.
150. Smith P. (2008). Antimicrobial resistance in aquaculture. *Rev. sci. tech. Off. int. Epiz.*, 27, 1, 243-264.

151. Phillips I., Casewell M., Cox T., Groot B., Friis C., Jones R., Nightingale C., Preston R., Waddell J. (2004). Does the use of antibiotics in food animals pose a risk to human health? A critical review of published data. *J. Antimicrob. Chemother.*, 53, 28-52.
152. Letchumanan V., Yin W.-F., Lee L.-H., Chan K.-G. (2015). Prevalence and antimicrobial susceptibility of *Vibrio parahaemolyticus* isolated from retail shrimps in Malaysia. *Front. Microbiol.*, 6, 1-11. Article 33.
153. Han F., Walker R. D., Janes M. E., Prinyawiwatkul W., Ge B. (2007). Antimicrobial susceptibilities of *Vibrio parahaemolyticus* and *Vibrio vulnificus* isolates from Louisiana gulf and retail raw oyster. *Appl. Environ. Microbiol.*, 73, 21, 7096-7098.
154. Reantaso M. B., Subasinghe R., Karunasagar I., Boyd C. (2013). FAO/MARD technical workshop on early mortality syndrome (EMS) or acute hepatopancreatic necrosis syndrome (AHPNS) of cultured shrimp. FAO Fisheries and Aquaculture Report No.1053.
155. Garrett T. R., Bhakoo M., Zhang Z. (2008). Bacterial adhesion and biofilms on surfaces. *Progress in Natural Science*, 18, 1049-1056.
156. Garcia-Gonzalo D., Pagan R. (2015). Influence of environmental factors on bacterial biofilm formation in the food industry: A review. *PostDoc. Journal*, 3, 6, 3-13.
157. Bryers J. D., Ratner B. D. (2004). Bioinspired implant materials befuddle bacteria. *ASM News*, 70, 5, 232-237.
158. Tsuneda S., Aikawa H., Hayashi H., Yuasa A., Hirata A. (2003). Extracellular polymeric substances responsible for bacterial adhesion onto solid surface. *FEMS Microbiol. Lett.*, 223, 287-292.
159. Simoes M., Simoes L. C., Vieira M. J. (2010). A review of current and emergent biofilm control strategies. *Food Science and Technology*, 43, 573-583.
160. Hall-Stoodley L., Stoodley P. (2002). Developmental regulation of microbial biofilms. *Curr. Opin. Microbiol.*, 13, 228-233.
161. Donlan R. M. (2001). Biofilm formation: A clinically relevant microbiological process. *Clin. Infect. Dis.*, 33, 1387-1392.
162. Van Houdt R., Michiels C. W. (2010). Biofilm formation and the food industry, a focus on the bacterial outer surface. *J. Appl. Microbiol.*, 1-15.
163. Hori K., Matsumoto S. (2010). Bacterial adhesion: From mechanism to control. *Biochem. Eng. J.*, 48, 424-434.

164. Srey S., Jahid I. K., Ha S.-D. (2013). Biofilm formation in food industries: A food safety concern. *Food Control*, 31, 572-585.
165. Elexson N., Yaya R., Nor A. M., Kantilal H. K., Ubong A., Yoshitsugu N., Nishibuchi M., Son R. (2014). Biofilm assessment of *Vibrio parahaemolyticus* from seafood using Random Amplified Polymorphism DNA-PCR. *Int. Food Res. J.*, 21, 1, 59-65.
166. Mizan Md. F. R., Jahid I. K., Ha S.-D. (2015). Microbial biofilms in seafood: A food-hygiene challenge. *Food Microbiol.*, 49, 41-55.
167. Kostakioti M., Hadjifrangiskou M., Hultgren S. J. (2013). Bacterial biofilms: Development, dispersal and therapeutic strategies in the dawn of the postantibiotic era. *Cold Spring Harb. Perspect. Med.*, 3, 1-23.
168. Mizan Md. F. R., Jahid I. K., Kim M., Lee K.-H., Kim T. J., Ha S.-D. (2016). Variability of biofilm formation correlates with hydrophobicity and quorum sensing among *Vibrio parahaemolyticus* isolates from food contact surfaces and distribution of genes involved in biofilm formation. *Biofouling*, 32, 4, 497-509.
169. Cortés M. E., Bonilla J. C., Sinisterra R. D. (2011). Biofilm formation, control and novel strategies for eradication. Science against microbial pathogens: communicating current research and technological advances, 896-905.
170. Elexson N., Son R., Rukayadi Y., Tuan Zainazor T. C., Nor Ainy M., Nakaguchi Y., Mitsuaki N. (2013). Biosafety of *Vibrio parahaemolyticus* biofilm from seafood using herbs and spices. *Journal of Life Medicine*, 1, 3, 71-82.
171. Poole K. (2002). Mechanisms of bacterial biocide and antibiotic resistance. *J. Appl. Microbiol.*, 92, 55S-64S.
172. Jung G. B., Nam S. W., Choi S., Lee G.-J., Park H.-K. (2014). Evaluation of antibiotic effects on *Pseudomonas aeruginosa* biofilm using Raman spectroscopy and multivariate analysis. *J. Opt. Soc. Am.*
173. Madigan M. T., Martinko J. M., Stahl D. A., Clark D. P. (2010). Brock of biology microorganisms. Benjamin Cummings, 13th edition.
174. Marks K. R. (2011). Investigating the fluoroquinolone-topoisomerase interaction by use of novel fluoroquinolone and quinazoline analogs. Ph.D dissertation of Iowa University.
175. Konaklieva M. I. (2014). Molecular targets of beta-lactam-based antimicrobial: Beyond the usual suspects. *Antibiotics*, 3, 128-142.

176. Suginaka H., Kotani S., Takata N., Ogawa M. (1980). Effect of cefotaxime (HR-756) on biosynthesis of cell wall peptidoglycan in *Pseudomonas aeruginosa* KM338 and *Escherichia coli*. *FEMS Microbiol. Lett.*, 8, 79-82.
177. LeFrock J. L., Prince R. A., Left R. D. (1982). Mechanism of action, antimicrobial activity, pharmacology, adverse effects, and clinical efficacy of cefotaxime. *Pharmacotherapy*, 2, 174-184.
178. Huang K. C., Mukhopadhyay R., Wen B., Gitai Z., Wingreen N. S. (2008). Cell shape and cell wall organization in Gram-negative bacteria. *PNAS*, 105, 49, 19282-19287.
179. Ginsberg C., Brown S., Walker S. (2008). Bacterial cell wall components. Springer - Verlag Berlin Heidelberg, 1535-1600.
180. Zeng X., Lin J. (2013). Beta-lactamase induction and cell wall metabolism in Gram-negative bacteria. *Front Microbiol*, 4, 1-9. Article 128.
181. Typas A., Banzhaf M., Gross C. A., Vollmer W. (2012). From the regulation of peptidoglycan synthesis to bacterial growth and morphology. *Nat. Rev. Microbiol.*, 10.
182. Bugg T. D. H., Braddick D., Dowson C. G., Roper D. I. (2011). Bacterial cell wall assembly: still an attractive antibacterial target. *Trends Biotechnol.*, 29, 167-173.
183. Izaki K., Matsushashi M., Strominger J. L. (1968). Biosynthesis of the peptidoglycan of bacterial cell walls. *The Journal of Biological Chemistry*, 243, 11, 3180-3192.
184. Tomioka S., Ishino F., Tamaki S., Matsushashi M. (1982). Formation of hyper-crosslinked peptidoglycan with multiple crosslinkages by a penicillin-binding protein 1A of *Escherichia coli*. *Biochem. Biophys. Res. Commun.*, 106, 4, 1175-1182.
185. Heijenoort J. (2001). Formation of the glycan chains in the synthesis of bacterial peptidoglycan. *Glycobiology*, 11, 3, 25R-36R.
186. Silver L. L. (2003). Novel inhibitors of bacterial cell wall synthesis. *Microbiology*, 6, 431-438, 431-438.
187. Wise E. M., Park J. T. (1965). Penicillin: Its basic site of action as an inhibitor of a peptide cross-linking reaction in cell wall mucopeptide synthesis. *Microbiology*, 54.
188. Neu H. C. (1985). Relation of structural properties of beta-lactam antibiotics to antibacterial activity. *The American Journal of Medicine*, 79, 2A.
189. Bugg T. D. H., Walsh C. T. (1992). Intracellular steps of bacterial cell wall peptidoglycan

biosynthesis : Enzymology, antibiotics, and antibiotic resistance. *Nat Prod Rep*, 199-215.

190. Scheffers D.-J., Pinho M. G. (2005). Bacterial cell wall synthesis: New insights from localization studies. *Microbiol. Mol. Biol. Rev.*, 69, 4, 585-607.
191. Sauvage E., Kerff F., Terrak M., Ayala J. A., Charlier P. (2008). The penicillin-binding proteins: structure and role in peptidoglycan biosynthesis. *FEMS Microbiol. Rev.*, 32, 234-258.
192. Beveridge T. J. (1999). Structures of Gram-negative cell walls and their derived membrane vesicles. *J. Bacteriol.*, 181, 16, 4725-4733.
193. Kumar A., Schweizer H. P. (2005). Bacterial resistance to antibiotics: active efflux and reduced uptake. *Adv. Drug Deliv. Rev.*, 57, 1486-1513.
194. Wright G. D. (2005). Bacterial resistance to antibiotics: Enzymatic degradation and modification. *Adv. Drug Deliv. Rev.*, 57, 1451-1470.
195. Lambert P. A. (2005). Bacterial resistance to antibiotics: Modified target sites. *Adv. Drug Deliv. Rev.*, 57, 1471-1485.
196. Sanders C. C., Sanders W. E. Jr. (1992). Beta-lactam resistance in Gram-negative bacteria: Global trends and clinical impact. *Clin. Infect. Dis.*, 15, 824-839.
197. Babic M., Hujer A. M., Bonomo R. A. (2006). What's new in antibiotic resistance ? Focus on beta-lactamases. *Drug Resist. Updat.*, 9, 142-156.
198. Bauernfeind A. (1986). Classification of beta-lactamases. *Review of Infectious Diseases*, 8, 5, S470-S481.
199. Ozturk H., Ozkirimli E., Ozgur A. (2015). Classification of beta-lactamases and penicillin binding proteins using ligand-centric network models. *Plos One*, 10, 2, 1-23.
200. Bush K., Jacoby G. A. (2010). Updated functional classification of beta-lactamases. *Antimicrob. Agents Chemother.*, 54, 3, 969-976.
201. Nikaido H. (1985). Role of permeability barriers in resistance to beta-lactam antibiotics. *Pharmac. Ther.*, 27, 197-231.
202. Saini A., Bansal R. (2012). Insights on the structural characteristics of NDM-1: The journey so far. *Adv Biol Chem*, 2, 323-334.
203. Brodersen D. E., Clemons W. M., Carter A. P., Morgan-Warren R. J., Wimberly B. T., Ramakrishnan V. (2000). The structural basis for the action of the antibiotics tetracycline,

- pactamycin, and hygromycin B on the 30S ribosomal subunit. *Cell*, 30, 1143-1154.
204. Chopra I., Roberts M. (2001). Tetracycline antibiotics: Mode of action, applications, molecular biology, and epidemiology of bacterial resistance. *Microbiol. Mol. Biol. Rev.*, 65, 2, 232-260.
205. Speer B. S., Shoemaker N. B., Salyers A. A. (1992). Bacterial resistance to tetracycline: Mechanisms, transfer, and clinical significance. *Clin. Microbiol. Rev.*, 5, 4, 387-399.
206. Roberts M. C. (2003). Tetracycline therapy: Update. *Clin. Infect. Dis.*, 36, 462-467.
207. Schnappinger D., Hillen W. (1996). Tetracyclines: antibiotic action, uptake, and resistance mechanism. *Arch Microbiol*, 165, 359-369.
208. Card R. M., Mafura M., Hunt T., Kirchner M., Weile J., Rashid M.-U., Weintraub A., Nord C. E., Anjum M. F. (2015). Impact of ciprofloxacin and clindamycin administration on Gram-negative bacteria isolated from healthy volunteers and characterization of the resistance genes they harbor. *Antimicrob. Agents Chemother.*, 59, 8, 4410-4416.
209. Yoshida H., Nakamura M., Bogaki M., Ito H., Kojima T., Hattori H., Nakamura S. (1993). Mechanism of action of quinolones against *Escherichia coli* DNA gyrase. *Antimicrob. Agents Chemother.*, 37, 4, 839-845.
210. Hawkey P. M. (2003). Mechanism of quinolone action and microbial response. *J. Antimicrob. Chemother.*, 51, S1, 29-35.
211. Hooper D. C. (2000). Mechanisms of action and resistance of older and newer fluoroquinolones. *Clin. Infect. Dis.*, 31, 2, S24-8.
212. Drlica K., Malik M., Kerns R. J., Zhao X. (2008). Quinolone-mediated bacterial death. *Antimicrob. Agents Chemother.*, 52, 2, 385-392.
213. Neugebauer U., Schmid U., Baumann K., Ziebuhr W., Kozitskaya S., Holzgrabe U., Schmitt M., Popp J. (2007). The influence of fluoroquinolone drugs on the bacterial growth of *S. epidermidis* utilizing the unique potential of vibrational spectroscopy. *J. Phys. Chem. A*, 111, 15, 2898-2906.
214. Mlynarikova K., Samek O., Bernatova S., Ruzicka F., Jezek J., Haronikova A., Siler M., Zemanek P., Hola V. (2015). Influence of culture media on microbial fingerprints using Raman spectroscopy. *Sensors*, 15, 29635-29647.
215. Oliveira F. S. S., Giana H. E., Silveira Jr. L. (2012). Discrimination of selected species of pathogenic bacteria using near-infrared Raman spectroscopy and principal components

analysis. *J. Biomed. Opt.*, 17, 10, 107004-1 - 107004-8.

216. Ramoji A., Galler K., Glaser U., Henkel T., Mayer G., Dellith J., Bauer M., Popp J., Neugebauer U. (2016). Characterization of different substrates for Raman spectroscopic imaging of eukaryotic cells. *J. Raman Spectrosc.*, 47, 773-786.
217. Al-Qadiri H. M., Al-Alami N. I., Lin M., Al-Holy M., Cavinato A. G., Rasco B. A. (2008). Studying of the bacterial growth phases using fourier transform infrared spectroscopy and multivariate analysis. *J. Rapid Methods Autom. Microbiol.*, 16, 73-89.
218. Czamara K., Majzner K., Pacia M. Z., Kochan K., Kaczor A., Baranska M. (2014). Raman spectroscopy of lipids: a review. *J. Raman Spectrosc.*, 46, 4-20.
219. Movasaghi Z., Rehman S., Rehman I. U. (2007). Raman spectroscopy of biological tissues. *Appl Spectrosc Rev*, 42, 493-541.
220. Schuster K. C., Reese I., Urlaub E., Gapes J. R., Lendl B. (2000). Multidimensional information on the chemical composition of single bacterial cells by confocal Raman microspectroscopy. *Anal. Chem.*, 72, 22, 5529-5534.
221. Harz M., Rosch P., Peschke K.-D., Ronneberger O., Burkhardt H., Popp J. (2005). Micro-Raman spectroscopic identification of bacterial cells of the genus *Staphylococcus* and dependence on their cultivation conditions. *Analyst*, 130, 1543-1550.
222. Jenkins A. L., Larsen R. A., Williams T. B. (2005). Characterization of amino acids using Raman spectroscopy. *Spectrochim. Acta Pt. A*, 61, 1585-1594.
223. Xie C., Li Y.-Q. (2003). Confocal micro-Raman spectroscopy of single biological cells using optical trapping and shifted excitation difference techniques. *J Appl Phys*, 93, 5.
224. Hlaing M. M., Dunn M., Stoddart P. R., McArthur S. L. (2016). Raman spectroscopic identification of single bacterial cells at different stages of their lifecycle. *Vib. Spectrosc.*, 86, 81-89.
225. Gniadecka M., Wulf H. C., Mortensen N. N., Nielsen O. F., Christensen D. H. (1997). Diagnosis of basal cell carcinoma by Raman spectroscopy. *J. Raman Spectrosc.*, 28, 125-129.
226. Notingher I. (2007). Raman spectroscopy cell-based biosensors. *Sensors*, 7, 1343-1358.
227. Movasaghi Z., Rehman S., Rehman I. (2008). Fourier Transform Infrared (FTIR) spectroscopy of biological tissues. *Appl. Spectrosc. Rev.*, 43, 2, 134-179.

228. Xu J., Turner J. W., Idso M., Biryukov S. V., Rognstad L., Gong H., Trainer V. L., Wells M. L., Strom M. S., Yu Q. (2013). In situ strain-level detection and identification of *Vibrio parahaemolyticus* using surface-enhanced Raman spectroscopy. *Anal. Chem.*, 85, 2630-2637.
229. Costerton J. W. (1999). Introduction to biofilm. *Int. J. Antimicrob. Agents*, 11, 217-221.
230. Han N., Mizan Md. F. R., Jahid I. K., Ha S.-D. (2016). Biofilm formation by *Vibrio parahaemolyticus* on food and food contact surfaces increases with rise in temperature. *Food Control*, 70, 161-166.
231. Jovetic S., Zhu Y., Marcone G. L., Marinelli F., Tramper J. (2010). Beta-lactam and glycopeptide antibiotics: first and last line of defense? *Trends Biotechnol.*, 28, 12, 596-604.
232. Toussaint K. A., Gallagher J. C. (2015). Beta-lactam/Beta-lactamase inhibitor combinations: From then to now. *Ann Pharmacother*, 49, 1, 86-98.
233. Schmitt J., Flemming H.-C. (1998). FTIR-spectroscopy in microbial and material analysis. *Int. Biodeterior. Biodegradation*, 41, 1-11.
234. Bycroft B. W., Shute R. E. (1985). The molecular basis for the mode of action of beta-lactam antibiotics and mechanisms of resistance. *Pharm. Res.*, 2, 3-14.
235. Malouin F., Bryan L. E. (1986). Modification of penicillin-binding proteins as mechanisms of beta-lactam resistance. *Antimicrob. Agents Chemother.*, 30, 1, 1-5.
236. Ruiz J. (2003). Mechanisms of resistance to quinolones: target alterations, decreased accumulation and DNA gyrase protection. *J. Antimicrob. Chemother.*, 51, 1109-1117.
237. Hooper D. C. (2001). Mechanisms of action of antimicrobials: Focus on fluoroquinolones. *Clin. Infect. Dis.*, 32, Suppl 1, S9-S15.
238. Hamasha K., QMohaidat Q. I., Putnam R. A., Woodman R. C., Palchaudhuri S., Rehse S. J. (2013). Sensitive and specific discrimination of pathogenic and nonpathogenic *Escherichia coli* using Raman spectroscopy—a comparison of two multivariate analysis techniques. *Biomed. Opt. Express*, 4, 4, 481-489.
239. Anes J., McCusker M. P., Fanning S., Martins M. (2015). The ins and outs of RND efflux pumps in *Escherichia coli*. *Front. Microbiol.*, 6, 587. Article 587.
240. Day L. E. (1966). Tetracycline inhibition of cell-free protein synthesis. *J. Bacteriol.*, 92, 1, 197-203.

241. Freeman B. A., Circo R. (1963). Effect of tetracyclines on the intracellular amino acids of molds. *J. Bacteriol.*, 86, 38-44.
242. Ling V., Morin C. L. (1971). Inhibition of amino acid transport in rat intestinal rings by tetracycline. *Biochim. Biophys. Acta*, 249, 252-259.
243. Redgrave L. S., Sutton S. B., Webber M. A., Piddock L. J. V. (2014). Fluoroquinolones resistance: Mechanisms, impact on bacteria, and role in evolutionary success. *Trends Microbiol.*, 22, 8, 438-445.
244. Blondeau J. M. (2004). Fluoroquinolones: Mechanism of action, classification, and development of resistance. *Surv. Ophthalmol.*, 49, S73-S78. Supplement 2.
245. Drlica K. (1999). Mechanism of fluoroquinolone action. *Curr. Opin. Microbiol.*, 2, 504-508.
246. Carman R. J., Simon M. A., Fernandez H., Miller M. A., Bartholomew M. J. (2004). Ciprofloxacin at low levels disrupts colonization resistance of human fecal microflora growing in chemostats. *Regul. Toxicol. Pharmacol.*, 40, 319-326.
247. Samanidou V. F., Demetriou C. E., Papadoyannis I. N. (2003). Direct determination of four fluoroquinolones, enoxacin, norfloxacin, ofloxacin, and ciprofloxacin, in pharmaceuticals and blood serum by HPLC. *Anal. Bioanal. Chem.*, 375, 623-629.
248. Bernatova S., Samek O., Pilat Z., Sery M., Jezek J., Jakl P., Siler M., Krzyzanek V., Zemanek P., Hola V., Dvorackova M., Ruzicka F. (2013). Following the mechanisms of bacteriostatic versus bactericidal action using Raman spectroscopy. *Molecules*, 18, 13188-13199.
249. Wolfson J. S., Hooper D. C. (1985). The fluoroquinolones: Structures, mechanisms of action and resistance, and spectra of activity in vitro. *Antimicrob. Agents Chemother.*, 28, 4, 581-586.
250. Saifedden G., Farinazleen G., Nor-Khaizura A., Kayali A. Y., Nakaguchi Y., Nishibuchi M., Son R. (2016). Antibiotic susceptibility profile of *Vibrio parahaemolyticus* isolated from shrimp in Selangor, Malaysia. *Int. Food Res. J.*, 23, 6, 2732-2736.
251. Joseph S. W., Debell R. M., Brown W. P. (1978). In vitro response to chloramphenicol, tetracycline, ampicillin, gentamicin, and beta-lactamase production by halophilic *Vibrios* from human and environmental sources. *Antimicrob. Agents Chemother.*, 13, 2, 244-248.
252. Kotra L.P., Mobashery S. (1998). Beta - lactam antibiotics, Beta -lactamases and bacterial resistance. *Bull. Inst. Pasteur*, 96, 139-150.

253. Denis F., Dosso M., Sow A., Mounier M. (1986). Les nouvelles cephalosporines. Structure - Pharmacocinetique - Activite. *Medicine et Maladies Infectieuses*, 4 bis, 236-240.
254. Bush K., Jacoby G. A., Medeiros A. A. (1995). A functional classification scheme for beta-lactamases and its correlation with molecular structure. *Antimicrob. Agents Chemother.*, 39, 6, 1211-1233.
255. Wike M. S., Lovering A. L., Strynadka N. C. J. (2005). Beta-lactam antibiotic resistance: a current structural perspective. *Curr. Opin. Microbiol.*, 8, 525-533.
256. Majiduddin F. K., Materon I. C., Palzkill T. G. (2002). Molecular analysis of beta-lactamase structure and function. *Int. J. Med. Microbiol.*, 292, 127-137.